NASA CONTRACTOR REPORT

NASA CR-1901

NASA CR-1901

FUNDAMENTAL LIMITATIONS ON V/STOL TERMINAL GUIDANCE DUE TO AIRCRAFT CHARACTERISTICS

by Julian Wolkovitch, Charles W. LaMont, and D. William Lochtie

Prepared by
MECHANICS RESEARCH, INC.
Los Angeles, Calif. 90045
for Langley Research Center

NATIONAL AERONAUTICS AND SPACE ADMINISTRATION • WASHINGTON, D. C. • DECEMBER 1971

1. Report No.	2. Government Accession No.	3. Recipient's Catalog No.
NASA CR-1901		

4. Title and Subtitle	5. Report Date
FUNDAMENTAL LIMITATIONS ON V/STOL TERMINAL GUIDANCE DUE TO AIRCRAFT CHARACTERISTICS	December 1971
	6. Performing Organization Code

7. Author(s)	8. Performing Organization Report No.
Julian Wolkovitch, Charles W. LaMont, and D. William Lochtie	
	10. Work Unit No.

9. Performing Organization Name and Address	11. Contract or Grant No.
Mechanics Research Inc. 9841 Airport Boulevard Los Angeles, California 90045	NAS1-9163
	13. Type of Report and Period Covered
12. Sponsoring Agency Name and Address	Contractor Report
National Aeronautics and Space Administration Washington, D.C. 20546	14. Sponsoring Agency Code

15. Supplementary Notes

16. Abstract

A review is given of limitations on approach flight paths of V/STOL aircraft, including limits on descent angle due to maximum drag/lift ratio. A method of calculating maximum drag/lift ratio of tilt-wing and deflected slipstream aircraft is presented.

Derivatives and transfer functions for the CL-84 tilt-wing and X-22A tilt-duct aircraft are presented. For the unaugmented CL-84 in steep descents the transfer function relating descent angle to thrust contains a right-half-plane zero. Using optimal control theory, it is shown that this zero causes a serious degradation in the accuracy with which steep flight paths can be followed in the presence of gusts.

17. Key Words (Suggested by Author(s))	18. Distribution Statement
V/STOL aircraft V/STOL descent angle limitations V/STOL flight dynamics	Unclassified - Unlimited

19. Security Classif. (of this report)	20. Security Classif. (of this page)	21. No. of Pages	22. Price*
Unclassified	Unclassified	181	$3.00

*For sale by the National Technical Information Service, Springfield, Virginia 22151

TABLE OF CONTENTS

Page

LIST OF SYMBOLS vii

LIST OF ILLUSTRATIONS xiii

LIST OF TABLES xvi

SUMMARY 1

CHAPTER

I PURPOSE AND SCOPE OF THIS REPORT 3

The Purpose of This Report 3

Contents of the Report 5

Acknowledgement 6

II LIMITS ON NOMINAL FLIGHT PROFILES FOR V/STOL AIRCRAFT AT LOW SPEEDS 7

The Requirement for High Drag/Lift Ratio 7

Drag/Lift Ratio of "Passive-Lift" Configurations 11

Direct increase of parasite drag 15

Reverse-thrust propellers 16

Reverse thrust jet engines 20

Tilt-rotor configurations 21

Slipstreamed - Wing Configurations 23

Tilt-wing descent boundaries 29

Jet Lift and Ducted Fan V/STOL Aircraft 31

Jet Flap and "Blown Flap" Aircraft 33

Limitations on Climb-out Performance 34

Limitations on Constant-Acceleration Flight Paths in the Vertical Plane 36

Limitations on Lateral Curvature of the Flight Path 38

TABLE OF CONTENTS (CONTINUED)

CHAPTER		Page
III	ANALYTIC PREDICTION OF DESCENT BOUNDARIES FOR TILT-WING AND DEFLECTED SLIPSTREAM AIRCRAFT ...	40
	Introduction	40
	Description of the Method	41
	Computation of Isolated Propeller Net Thrust, Gross Thrust, and Normal Force	42
	Computation of Wing Forces	46
	Computation of Total Lift and Drag	50
	Correlation with Experiment within the Unstalled Region	52
	Calculation of Descent Boundaries for the XC-142A	52
	General Procedure for Calculating Descent Boundaries	55
	Geometric and Aerodynamic Characteristics of the XC-142A	55
	Calculated and Experimental Descent Boundaries	67
IV	EFFECT OF DESCENT ON TRANSFER FUNCTIONS OF TILT-WING AND TILT-DUCT V/STOL AIRCRAFT	70
	Introduction	70
	Calculation and Validation of CL-84 Stability Derivatives	71
	The Effect of Descent Angle on the CL-84 Longitudinal Transfer Functions	74
	Longitudinal transfer function denominators	76
	Pitch attitude/longitudinal stick deflection transfer function	76
	Speed/longitudinal stick deflection transfer function	76
	Height error/longitudinal stick deflection transfer function	77

TABLE OF CONTENTS (CONTINUED)

		Page
	Height error/collective transfer function	80
	The Effect of Descent on the CL-84 Lateral Transfer Functions	85
	Lateral transfer function denominators	85
	Bank angle/lateral stick deflection transfer function numerators	85
	Lateral ground velocity/pedal deflection transfer function numerators	86
	Lateral ground velocity/lateral stick deflection transfer function numerators	86
	Calculation and Validation of X-22A Derivatives and Transfer Functions	87
CHAPTER		
V	PREDICTION OF THE BEST ACCURACY ACHIEVABLE FOR V/STOL TERMINAL GUIDANCE	91
	Introduction and Summary	91
	Transfer Function and Mean Square Error of an Optimal Regulator	92
	Example of calculation of optimum regulator transfer function	95
	Example of calculation of mean square error	97
	A Simple Formula for the Mean Square Error of an Optimal Regulator	100
	Applicability of Wiener Regulator Theory to V/STOL Control	102
	Nonstationary inputs and aircraft dynamics	103
	Instability of the aircraft	104
	Nonlinearities	104
	Different points of application of signal and noise	104
	Multiloop control	105

TABLE OF CONTENTS (CONTINUED)

		Page
	Optimal Control of the CL-84	105
	Alternative Control Techniques	111
	Gust Models	112
	Optimal Control of the X-22A Tilt-Duct Aircraft	113
	Implications of Optimal Control Theory for Other V/STOL Configurations	114
CHAPTER VI	CONCLUSIONS AND RECOMMENDATIONS	116
	Conclusions	116
	Recommendations	117
APPENDIX A - CL-84 TRANSFER FUNCTIONS AND DERIVATIVES		119
APPENDIX B - X-22A STABILITY DERIVATIVES		151
REFERENCES		164

LIST OF SYMBOLS

A	aspect ratio
C	Laplace transform of c
C_D	drag coefficient, $D/\frac{1}{2}\rho V_A^2 S$
C_{D_i}	induced drag coefficient, $D_i/\frac{1}{2}\rho V_A^2 S$
C_{D_o}	parasite drag coefficient, $D_o/\frac{1}{2}\rho V_A^2 S$
C_L	lift coefficient $L/\frac{1}{2}\rho V_A^2 S$
C_L", C_X"	lift and drag coefficients referred to slipstream dynamic pressure
C_{T_s}	thrust coefficient referred to slipstream dynamic pressure
c	general system response
D	propeller diameter, ft.,
D	drag, lbs
D_i	induced drag, lbs
D_o	drag not due to lift, parasite drag, lbs
e	span-efficiency factor
F_c	controller transfer function
g	acceleration due to gravity, fps^2
h	height above unperturbed flight path, ft

h_e height error, defined in Figure 25, ft

h_g inertial height above ground, ft

I_x roll inertia, lbs-ft^2

I_y pitch inertia, lbs-ft^2

I_z yaw inertia, lbs-ft^2

I_{xz} product of inertia lbs-ft^2

i_T tail incidence

i_w angle of wing chord line to datum, radians

i_{TL} angle of thrust line to chord, radians

$j\omega$ imaginary part of s

k a constant

k_η thrust turning loss factor

L rolling moment, lbs-ft

L lift, lbs

M pitching moment, lbs-ft

M Laplace transform of system error

m airplane mass, slugs

m mass flow, slugs per sec

m system error

N yawing moment, lbs-ft

N	Laplace transform of n
N	number of propellers
n	noise (i.e., disturbance) time history
n_z	normal acceleration, g's
P	minimum phase transfer function factor
p	roll rate, rad/sec
$\bar{Q}$	nonminimum phase transfer function factor
q	pitch rate, rad/sec
R	propeller radius, ft
R	Laplace transform of r
r	yaw rate rad/sec
r	general system input
r.m.s	root-mean-square value
S	wing reference area, ft^2
S.A.S.	denotes stability augmenter system
s	Laplace transform complex variable, $s = \sigma + j\omega$
S_p	actuator disc area, ft^2
T	thrust lb
T_c	thrust coefficient, $= 2T/\rho V_\infty{}^2 S_p$
T_c''	thrust coefficient based on slipstream dynamic pressure, $= 2T/\rho V_{ss}^2 S_p$
t	time, sec
U_o	unperturbed velocity along the z-axis, fps
u	perturbation velocity along the x-axis, fps
u	forward speed perturbation

V	inertial speed or airspeed in still air, fps
V_A	airspeed, fps
V_D	resultant flow velocity at actuator disc, fps
V_I	inertial speed, fps
V_R	resultant flow velocity at wing, fps
V_{ss}	flow velocity in fully developed slipstream, fps
V_w	horizontal wind speed relative to the ground, fps
V_∞	free-stream airspeed, fps
v	perturbation velocity along the y-axis, fps
W	gross weight, lbs
w	perturbation velocity along the z-axis, fps
X	force along x-axis, lbs
x	ground distance, ft
$\dot{x}$	ground speed, fps
w_g	w-gust velocity component fps
Y	force along y-axis, lb
y	lateral deviation from unperturbed flight path, ft
Z	force along z-axis, lbs
$ZI_{x,z,}$	inertia about x or z axis in stability axes
α	angle of attack of wing or thrust line, as appropriate, radians
α_D	angle between V_D and the shaft axis, radians
α_o	angle of attack of wing reference chord line at zero lift with power-off, radians
α_{OL}	angle of zero lift chord line to wing chord line, radians

α_{ss}	angle of fully-developed slipstream to free-stream, radians
α_T	$\alpha + i_w$, wing total angle of attack, radians
α_{TL}	angle of shaft to free-stream, radians
α_w	effective angle of attack of wing, radians
$\dot{\gamma}$	rate of change of flight path angle, rad/sec
γ_A	equivalent flight path angle in still air, positive for climb, radians
γ, γ_I	angle of flight path to the horizontal, positive for climb, radians
γ_o	unperturbed flight path angle, positive for climb, radians
δ	controller output (i.e., control deflection)
δ_A	roll control deflection
δ_E	pitch attitude control deflection
δ_F	flap deflection
δ_R	yaw control deflection
δ_T	thrust control deflection
χ	local angle of attack, radians
χ	azimuthal flight path direction, radians
χ_{max}	limiting local angle of attack for buffeting, radians
χ_{ss}	angle of gross thrust vector to shaft, radians
θ_o	collective pitch, radians
θ_{ZLL}	angle of zero lift chord line to shaft, radians
v_h	$\left[\text{thrust of one propeller}/2\rho(\frac{\pi}{4})D^2\right]^{\frac{1}{2}}$, fps

ρ	air density, slug-ft^3
σ	real part of s
τ_e	effective time delay, secs
Φ_{nn}	noise power spectrum
Φ_{mm}	output power spectrum
$\Phi_{w_g w_g}$	gust spectrum, ft^2-sec^2/rad-sec^{-1}
ω_b	gust break frequency rad/sec

Mathematical Symbols

$\approx$	approximately equals
$\overbrace{x}$	mean value of x
x^+	factor of x containing all the left-half-plane poles and zeros
x^-	factor of x containing all the right-half-plane poles and zeros
$\left[x\right]_+$	expansion of x in partial fractions, omitting partial fractions with right-half-plane zeros
$\left[x\right]_-$	expansion of x in partial fractions, omitting partial fractions with left-half-plane zeros
$\bar{x}$	complex conjugate of x

LIST OF ILLUSTRATIONS

Figure		Page
1	Forces Acting on an Aircraft Flying a Straight-Line Accelerating Descent	8
2	Effect of Head and Tail Winds on Descent Angle	8
3	Alternative Approach Flight Profiles	10
4(a)	Approach Characteristics of a Passive-Lift STOL Transport as a Function of Lift Coefficient	10
4(b)	Maximum Lift Coefficient Comparison	13
5	Effect of Reverse-Thrust Propellers on Descent Angle of a Passive-Lift STOL Aircraft	19
6	Helicopter and Tilt-Rotor Descent Boundaries	22
7	Explanation of Descent Boundaries for Tilt-Wing and Deflected Slipstream Configurations (from Ref. 11)	24
8	Breguet 941/McDonnell Douglas 188 Flight Envelopes for Preapproach and Wave-off Configuration	26
9	Breguet 941/McDonnell Douglas 188 Flight Envelopes for Approach and Landing Configuration	27
10	XC-142A Buffet Boundaries	30
11	Descent Boundaries for a Tilt-Duct Aircraft (DOAK VZ-4)	32
12	Trade-off Between Horizontal and Vertical Acceleration for a Given Total Normal Acceleration Capability	39
13	Induced Velocities and Total Velocities in the Slipstream	43
14	Propeller-Wing Slipstream Force Vectors at Forward Speed	43

Figure		Page
15	Angular Relationships of Wing-Propeller Configuration and Slipstream Reaction Forces (Static Case)	47
16	Initial and Final Gross Thrust Vectors	49
17(a)	Correlation of Lift and Estimated Buffet Onset with Figure 16, Ref. 10	53
17(b)	Correlation of Longitudinal Force and Estimated Buffet Onset with Figure 16, Ref. 10	54
18	Three-View Drawing of 1/11 Scale XC-142A Model of Reference 23	56
19	Zero Lift Drag Data, XC-142A	60
20(a)	XC-142A 1/11 Scale Model Local Angle of Attack at Maximum Lift	63
20(b)	Flap Effectiveness for XC-142A 1/11 Scale Model ..	63
21(a)	XC-142A Zero Lift Angle Characteristics	66
21(b)	Flap Effectiveness, XC-142A	66
22	Comparison of Predicted and Measured Descent Boundaries for the XC-142A	68
23	Three-View Drawing of CL-84 Tilt-Wing Aircraft ...	72
24	Time History of Longitudinal-Control Step Pull-and-Hold Maneuver with Pitch-Attitude SAS Off and Pitch-Rate SAS on Airspeed of 42 Knots; Wing Incidence of 40°; Flap Incidence of 24°	75
25	Definition of Height Error	78
26	Effect of Descent Angle on Height Error Response for CL-84 at 42 Knots Airspeed with S.A.S. Off ...	81
27(a)	Effect of Descent Angle on Height Error Response for CL-84 at 42 Knots Airspeed with S.A.S. On	83
27(b)	Effect of Descent and Stability Augmenter System on Pitch Attitude Response to Unit Step Input in Collective Pitch for CL-84 at 42 knots Airspeed at Sea Level	84

Figure		Page
28	Three-View Drawing of Bell X-22A Tilt-Duct V/STOL Aircraft	88
29	Dynamic Lateral-Directional Stability (Dutch Roll) for X-22A with S.A.S. On.	90
30	Regulator Block Diagram	93
31	Effect of Nonminimum Phase Transfer Function on Mean Square Error	93
32	Effect of Nonminimum Phase Characteristics on Step Response of a Second Order System	99
33	Gust Spectrum Break Frequency as a Function of Airspeed and Altitude	107
34	Graphical Representation of Evaluation of Right-Half Plane Residue	107
35	Effect of Gust Break Frequency on Minimum Achievable Gust Response with Optimum Single-Loop Control	110

LIST OF TABLES

Table		Page
1	Operating States of Reverse-Thrust Propellers	17
2	XC-142A Basic Dimensional Data	58
3	XC-142A Configuration Parameters	58
4	Zero Lift Drag Coefficient Data, XC-142A	59
5	Angle of Attack at Maximum Lift - XC-142A	61
6	Flap Effectiveness Data - XC-142A	64
7	Flight Conditions Studied for CL-84	73
8	Flight Conditions Studied for the X-22A	87

FUNDAMENTAL LIMITATIONS ON V/STOL TERMINAL GUIDANCE DUE TO AIRCRAFT CHARACTERISTICS

By Julian Wolkovitch, Charles W. LaMont, and D. William Lochtie
Mechanics Research, Inc.

SUMMARY

For V/STOL aircraft, the possible terminal flight paths and the accuracy with which these flight paths can be followed are limited. A review is given of the limitations on possible flight paths, and it is shown that a principal cause of these limitations is the inability to generate sufficient drag at high lift coefficients. The reasons for this limitation on drag/lift ratio are explained, and a new method is presented for calculating the maximum drag/lift ratio of tilt-wing and deflected-slipstream configurations. The method uses momentum theory and requires power-off stall characteristics. The predictions of the method are shown to be in reasonable agreement with measured steep descent buffet boundaries for the XC-142A tilt-wing aircraft.

Stability derivatives and transfer functions for the CL-84 tilt-wing aircraft and for the X-22A tilt-duct aircraft are presented for low-speed level and descending flight. For the tilt-wing aircraft, a significant effect of descent angle occurs in the transfer function relating flight path angle to thrust. In steep low speed descents, a right half-plane zero appears which causes the response to move in the wrong direction a few seconds after the input is applied. Optimal control theory is used to calculate the minimum achievable r.m.s. deviation from the flight path due to random gusts. It is shown that, when the above right-half-plane zero approaches the gust break frequency, the accuracy with which the aircraft can follow the desired flight path is seriously degraded.

Page intentionally left blank

CHAPTER I

PURPOSE AND SCOPE OF THIS REPORT

The Purpose of This Report

V/STOL aircraft must be able to operate in confined air spaces if full advantage is to be taken of their capability for zero or small ground roll distance. This implies the capability to descend at steep angles and low speeds. It has been found that for almost all V/STOL aircraft, severe limitations exist on the steepness of the flight path that can be achieved at low speeds. These limitations stem from two causes

(1) inability to generate the steady aerodynamic forces required to follow the desired flight path, due to limits such as stall and buffet, and insufficient drag.

(2) poor accuracy of following the desired flight path, due to unsatisfactory response of the aircraft to gusts and to command control inputs, inadequate pilot displays, etc.

The purpose of this report is to investigate the above limitations for typical V/STOL aircraft, to indicate their importance, and to describe feasible methods of removing or relaxing the limitations.

The report concentrates on limitations which are "fundamental" for a given aircraft. A "fundamental" limitation is defined as one that can only be removed by changing the overall vehicle geometric, aerodynamic, or control system characteristics. For example, at typical approach speeds, the steepness of the approach of tilt-wing aircraft is restricted by inability to generate sufficient steady drag from the wing-propeller combination. This is regarded as a "fundamental" limitation of this type of aircraft, since it can only be relieved by a major modification

such as increased leading edge droop, or a more effective flap system. Limitations such as poor pilot vision of his touchdown point in VFR flight, inadequate or badly-arranged displays for IFR flight, etc., can be relieved without major modifications to the vehicle and are therefore not regarded as "fundamental."

The scope of this report embraces all types of V/STOL aircraft other than helicopters. A study on the characteristics of helicopters in steep approaches was performed in parallel with the research reported here, the results are presented in Reference 1. In this report the term "V/STOL aircraft" specifically excludes helicopters.

The contents of the report are summarized below; however, before this summary it is necessary to explain some terms used throughout the report. These are "nominal flight profile", "nominal flight path" and "nonminimum phase system".

A nominal flight profile is defined here as a time history of a combination of vehicle state variables such as airspeed, descent angle, normal acceleration, etc., which is feasible in that the required aerodynamic forces can be generated by the aircraft, regarding it as a point mass. For example, an approach consisting of a turn, followed by a level deceleration transisting to a constant-speed descent would constitute a nominal flight profile, provided the aircraft could pull the 'g's required for the turn, and could produce the drag required for deceleration and steady descent without exceeding stall or buffet boundaries. A nominal flight path is a nominal flight profile which involves no change in airspeed.

A nonminimum phase system is one having a relevant transfer function containing one or more right-half plane zeros. As shown in standard references in control theory (e.g., Reference 2), such zeros limit the precision with which the desired flight path can be followed, in the presence of disturbances such as gusts.

Contents of the Report

Chapter II presents a review of the nominal flight profile capabilities of current V/STOL aircraft configurations. The equivalence of descent capability and deceleration capability is explained. Examples of the limits on nominal flight profiles for various types of V/STOL aircraft are presented. This chapter contains nothing new, but it collects together some hitherto scattered data, and sets the stage for the detailed technical analyses that follow, by explaining their relevance to practical problems.

Chapter III presents a new method for calculating descent/deceleration capabilities of tilt-wing and deflected-slipstream configurations. The method uses momentum theory to predict the power-on descent/deceleration boundaries in terms of the power-off stall characteristics of the configuration. A worked example is given for the XC-142, showing that the method gives fair agreement with experimental data for descent angle buffet boundaries.

Chapter IV discusses the dynamics of representative tilt-wing and tilt-duct aircraft in small-perturbations from constant-speed approaches. The flight path angles considered cover the range from level flight to the steep descent buffet boundary. Stability derivatives for the Canadair CL-84 tilt-wing aircraft were calculated using the MOSTAB modular stability derivative program described in Reference 1. The accuracy of the derivatives is verified by using them to calculate time histories of the response to pilot control inputs. It is shown that these time histories agree closely with time histories obtained from flight test data. Chapter IV also presents transfer functions for the Bell X-22A tilt-duct aircraft in low-speed level and descending flight. These transfer functions were calculated using

derivatives supplied by the manufacturer. The significance of the above transfer functions in determining limits on the accuracy of flight path control is described in Chapter V.

In Chapter V, optimal control theory is applied to determine the minimum achievable r.m.s deviation from a nominal flight path, for any given stationary random gust environment. It is shown that, for the tilt-wing aircraft considered, significant increase in the minimum achievable r.m.s. deviation occurs when the descent angle becomes steep. This loss in accuracy of flight path control is shown to be caused by the appearance of a right-half-plane zero in the transfer function relating flight path angle to collective propeller pitch, (which is the primary means of flight path control at low speeds). Methods of alleviating this nonminimum phase effect are discussed. It is shown that the right-half plane zero can be removed through feedbacks of pitch attitude and rate to the pitch attitude control. In contrast to the tilt-wing configuration, the tilt-duct aircraft is free of critical nonminimum phase effects, and is predicted to be capable of following relatively steep nominal flight paths with good accuracy.

Chapter VI states the major conclusions of the report and lists some recommendations for further research.

Appendix A contains tables of derivatives and transfer functions for the CL-84. Appendix B contains derivatives for the X-22A.

Acknowledgement

Grateful acknowledgment is made to Mr. F. C. Phillips of Canadair Limited, who provided much valuable data on the CL-84.

CHAPTER II

LIMITS ON NOMINAL FLIGHT PROFILES FOR V/STOL AIRCRAFT AT LOW SPEEDS

The Requirement for High Drag/Lift Ratio

Initially, consider straight-line flight in calm air. This represents the simplest case for analysis. The combinations of airspeed, descent angle, and deceleration which are feasible for a given aircraft configuration are determined by the balance of aerodynamic, inertial and gravitational forces as shown in Figure 1. The key aerodynamic parameter is the drag/lift ratio, which from Figure 1 is related to flight path angle and deceleration by

$$\frac{D}{L} = \tan(-\gamma) - \frac{\frac{dV}{dt}}{g \cos(-\gamma)} \qquad (1)$$

In most instances (D/L) max is limited, for reasons discussed below, and the steepest descent angle is given by

$$(-\gamma)_{max} = \tan^{-1} (D/L)_{max} \qquad (2)$$

At this descent angle the deceleration capability is zero.

It is advantageous to have a high $(D/L)_{max}$ for the following reasons

(1) to permit approaches to confined areas, e.g., in city-centers,

(2) to facilitate downwind approaches and to cope with wind shears

(3) to minimize the time required to decelerate from cruise to touchdown

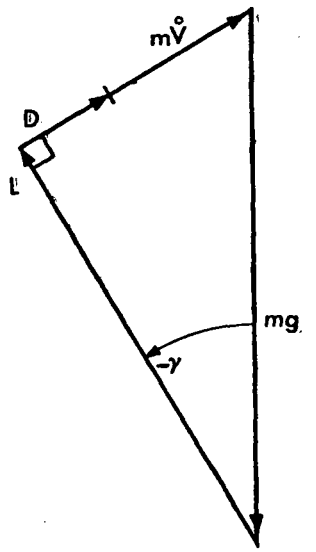

Figure 1. Forces Acting on an Aircraft Flying a Straight-Line Accelerating Descent

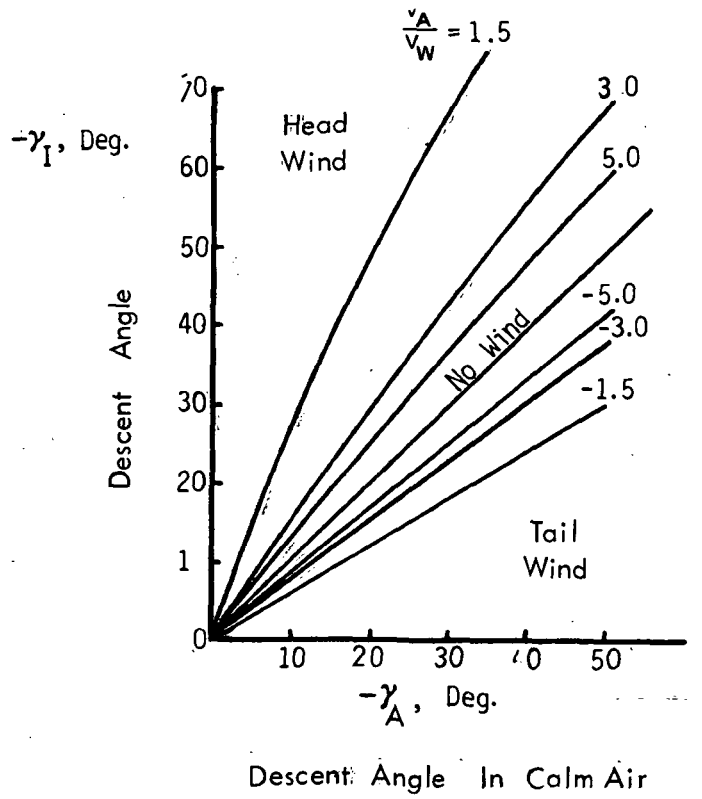

Figure 2. Effect of Head and Tail Winds on Descent Angle

A brief explanation of items (2) and (3) is given below.

Consider an airplane descending at an angle $-\gamma_A$ and speed V_A relative to the wind, which is blowing with horizontal velocity V_w, positive for headwind. Assuming steady conditions, the descent angle relative to inertial space is $-\gamma_I$ where

$$-\gamma_I = \tan^{-1} \left\{ \frac{\tan(-\gamma_A)}{1 - \frac{V_w}{V_A \cos(-\gamma_A)}} \right\} \qquad (3)$$

For V/STOL aircraft $\frac{V_w}{V_A}$ is much larger than for conventional aircraft, and γ_A is also increased in most cases. Both these factors combine to increase the difference between γ_I and γ_A ($= (D/L)_{max}$). This is beneficial for headwinds but correspondingly adverse for tailwinds, as shown in Figure 2 which graphs Eq. 3. The implications for wind-shears are obvious, from Figure 2.

The time occupied in decelerating and descending from cruise speed and altitude to touchdown is less productive than the time spent in cruise, because of the lower average speed. For efficient operation this unproductive time should be minimized. Considering the contribution of the approach to this unproductive time leads to the conclusion that the highest possible value of $(D/L)_{max}$ should be used to minimize the time spent on the approach. However, it is not readily apparent how this (D/L) should be applied, i.e., whether it should be used for increasing deceleration or to increase descent angle. The problem is illustrated by the following simple example, taken from Reference 3.

Figure 3 compares two alternative approach profiles. One is a

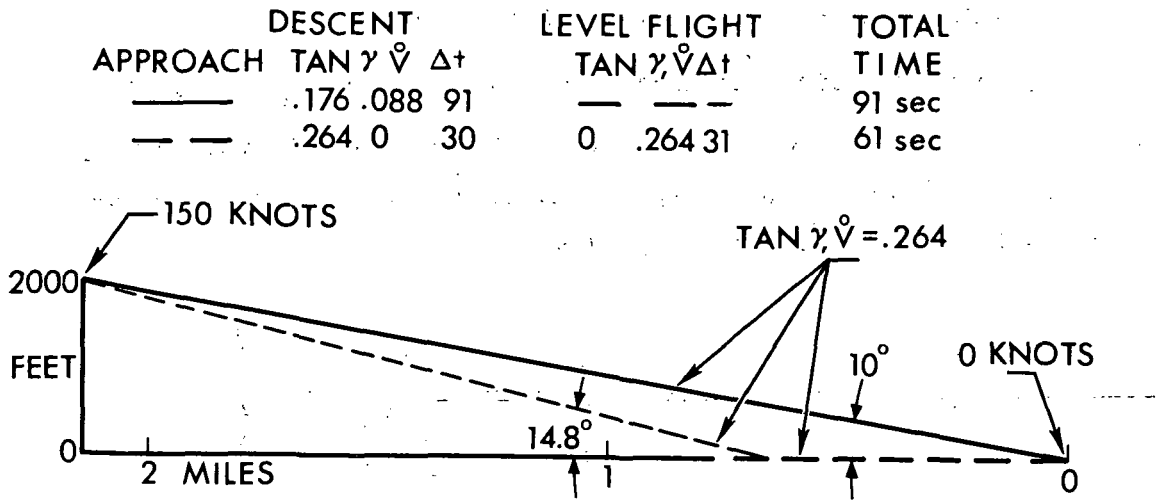

Figure 3. - Alternative Approach Flight Profiles

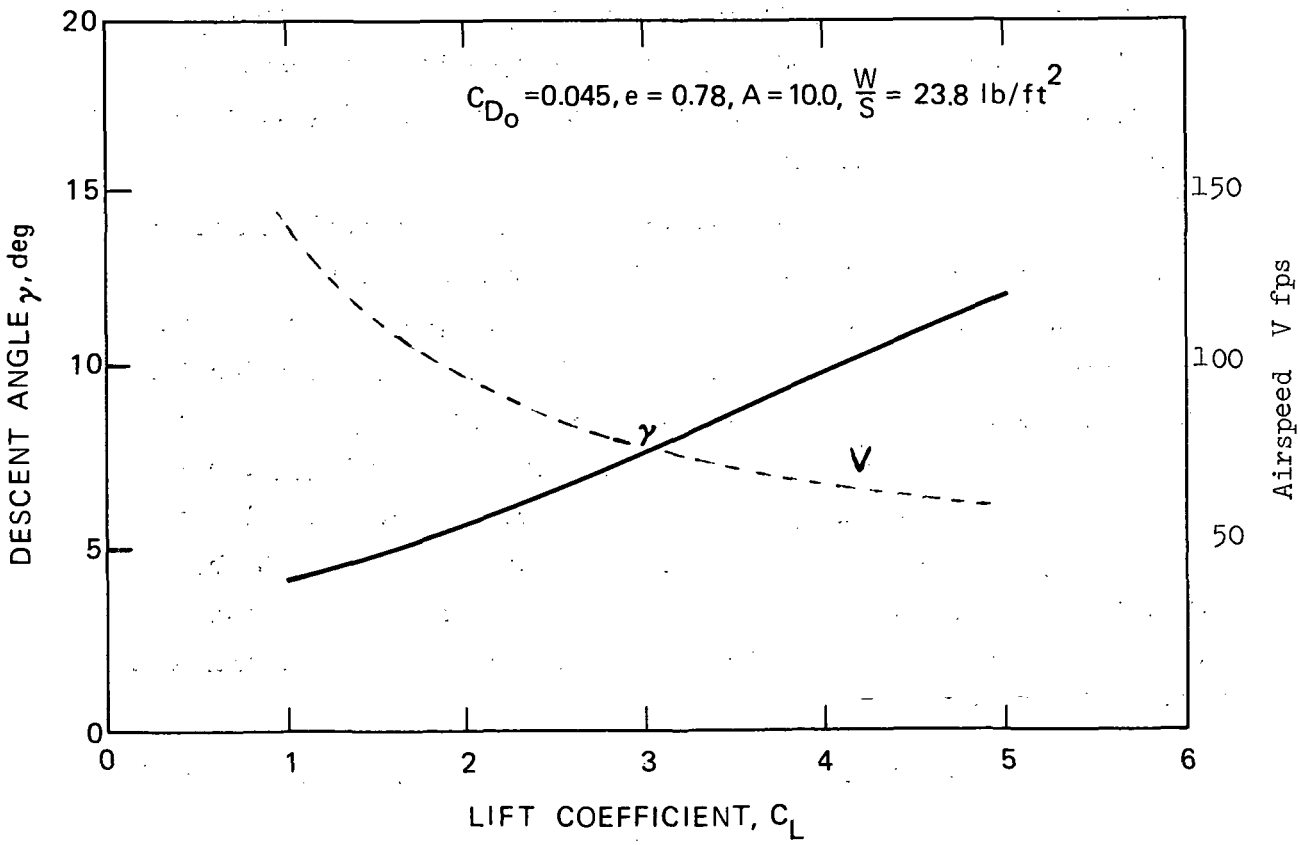

Figure 4(a) - Approach Characteristics of a Passive-Lift STOL Transport as a Function of Lift Coefficient

straight-line 10 degree descent with a constant deceleration of 0.088 g's. The other approach consists of two straight-line segments, the first at 14.8 degrees with no deceleration and the second at 0 degrees with 0.264 g's deceleration. Both approaches require the aircraft to fly at $(D/L)_{max} = 0.264$ continuously. The two-segment approach requires only 61 seconds, compared to 91 seconds for the "straight-in" approach. Undoubtedly, further savings can be achieved through more complicated approach profiles. Several references have studied the optimization of approach flight paths within given constraints as $(D/L)_{max}$. It is certainly interesting to determine the optimum approach profile for a given $(D/L)_{max}$; however, the time required for such an approach can always be reduced by increasing $(D/L)_{max}$. Thus, in studying fundamental limitations on V/STOL terminal guidance, it is more relevant to consider the aerodynamic factors limiting $(D/L)_{max}$ for various configurations. Only when these have been satisfactorily determined is it worthwhile to perform optimization calculations of the type described above.

The above discussions explain the emphasis of this report on $(D/L)_{max}$ as a fundamental limiting parameter for V/STOL approaches. Later sections of this report discuss the factors limiting $(D/L)_{max}$ and indicate how the limits may be alleviated.

Drag/Lift Ratio of "Passive-Lift" Configurations

Most STOL aircraft in current commercial service are of the category which we shall call "passive-lift" in which the powerplant makes no substantial contribution to the lift. The DeHavilland Twin-Otter is a well-known example of this type.

The drag/lift characteristics of a passive-lift aircraft can be expressed in coefficient form as

$$C_D = C_{D_o} + \frac{(C_L)^2}{\pi A e} \qquad (4)$$

where C_{D_o} is the coefficient of parasite drag (i.e., drag not induced by lift).

For a typical passive-lift configuration of the Twin-Otter category $C_{D_o} = 0.045$, $e = 0.78$, $A = 10$, giving $C_D = 0.045 + 0.041 (C_L)^2$. The resulting descent angle and airspeed are graphed on Figure 4(a). The airspeed was calculated from the standard formula:

$$V_{min} = \left(\frac{2}{\rho} \cdot \frac{W}{S} \cdot \frac{\cos \gamma}{C_{L_{max}}} \right)^{1/2} \qquad (5)$$

As Figure 4(a) demonstrates, a substantially slower and steeper descent results from increasing $C_{L_{max}}$. The possibilities for accomplishing this will now be discussed.

Passive-lift aircraft using leading edge slots and double-slotted flaps are usually limited to lift coefficients of 2.8 to 2.9. In part this is due to the necessity to maintain adequate margin of thrust over drag to permit go-around following a balked landing (see Reference 4). However, an additional factor is the mechanical complexity involved in constructing a flap system that will permit $C_{L_{max}} > 3.0$ when extended without excessive cruise drag in the retracted position. This can be appreciated by considering Figure 4(b) which shows two-dimensional test data taken from Reference 5.

Note that much of the advantage of slots and flaps stems from the increased wing area they provide through increasing the projected chord, c_p, (a sliding doubled-slotted flap + slat can extend c_p by 40 percent). Again mechanical complexity limits the percentage

NOTE: ALL C_L's ARE REFERRED TO THE PROJECTED CHORD, C_p

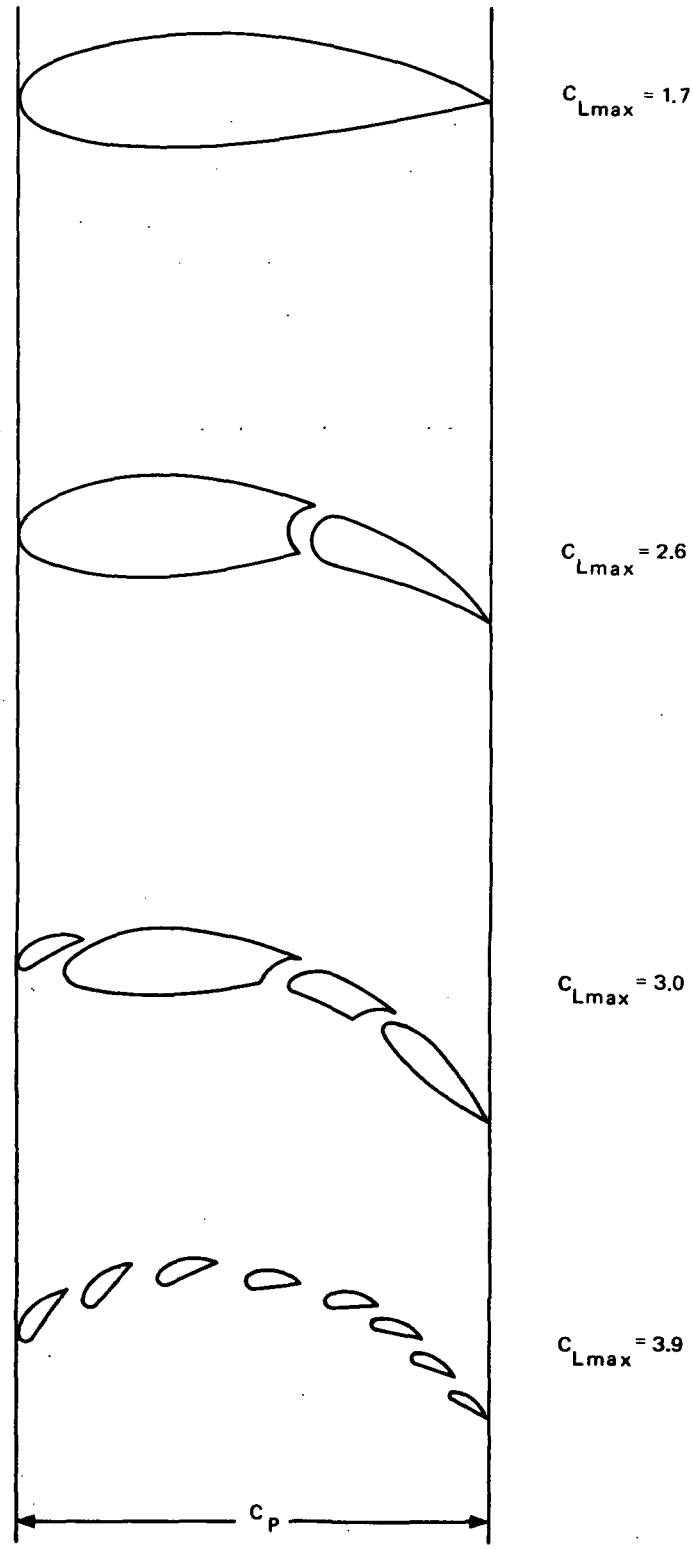

Figure 4(b) - Maximum Lift Coefficient Comparison

extension of c_p that is possible, but recent tests (Reference 6) of spanwise extension of the wing tips indicate that this may be a practical alternative to the customary chordwise extension. The increase in wing area obtained by tip extension can reduce the approach speed, but does not necessarily yield a steeper approach, since the increase in aspect ratio tends to reduce the induced drag.

It is by no means certain that the ultimate lift capabilities of passive-lift configurations have been approached. The maximum lift coefficient of wings of moderate aspect ratio is substantially less than that the maximum two-dimensional section lift coefficient. This is made clear in Reference 7, which summarizes the existing theories for predicting $C_{L_{max}}$ for general wings, specified only by their planform. All the theories predict

$$C_{L_{max}} = kA \qquad (6)$$

where k varies from 0.85 to 1.9 according to the particular theory. None of the theories predicts the leveling-off of $C_{L_{max}}$ that actually occurs due to wing-stalling for A greater than about 7, as two-dimensional conditions are approached.*

Hancock (Reference 8) concludes that k in Eq. 6 should be 0.85, but admits that his theory does not agree with experimental data, which indicate a value of k of about 1.9. Hancock shows that the published theories which give k = 1.9 are based on unsound arguments, and that any agreement between these theories and experiment is fortuitous.

---

*Note that this discussion does not include STOL aircraft with active boundary layer control (B.L.C.) using blowing and/or sucking to delay stall. Such aircraft are discussed later in this chapter.

This gap between theory and experiment is disturbing. Until it is resolved, it is prudent to use experimental data on specific configurations to predict $C_{L_{max}}$ of passive-lift-aircraft. From Figure 4(a), it is apparent that the attainment of high-lift coefficients does not produce sufficient induced drag to achieve a very steep flight path.

Returning to Eq. 4, we see that an alternative method of increasing $-\gamma$ is to increase the parasite drag coefficient C_{D_o} or decrease the induced drag factor e. It is difficult to change the latter while still retaining high $C_{L\ max}$, so the most practical alternative is to increase C_{D_o}. There are several ways in which this can be accomplished.

(1) direct increase of parasite drag through spoilers or dive-brakes
(2) reverse-thrusting propellers (sometimes called "Beta" control)
(3) reverse thrusting jet engines

Each of these alternatives will now be discussed.

Direct increase of parasite drag. - Parasite drag devices such as spoilers and dive-brakes are not well suited to low-speed conditions because their drag varies as $(1/2)\rho V^2$. Thus for the example aircraft of Figure 3, from Eq. (4) at $C_L = 3.0$

$$C_D = \underset{\text{parasite}}{0.045} + \underset{\text{induced}}{0.37} = \underset{\text{total}}{0.415} \qquad (7)$$

To double the descent angle by increasing parasite drag would demand raising the parasite drag coefficient to 0.46.

$$C_{D_o} = 0.83 - 0.37 = 0.46 \qquad (8)$$

The ratio of the area of the required dive-brake to the wing area, is given by

$$\Delta C_{D_o} = 0.46 - 0.045 = 0.415 = (S_{\text{dive-brake}}/S)\ (C_{D\ \text{dive-brake}}/0.045) \tag{9}$$

Taking C_D dive-brake as 0.90, this gives the ratio of dive-brake araa to wing area as

$$S_{\text{spoiler}}/S = 0.415 \times \left(\frac{0.045}{0.90}\right) = 8.3\% \tag{10}$$

It is difficult to find a location for dive-brakes of such a size where they will neither cause an appreciable loss of lift nor interfere with controllability by causing buffeting at the tail. For higher lift coefficients (i.e., "active" lift configurations) the required dive-brake area increases, and these disadvantages become even more severe. The net conclusion follows that dive-brakes offer only small benefits for STOL aircraft.

Reverse-thrust propellers. - To appreciate the problems and potential advantages of reverse thrust propellers (sometimes called "Beta-control") it is necessary to understand that a propeller thrusting in the opposite direction to which it is moving may have several states of operation, some steady, others very unsteady. These states are defined by reference to a quantity v_h, defined in terms of propeller radius, R, and air density, ρ, as:

$$v_h = \sqrt{\frac{\text{Thrust of one propeller}}{2\rho\pi R^2}} \tag{11}$$

The parameter v_h has the dimensions of velocity and is known as the "thrust velocity" or the "hover induced velocity at the propeller disc". The behavior of any reverse-thrust propeller is determined

by the ratio V/v_h as shown in Table 1.

TABLE 1.

OPERATING STATES OF REVERSE-THRUST PROPELLERS

V/v_h	Operating State	Characteristics
0 to = 0.7	"Powered Descent"	Thrust fairly steady, propeller takes power from engine.
= 0.7 to = 1.5	"Vortex-Ring"	Thrust fluctuations occur, (as high as $\pm$ 30 percent of mean thrust). Takes power from engine.
= 1.5 to = 1.8	"Autorotative"	Thrust steady, propeller windmills with no power required from engine.
> = 1.8	"Windmill-Brake"	Thrust steady, propeller requires braking action from engine to maintain a given thrust.

The vortex-ring state is analyzed in Reference 1, where it is shown that the unsteady condition is caused by a breakdown in the protective sheath of vorticity which surrounds the slipstream. This vorticity takes up the shear velocity differential between the flow inside the slipstream and the free-stream flow. In the region $0.7 < V/v_h < 1.5$ a steady sheath of vorticity cannot be produced, and the slipstream forms, collapses, and reforms in a cyclic manner. These characteristics are only slightly dependent on the geometry of the particular propeller employed.

To see how this affects descent angle at a given speed, consider the example aircraft of Figure 4(a) at $C_L = 3$, V = 70 fps. A propeller diameter is 0.17 of the span is assumed. The power-off drag/lift ratio is 0.138, giving $\gamma = -\tan^{-1}(D/L) = -7.9$ degrees. The required drag increment to attain a steeper γ is $\Delta D/L = -\tan\gamma - 0.138$ where ΔD is to be supplied by the reverse thrust of two propellers.

Manipulating Eq. 11 yields

$$v_h = \sqrt{\frac{(\Delta D/L)\ (1/2)\rho V^2\ S\ C_L}{2(2\ \rho\ \pi R^2)}} \tag{12}$$

which simplifies to

$$\frac{v_h}{V} = \sqrt{\frac{(\Delta D/L)\ b^2\ C_L}{8\ \pi\ A\ R^2}} \tag{13}$$

Combining Eq. (13) with the data of Reference 1, summarized in Table 1, yields a method for assessing the feasibility of obtaining steep nominal flight paths through the use of reverse-thrust propellers. This is illustrated in Figure 5 for the example airplane. The descent angle can be increased from 7.9 degrees to 22 degrees without bringing the propeller into the vortex-ring state. This is a worthwhile improvement, especially considering the relatively minor airframe modifications required and the negligble weight penalty.

Little has been reported in the literature on this form of flight path control and it appears worthy of further investigation. This should include theoretical and wind-tunnel studies of the effects of the reversed propellers on buffet and tail effectiveness.

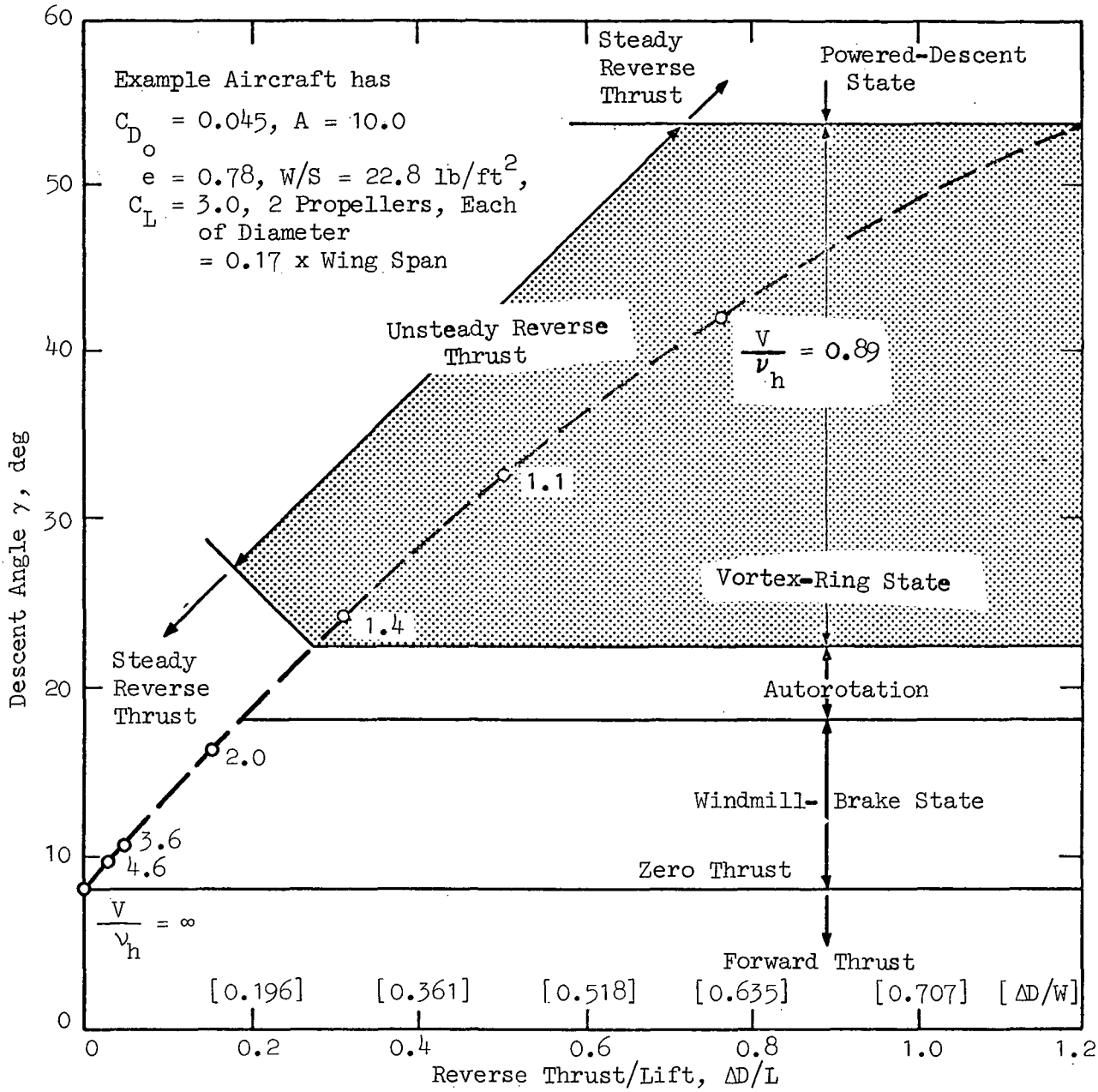

Figure 5. - Effect of Reverse-Thrust Propellers on Descent Angle of a Passive-Lift STOL Aircraft

Reverse thrust jet engines. - References 4 and 9 describe a method of drag augmentation in which a passive-lift STOL aircraft is fitted with two small jet engines located at the sides of the fuselage near the tail. These engines face "backwards" and provide thrust in the decelerating sense. The engines must be positioned carefully to avoid impingement of the jets on the wing with consequent loss of lift. However with proper engine location the wing lift actually increases, and the system was liked by pilots in simulator tests.

The weight penalty is about 1 lb per 8 lbs of thrust. Thus, for the example airplane of Figure 3 the descent could be steepened from 7.9 to 16 degrees at a cost of 1.8 percent of the gross weight. Typically this implies reducing the payload by about 8 percent.

Reference 4 states that the system was not incorporated in a production aircraft because of natural customer resistance to "mixed" powerplants. Weight and noise may also be objectionable. These factors appear to be the major disadvantages of this concept. There is no "v_h/V" limitation corresponding to the vortex-ring region for the reverse-thrust propeller because the jet engines need never be idled since the net thrust balance can be adjusted using both the jets and the propellers. Further, the system is applicable to "active-lift" types which depend on propeller slipstream for lift or control.

Apart from the short description in Reference 4 and 9 little has been published on this concept. It appears to merit further investigation. A systematic series of wind-tunnel tests should be performed to explore the effects of jet engine location. These tests should include flow vizualization to aid the optimum location of the reverse-thrust engines.

Tilt-rotor configurations. - The descent/deceleration limitations for tilt-rotor aircraft and "free-floating tilt-wing" configurations (as described in Reference 10) are similar to those for helicopters when expressed in terms of v_h. This parameter increases because of the higher disc-loading of these types, ranging from 5 lbs/ft^2 for the XV-3 to 25 lbs/ft^2 for the X-19A. Thus, in general, the boundaries on descent rate will be less stringent than for competitive helicopters. The boundaries are set by the vortex-ring state and by autorotation. Reference 1 presents a discussion of these boundaries for helicopters, which is also applicable to tilt-rotor aircraft. Hence only one typical result will be shown here.

Figure 6 shows boundaries for helicopter or tilt-rotor aircraft with a disc-loading of 6.2 lb/ft^2. The outer boundary of the vortex-ring state corresponds to r.m.s. mean-to-peak thrust fluctuations of 15 percent of the gross weight. The inner boundary corresponds to fluctuations of approximately double this intensity. To extend Figure 6 to other aircraft, the vortex-ring boundary may be scaled proportionately to the square root of disc loading. The autorotation boundary depends more critically upon the parasite drag and rotor profile drag, and should be calculated for each configuration.

Autorotation is commonly used in military operations and as a civil emergency procedure. The objections to autorotation as a standard procedure for routine I.L.S. approaches are as follows.

(1) To steepen the nominal flight path beyond the autorotation boundary (e.g., to cope with wind-shears) would require a braking action to be applied to the rotor. Such braking could, in principle, be provided by variable turbine inlet stators as used in some industrial gas turbines. However current FAA helicopter regulations preclude engine braking, as they require an override or free-wheel device to prevent stoppage of the rotor following engine failure.

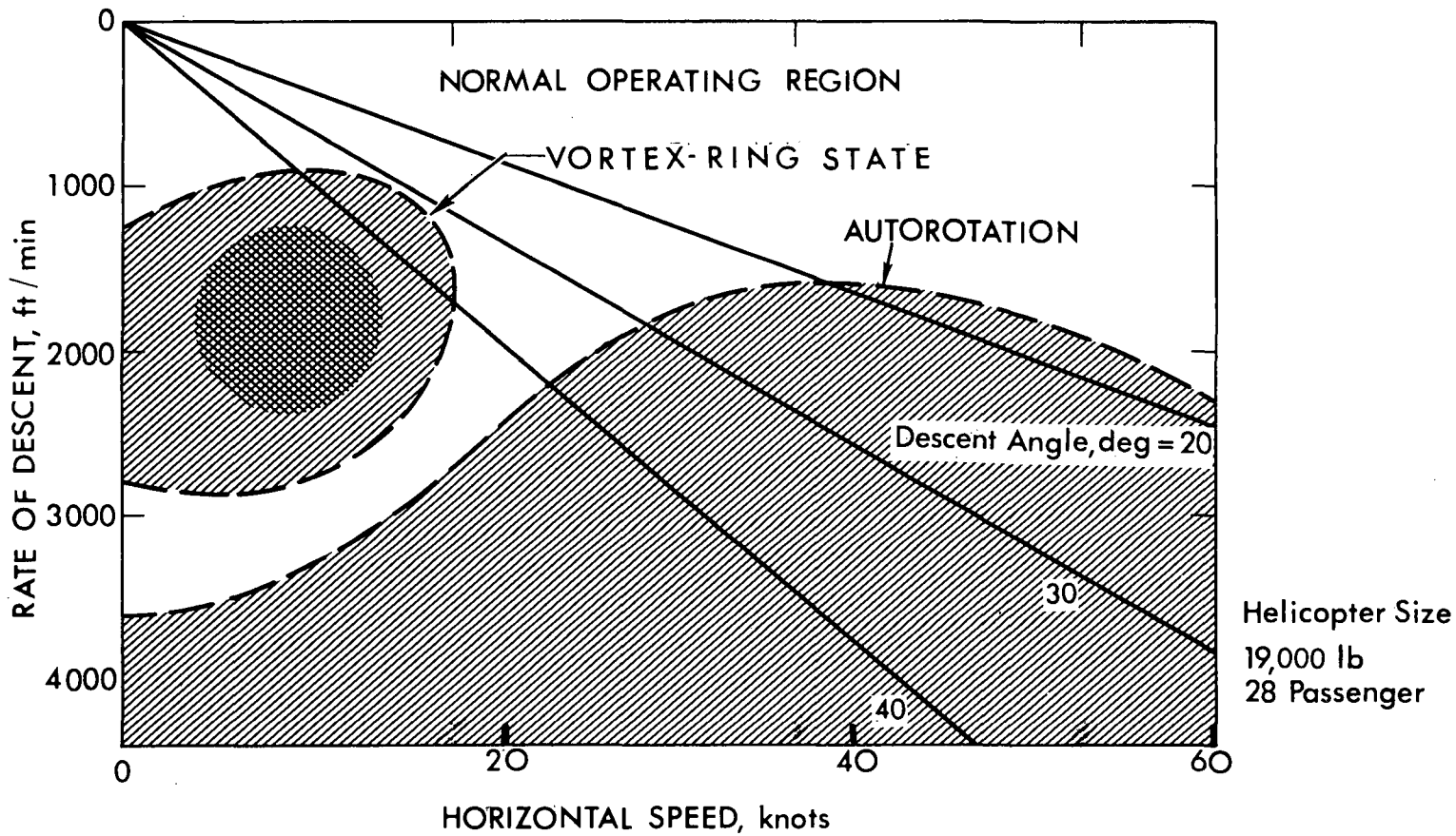

Figure 6. - Helicopter and Tilt-Rotor Descent Boundaries

(2) The rate of descent in autorotation may be too high to permit descent to be arrested following breakout from low cloud.

(3) At low speeds, recovery from autorotation to level flight may cause the aircraft to enter the vortex-ring state.

Slipstreamed-Wing Configurations

The term "slipstreamed-wing" is used to denote tilt-wing and deflected slipstream configurations.

Deflected slipstream and tilt-wing types both suffer severe limitations on their descent/deceleration capability. A simplified explanation of the cause of these limitations is given in Reference 11. This explanation is illustrated in Figure 7. By adding the free-stream and slipstream velocities vectorially the velocity vector at the wing can be deduced. If the inclination of this vector to the wing is too large the wing stalls, the onset of stall being marked by considerable buffeting. This stalled condition occurs when attempting steep descents.

Figure 7 suggests the possibility of predicting the max D/L of slipstreamed-wing aircraft from a knowledge of its power-off stall characteristics. This possibility is explored in Chapter III, where a theory is developed for calculating $(D/L)_{max}$ of slipstreamed-wing configurations.

Flight test results indicate that, although the condition for $(D/L)_{max}$ determines the maximum descent angle attainable at a given airspeed, this limit may not in fact be practical, because of requirements for maneuvering, go-around, control effectiveness, and control following engine failure. These considerations may dictate that descents shall be limited to angles less than those achievable from $(D/L)_{max}$

V_A AIRPLANE VELOCITY
V_S SLIPSTREAM VELOCITY
V_R RESULTANT VELOCITY OVER WING
α_W EFFECTIVE WING ANGLE OF ATTACK

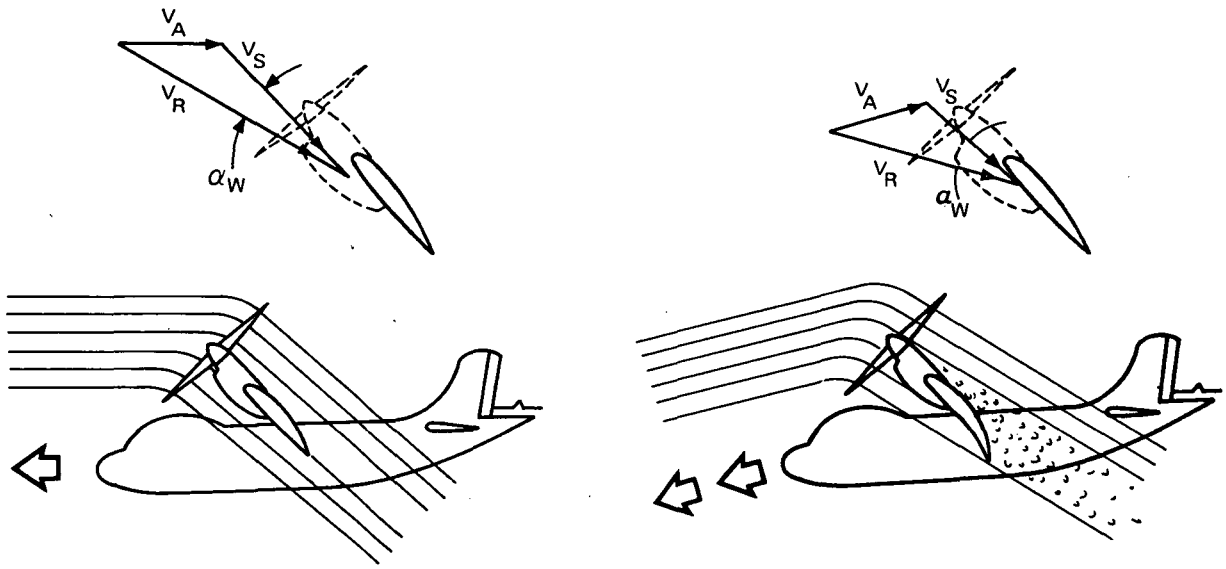

LEVEL FLIGHT—HIGH POWER
HIGH SLIPSTREAM VELOCITY
MODERATE WING ANGLE OF ATTACK
WING UNSTALLED

STEEP DESCENT – LOW POWER
LOW SLIPSTREAM VELOCITY
HIGH WING ANGLE OF ATTACK
WING STALLED

THE PROPELLER SLIPSTREAM CAN KEEP A PROPERLY DESIGNED WING FROM STALLING IN LEVEL TRANSITION FLIGHT, BUT THE STALLING PROBLEM BECOMES MORE SEVERE IN STEEP DESCENTS WITH LOW POWER.

Figure 7. - Explanation of Descent Boundaries for Tilt-Wing and Deflected Slipstream Configurations (from Ref. 11)

considerations alone. In the following section, descent characteristics of some typical slipstreamed-wing configurations are reviewed, and the relationships between boundaries based on $(D/L)_{max}$ and practical operational boundaries are indicated.

References 12 and 13 describe flight tests on the Breguet 941 deflected slipstream aircraft (also known as the McDonnell-Douglas 188), and Reference 14 presents similar data on the XC-142 tilt-wing aircraft. The measured descent boundaries for the Breguet 941 are shown in Figures 8 and 9, and for the XC-142A tilt-wing aircraft in Figure 10. Both these aircraft are highly developed "second-generation" representatives of their classes and considerable efforts have been made to give these aircraft good descent capabilities. Thus Figures 8, 9, and 10 illustrate the present state-of-the art in this area. A detailed discussion of the boundaries for each type now follows.

The following observations on Figures 8 and 9 apply to any deflected slipstream aircraft:

1. It is not possible to reduce thrust to zero at the lower velocities because slipstream is required to provide sufficient flow over control surfaces to maintain effective control.

2. The stall boundary is optimistic for two reasons: (1) some Δn_z must remain for maneuvering, and (2) minimum control effectiveness considerations may dictate higher speeds than stall speed.

3. From considerations of the altitude loss during the process of arresting a descent rate following "breakout" at 200 ft. ceilings, a maximum descent rate of 1000 f.p.m. is recommended in Reference 13 during the latter portions of the descent.

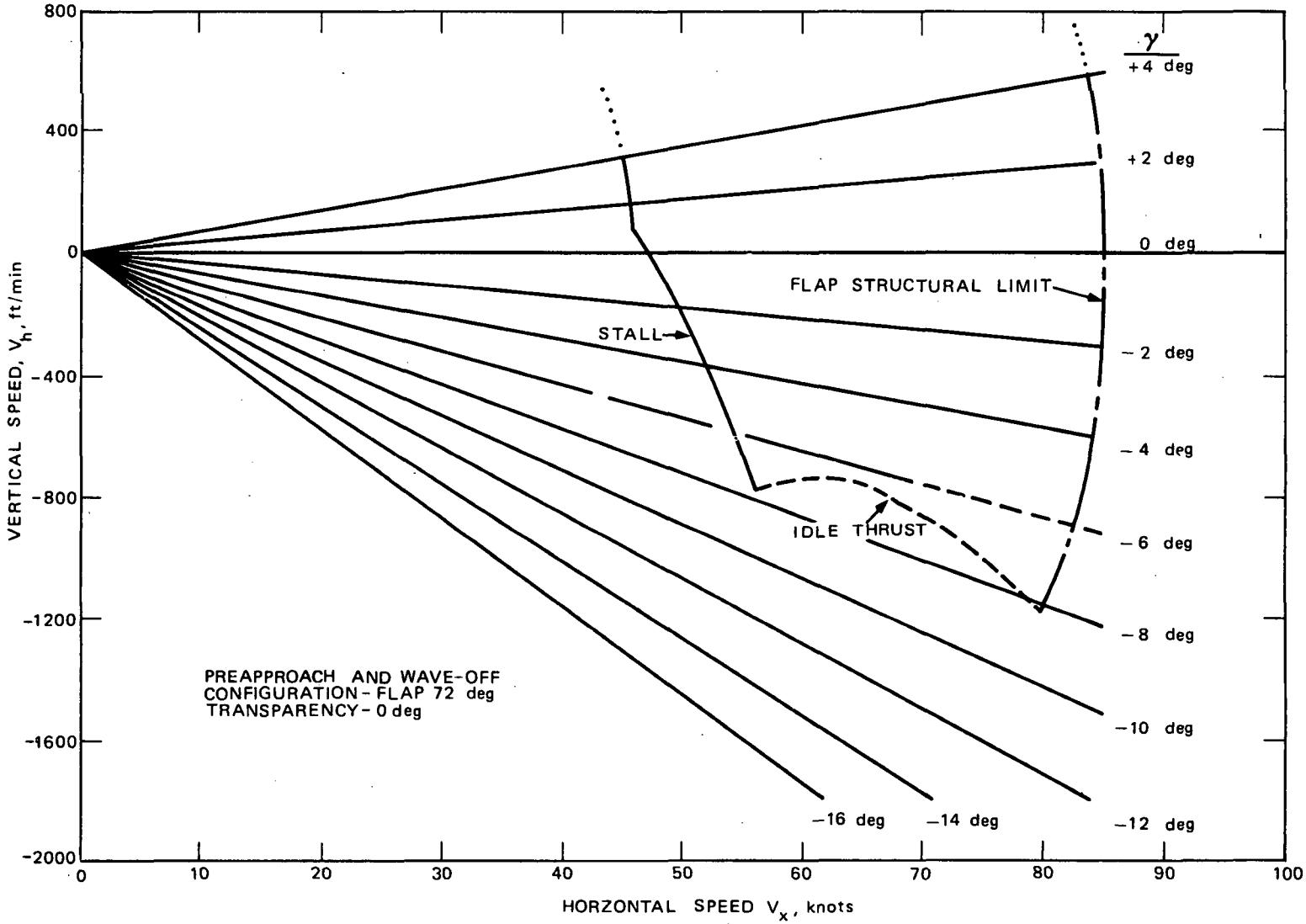

Figure 8. - Breguet 941/McDonnell Douglas 188 Flight Envelopes for Preapproach and Wave-Off Configuration

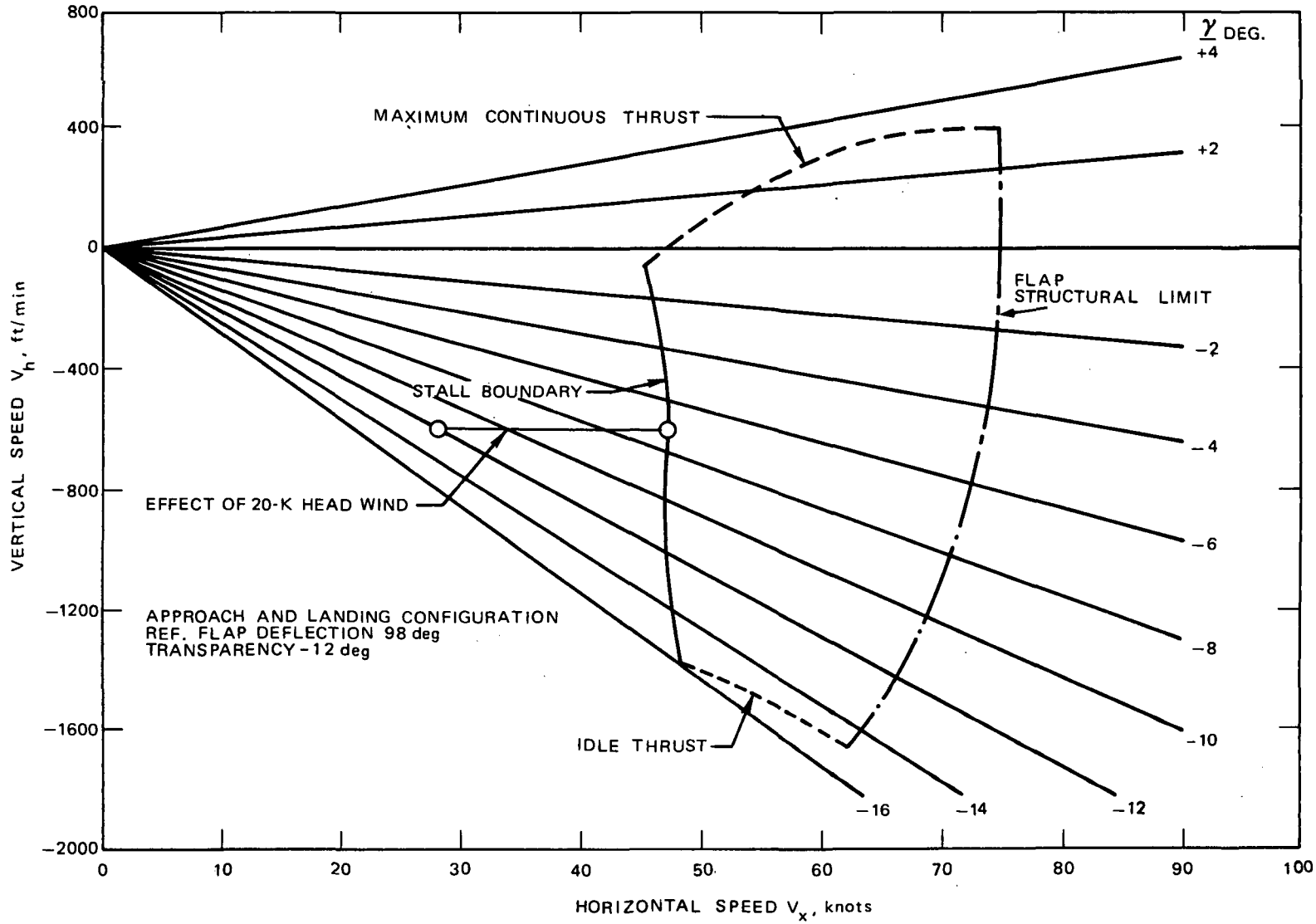

Figure 9. - Breguet 941/McDonnell Douglas 188 Flight Envelopes for Approach and Landing Configuration

As can be seen from Figure 8, this limits the maximum descent angle to less than 12 degrees at minimum speed, and to less than 8 degrees at the flap limit speed of 75 knots.

4. It is important to note that in the approach and landing configuration (98 degree flap) there is no wave-off capability (positive γ) should a single engine failure occur. This is not a desirable situation for commercial operation, nor is it permitted by FAA regulations. Therefore, it is necessary to use a "less draggy" configuration during approach or demonstrate that conversion to this state, following single engine failure, can be made sufficiently quickly that positive climb angles can be attained before the aircraft strikes the ground. The "pre-approach and wave-off" configuration of the Breguet 941 is shown in Figure 8 and corresponds to a reference flap setting of 72 degrees. This configuration permits single-engine climbs up to + 8 degrees. Thus, the wave-off requirement may dictate flap configurations which limit the descent angle to values considerably below the maximum capability of the vehicle.

Because of the considerable effort that has already been devoted to the "double-slotted flap and slat" wing system of the Breguet 941 and similar aircraft it is hard to discern any opportunity for significant increases in descent angle capability. However, fitting high power engines would improve the "wave-off" capability, thus permitting full benefit to be derived from the existing flap system.

The Breguet 941 has a capability called "transparency" whereby the inboard and outboard propeller blade angles can be varied independently, resulting in a warped lift distribution along the wing. This lift distribution is accompanied by higher induced drags. Thus, at a given airspeed, steeper descent angles are possible if transparency is used, as indicated by Figure 9. The limits of this technique are not presently known. However it might be possible to predict the effect of transparency on $(D/L)_{max}$ using the theory presented in Chapter III.

Tilt-wing descent boundaries. - For tilt-wing aircraft there exist two boundaries, as shown on Figure 10, corresponding to different types of buffet. High frequency, small amplitude, buffet occurs at the upper boundary. This is believed to be due to stalling of the tilted center-section of the wing which cannot be immersed in the slipstream of the four propellers. The buffet becomes more pronounced and of lower frequency as the lower boundary is approached. Military pilots state that the lower boundary is the practical limit to human tolerance for prolonged periods (Reference 14). For commercial passenger operation it is sensible to assume a more restrictive boundary. Note that despite a complete hover capability, and control of thrust vector rotation through 90 degree, descents along a 12 degree glide path at 50 knots are still impractical.

The theory of Chapter III relates the low frequency buffet boundary to the power-off stall characteristics of the wing, modified by the induced flow effects of the propellers. However these induced effects do not influence the portions of the wing not immersed in the slipstream. For example, Figure 10 shows that for the XC-142A at 30 knots, an 11 degree glide slope is attainable with 35 degrees of wing tilt. For a level fuselage condition, this means that the portions of the wing not immersed in the slipstream are experiencing local angles of attack of 11 + 35 = 46 degrees, well above the stall, with accompanying buffet.

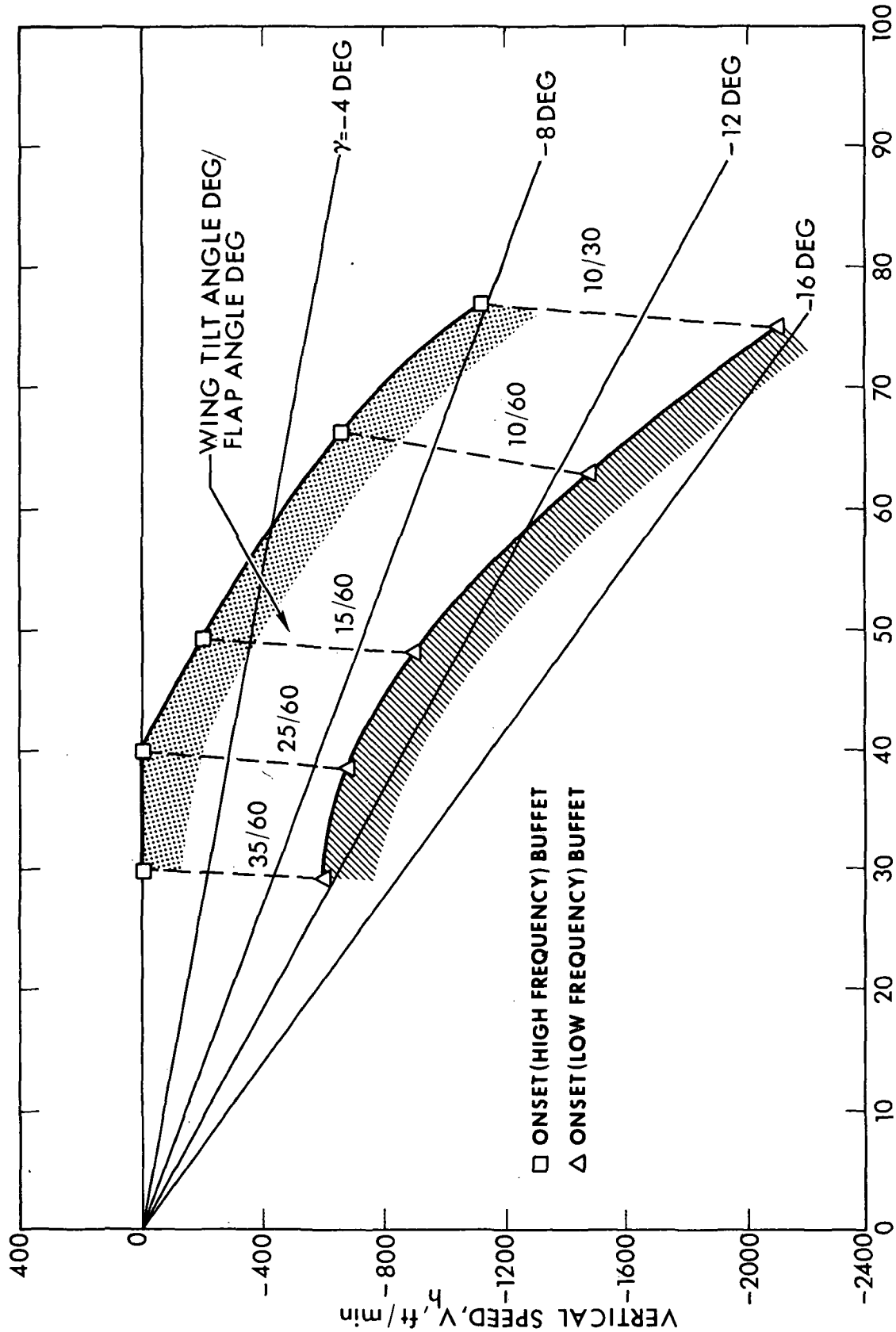

Figure 10. - XC-142A Buffet Boundaries

Some of the methods of obtaining steep descent for passive-lift aircraft are also applicable to tilt-wing and deflected slipstream aircraft. Again, dive-brakes are ineffective due to the low airspeed, and reverse-thrusting propellers do not appear to be compatible with the slipstreamed-wing concept. However, reverse jet engines may provide a feasible method of increasing descent capabilities, at the cost of a loss in payload to make up for the added engine weight.

Jet Lift and Ducted Fan V/STOL Aircraft

Ducted fan V/STOL aircraft such as the Bell X-22 and Doak VZ-4 experience limits on descent/deceleration capability due to flow separation around the lip of the duct. For the X-22 the phenomenon was noted (Reference 15) as the cause of "duct buzz", an unpleasant high-frequency vibration which permeated the entire aircraft. Little information is available on steep descent flight tests of the X-22 but from References 15 and 16 it appears that the descent angle may be limited to about 10 degrees at low speeds. More complete data is available on the Doak VZ-4 and Figure 11 (from Reference 17) shows the descent limits recorded in flight. Note that at 60 knots, the limiting angle of descent is only 6 degrees, beyond which severe buffet occurs.

Part of the buffet problem with the VZ-4 stems from its large wing which operates at an angle of attack, α, equal to the descent angle, $-\gamma$, when the fuselage altitude is level. Thus a moderate γ suffices to stall the wing, if the fuselage is kept approximately horizontal during descent.

Similar stall limitations to those discussed above apply to any vehicle in the portion of its flight regime where partially wing-supported flight is desired. For example, Reference 18 notes that XV-4B Hummingbird (a dual propulsion pure jet VTOL research aircraft) had many combinations of speed and descent angle which were unattainable

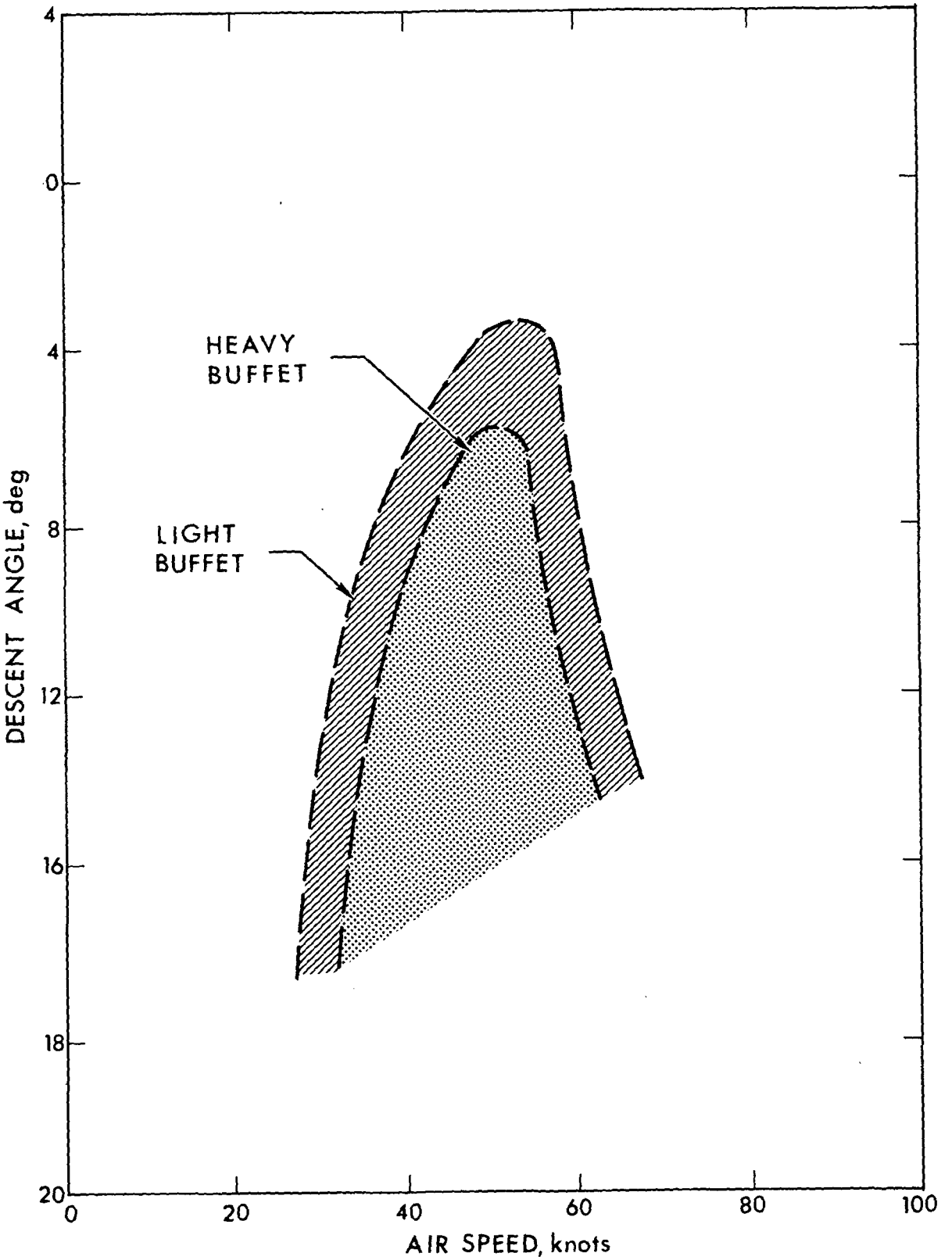

Figure 11. - Descent Boundaries for a Tilt-Duct Aircraft (DOAK VZ-4)

due to wing stall and/or buffet effects associated with flow separation over the wing at high angles of attack. Thus, despite the Hummingbird's hovering and high speed flight capabilities, it could not descend in equilibrium flight at 50 knots along a 12-degree glide slope.

Fan-in-wing aircraft such as the Ryan XV-5A also suffer from wing-stall limitations (Reference 19) and lip stall may also be severe because of the small duct lip radius imposed by the geometric constraints of the wing.

The prospects for improving descent boundaries for jet lift and ducted fan aircraft appear fairly good although they have yet to be demonstrated. Where wing stall is the culprit some increase of descent angle (assuming a level fuselage attitude) can be obtained by stall delaying devices such as slats and flaps. For some ducted fan configurations it may be possible to increase the duct inlet radius ("bell-mouth" effect) to delay lip separation. However, the phenomenon of flow separation for ducted fans is not well understood, and analytic prediction of descent capabilities appears to be beyond the current state-of-the-art.

Jet Flap and "Blown Flap" Aircraft

Under this heading we discuss descent limitations of two classes of STOL aircraft, both of which derive some of their lift through downward-directed jet sheets emanating near the wing trailing edge. The distinction between blown-flap and jet-flap types is one of degree. In the former, the jet extends over only a small fraction (e.g., 1/3) of the wing span, whereas the true jet-flap aircraft uses a full-span jet sheet, with approximately constant momentum per unit span.

Operationally, the blown flap is suited for "moderate STOL" where the $C_{L_{max}}$ requirements are easily achieved by a part-span jet

sheet with thrust/weight ratios about 0.3. The benefits of the increased C_L on descent angle are similar to the "passive-lift" example of Figure 4(a) with the added bonus that the non-uniform spanwise lift distribution decreases the induced drag efficiency factor e. For small thrust/weight ratios, the practical limits on descent capability may be set by wave-off requirements as discussed for the Breguet 941.

The jet flap is suited for "extreme STOL" where the maximum possible lift coefficient of the wing must be realized, and higher thrust/weight ratios can be afforded (e.g., T/W of about 0.6). Unfortunately, the jet flap suffers from a serious disadvantage as regards induced drag. Firstly, the uniform span-loading gives a high induced drag efficiency factor e, thus reducing C_{Di}. More important, the thin jet sheet tends to bend backwards parallel to the flight path considerably reducing the drag. This "thrust recovery" phenomenon (Reference 20) substantially reduces descent angle capability.

In summary, part-span blowing is a good way of extending the low speed capability of CTOL aircraft to yield "moderate" STOL performance. Full span blowing, as in the jet flap, gives lower air speed, but suffers from fundamental limits on descent capability. Probably the simplest way of overcoming these is through the use of reverse-jet engines as discussed previously.

Limitations on Climb-out Performance

The limitations on descent/deceleration capability discussed in the preceding sections are "fundamental" in that they cannot be alleviated merely by adding power. For example, adding power does nothing to improve the descent capabilities of a tilt-wing configuration, which are intrinsically limited by the stalling characteristics of the wing and the propeller diameter and location. By contrast, climb-out capability can always be improved by the addition of power. Climb

restrictions are thus of less importance to the present study and hence only a brief discussion is given below.

A steep climb angle at low air speeds is essential to V/STOL operation in urban environments. Helicopters, and other VTOL aircraft with thrust-to-weight ratios greater than unity plus the capability of vectoring that thrust vertically while maintaining a level fuselage, clearly have the greatest versatility in this respect. STOL aircraft on the other hand, especially passive-lift configurations, experience definite limits in maximum achievable angle of climb. For steady climbing flight;

$$\sin \gamma = T/W - D/W \tag{14}$$

where it is assumed that the thrust vector is essentially aligned with the flight path. For small γ, this expression differs from the expression for the glide descent angle (Eq. 1), by the positive term T/W. Thus, using the Twin-Otter example illustrated in Figure 5 , we can easily construct a similar maximum climb angle chart by simply adding the T/W increment. For example, for T/W = 0.5, we have:

$$\sin \gamma = 0.5 - \gamma \text{ descent} \tag{15}$$

Using Figure 3, for V = 100 fps, $C_L = 2$ and $\gamma_{descent} = -6$ degrees (-0.105 radians)

$$\gamma_{climb} = \sin^{-1} (0.5 - 0.105) = 22.7 \text{ degrees} \tag{16}$$

Reference 4, in reviewing the state-of-the-art for large passive-lift STOL's, suggests that climb angles in the order of 6 to 12 degrees are readily attained, while Reference 13 indicates that the Breguet 941 achieves 14 degrees in the take-off configuration. The certification

requirement for positive climb angles with one engine inoperative places severe demands on twin engine STOL aircraft. For the reasons explained above, this aspect of STOL nominal flight path capability falls beyond the scope of this report. However, it is important as a practical operational consideration.

Limitations on Constant-Acceleration Flight Paths in the Vertical Plane

Considering flight in the vertical plane, it can be shown that the rate of change of the flight path angle is given by

$$\frac{d\gamma}{dt} = (n_z - \cos\gamma)\frac{g}{V_I} \tag{17}$$

where n_z is the normal acceleration capability (load factor) of the aircraft, ($n_z = L/W$), and V_I is the inertial speed. The geometry of landing and take-off flare maneuvers is determined by $\frac{d\gamma}{dx}$, where x is the horizontal coordinate. Substituting $dx/dt = V_I \cos\gamma$ in Eq. (17), gives:

$$\frac{d\gamma}{dx} = \left(\frac{n_z}{\cos\gamma} - 1\right)\frac{g}{(V_I)^2} \tag{18}$$

The $1/V_I^2$ factor in Eq. (18) indicates that, for a given n_z, a STOL aircraft can obtain much more curvature of the flight path than its CTOL counterpart. For a given V_I, the maximum curvature of the flight path is determined by $n_{z\ max}$, which in turn is limited by one or more of the following considerations.

(1) stalling of lifting surfaces

(2) structural load limits

(3) limited normal force generation capability due to factors other than stall

(4) passenger comfort

Each of these factors will now be discussed.

Stalling of Lifting Surfaces: For passive-lift aircraft a typical approach speed is 1.3 V_s, giving $n_{z\ max} = 1.69$. Thus, from Eq. (18), at an approach speed of 80 knots the flare curvature is restricted to 7 degrees per 100 feet. This is quite a mild restriction. It implies that a flare from a 15 degree approach would require 1.69 g's to be held at 200 feet from the touchdown point, at a height of approximately 25 feet.

Structural Load Limits: These are typically + 3g, and -1g for large commercial aircraft, and are less restrictive than the other considerations discussed here for determining nominal flight paths.

Normal Force Generation Capability: For VTOL aircraft in very low speed flight at maximum design gross weight, the n_z is typically limited to 1.2 g, due to installed power limitations. This does not greatly restrict the curvature of the nominal flight path (determined from Eq. 18) because very low values of V_I can be obtained.

Passenger Comfort: There is a dearth of reliable data on the 'g' tolerance of the average fare-paying passenger. For some passengers the threshold of discomfort is approached during the landing roll of a large commercial jet. This involves deceleration from 110 knots to 40 knots in approximately 3000 feet, corresponding to a mean deceleration of 0.16 'g' over a period of 22 seconds. It is probable that a similar deceleration occuring in flight would be objectionable, due to the added effects of buffeting and gusts. In addition, psychological factors associated with fear of flying and loss of visual reference to the ground may further reduce passenger 'g' tolerance. Tentatively,

based on the author's experience, we suggest that maneuvers should be such that the acceleration experienced by any passenger are less than 1.0 incremental 'g' in the "eyeballs down" sense, and 0.5 'g' in all other directions.

Limitations on Lateral Curvature of the Flight Path

A given load factor capability, n_z, can be used to produce curvature of the flight path in the horizontal plane by banking the aircraft. For a given n_z, with γ small, so that $\cos \gamma = 1$, the horizontal and vertical accelerations can be traded according to the following equation.

$$g\, n_z = \left[(\dot{Vx})^2 + (g + V\dot{\gamma})^2 \right]^{1/2} \tag{19}$$

The required bank angle is given by

$$\cot \phi = \frac{g + V\dot{\gamma}}{\dot{Vx}} \tag{20}$$

These relationships are graphed on Figure 12, which demonstrates that the extra n_z required to maneuver laterally is quite small. Thus V/STOL aircraft can maneuver laterally without sacrificing much $\dot{\gamma}$ capability. This facilitates sidestep maneuvers required to align the aircraft with the runway following breakout from cloud. For a given sidestep flight path, the excess 'g' required is generally small for V/STOL aircraft because of the lower speed.

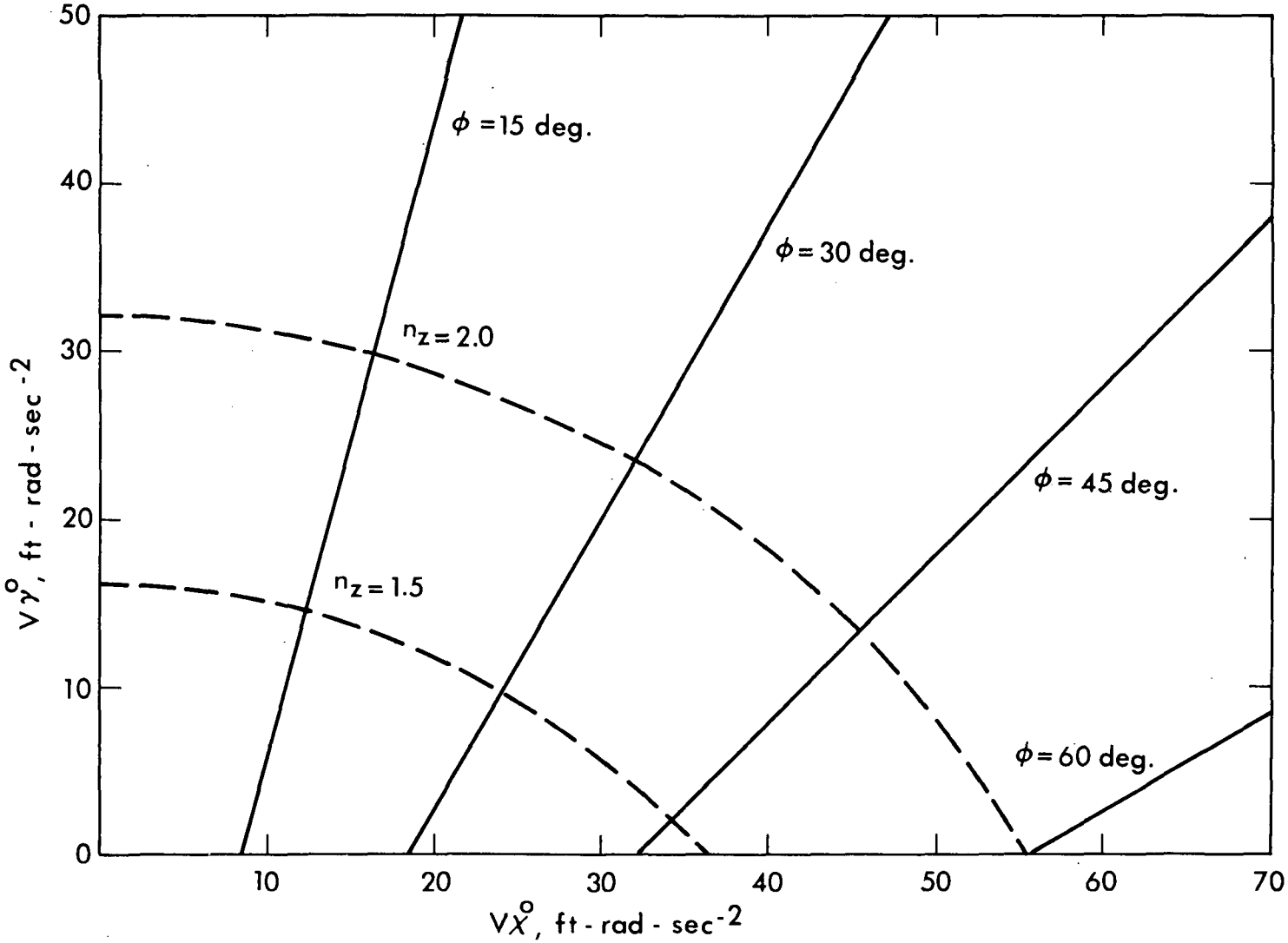

Figure 12. - Trade-off Between Horizontal and Vertical Acceleration for a Given Total Normal Acceleration Capability

CHAPTER III

ANALYTIC PREDICTION OF DESCENT BOUNDARIES FOR TILT-WING AND DEFLECTED SLIPSTREAM AIRCRAFT

Introduction

Considerable experimental evidence exists to show that the descent boundary of tilt-wing and deflected slipstream aircraft is associated with wing stalling. The mechanism whereby stalling sets a limit on $(D/L)_{max}$ is indicated in Figure 7, and there have been numerous qualitative descriptions of this phenomenon. It therefore seems plausible that the $(D/L)_{max}$ boundary of a general slipstreamed-wing configuration could be calculated from a knowledge of the power-off stall characteristics of the wing. This chapter describes a new method for calculating the lift and drag of a general wing-propeller combination. It is shown that the observed descent boundaries can be predicted with fair accuracy. The method requires data on the power-off characteristics of the wing, and uses momentum theory to correct these characteristics for power-induced effects. In this chapter, the method is used only to calculate the $(D/L)_{max}$ boundary of the XC-142A. In subsequent chapters, the method is applied to calculate stability derivatives for the CL-84 tilt-wing aircraft in level and descending flight. For the XC-142A, wind-tunnel model results were used as the source of power-off data. The predicted boundaries are of the same general form as the experimental boundaries observed in model and full scale tests, but give a limiting descent angle which at a given forward speed is about 8 degrees shallower than that obtained in full-scale flight tests. The discrepancy can be removed by introducing an arbitrary scale effect correction, increasing the angle of attack for power-off stall by 10 degrees to correct model results to full-scale. This scale correction is believed to be valid and reasonable, but cannot be fully justified until full-scale power-off data become available.

The predicted boundaries are very sensitive to the power-off stall characteristics, which in turn depend critically upon Reynolds number and wind-tunnel wall interference. This sensitivity limits the usefulness of the method for prediction of descent boundaries; however, it reflects important physical factors, and emphasizes the value of stall-delaying devices such as slats and slotted flaps, or boundary-layer control. Because of the sensitivity to stall effects, the theory is probably most useful as a basis for comparative (rather than absolute) predictions. It provides a method for assessing the relative effectiveness of alternative stall-delaying devices. The fact that theory predicts the correct general shape of the boundaries confirms the value of simple momentum concepts in the analysis of the complex flows around slipstreamed wings.

Description of the Method

The technical approach is generally similar to that employed by Kuhn (Reference 21). There are, nowever, numerous differences between details of Kuhn's method and the method presented here. These differences will be noted as they arise in the discussion. In both methods, the lift and drag of the wing are computed as the sum of two parts.

(1) The 'outer' flow: a part due to deflection of the free-stream by the wing. The mass flow that is deflected is assumed to $\rho \frac{\pi}{4} V_\infty \left[b^2 - N(D^2) \right]$, where V_∞ = free-stream velocity, ρ = density, b = wingspan, N = number of propellers, and D = diameter.*

---

* Kuhn chooses an 'outer' mass flow equal to $\rho \frac{\pi}{4} V \left[b^2 - N(D_s)^2 \right]$ where D_s is the diameter of the fully-developed slipstream. For most flight conditions of practical interest, the difference in the total lift and drag due to replacing D by D_s is slight. Neither choice is rigorous, and using D leads to much simpler mathematical expressions.

(2) The 'inner' flow: a part due to deflection of the slipstreams by the wing. This flow is assumed to be deflected parallel to the section zero lift-line.*

To compute the 'inner' flow, the slipstream mean airspeed at the wing must be known. This is derived using momentum theory, as explained below. Note that it is not assumed that the slipstream is parallel to the propeller axis, except at zero forward speed, or when the propeller axis is parallel to the direction of flight, as in cruise.**

Computation of Isolated Propeller Net Thrust, Gross Thrust, and Normal Force

Inviscid incompressible flow is assumed, with the fully developed slipstream static pressure equal to the free-stream static pressure. As shown in Figure 13, the mean induced velocity at the propeller disc, V_i, is assumed to be parallel to the shaft axis. The mean induced velocity in the fully developed slipstream is assumed to be $2V_i$, in the same direction. The resultant velocities at the disc and in the fully developed slipstream are obtained by summing the free-stream and the appropriate induced velocities, as indicated in Figure 13.

---

* This assumption has been verified by plotting flow deflection data from several tests on wing-propeller-flap combinations at zero forward speed. Kuhn assumed that this "static" flow deflection angle, θ, remains unchanged with forward speed; however, he did not correlate θ with the angle between the propeller axis and the zero lift-line, θ_{ZLL}.

** This is another point of difference between the present theory and that of Kuhn, in which it is assumed that the slipstream is always parallel to the propeller shaft.

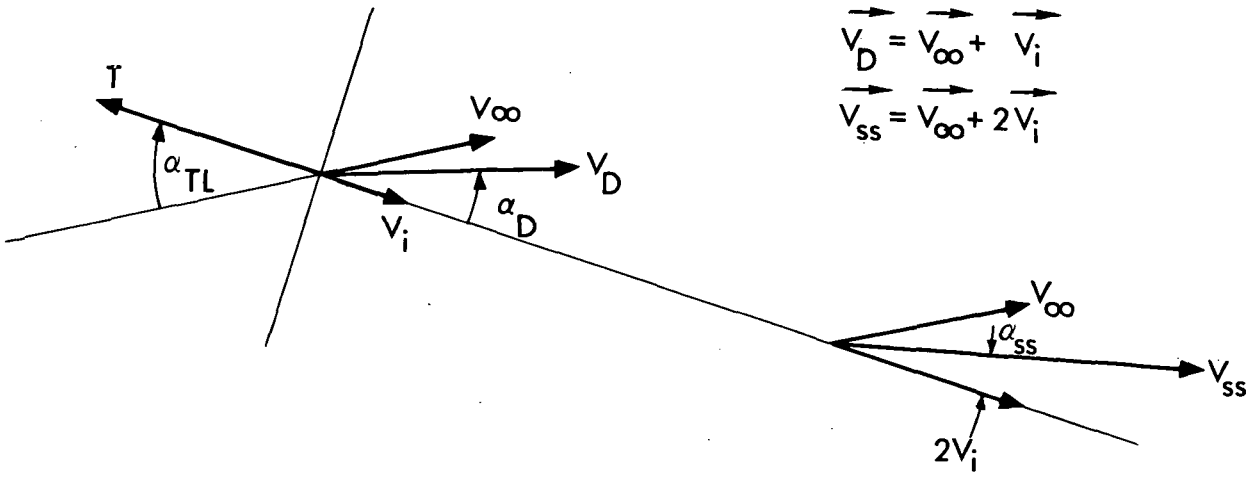

Figure 13. - Induced Velocities and Total Velocities in the Slipstream

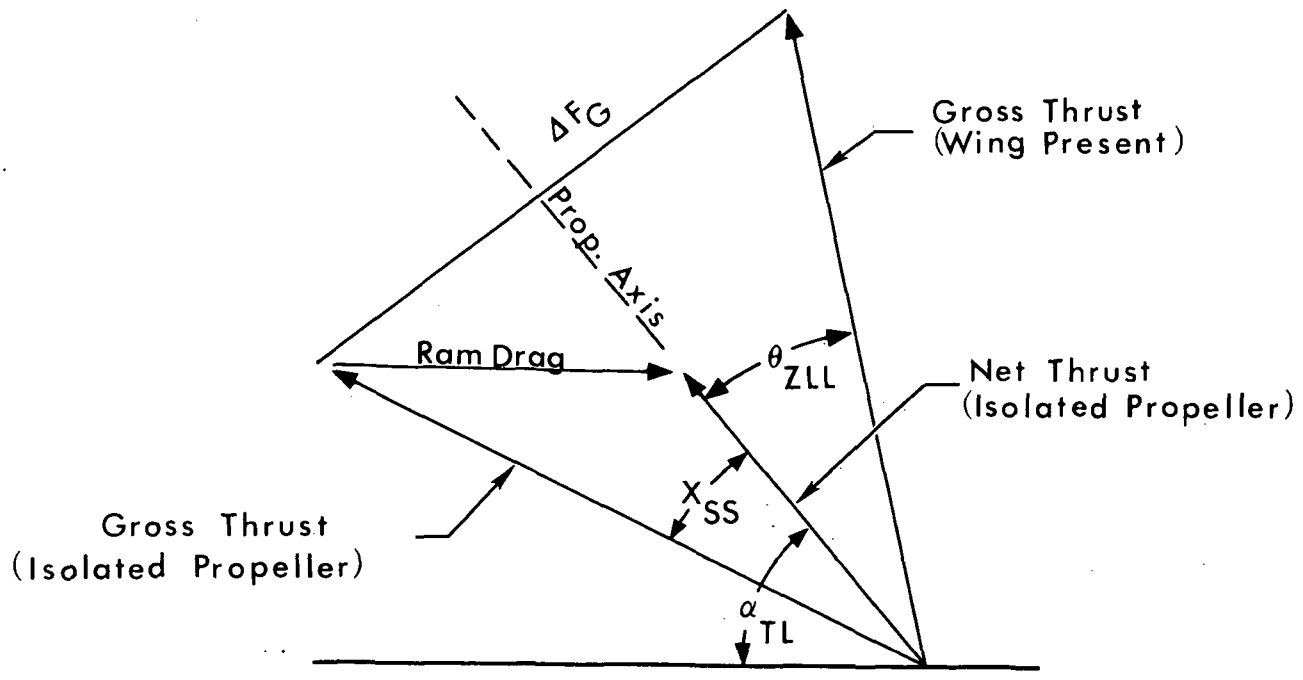

Figure 14. - Propeller-Wing-Slipstream Force Vectors at Forward Speed

The foregoing assumptions are standard in the momentum theory of propellers. It is also assumed that the mass flow through the propeller is proportional to the local resultant velocity $\vec{V}_D = \vec{V}_i + \vec{V}_\infty$, and an area equal to $S_p \cos \alpha_D$, where α_D is the angle of V_D to the shaft axis, i.e.:

$$\text{Mass Flow} = \rho V_D S_p \cos \alpha_D \tag{21}$$

This assumption is different from the standard assumption of momentum theory which replaces the above "area of capture" $S_p \cos \alpha_D$ by S_p. However, it has been found that Eq. (21) gives better agreement with experiment.*

From Figure 13 and Eq. (21), the thrust, T, is given by

$$T = \rho S_p \cos \alpha_D V_D 2V_i = \rho S_p 2V_i (V_i + V_\infty \cos \alpha_{TL}) \tag{22}$$

Defining a thrust coefficient $T_c = 2T/\rho V_\infty^2 S_p$, and manipulating Eq. (22), yields the following relationship for induced velocity, as a function of thrust coefficient, and of the inclination of the thrust line to the free stream, α_{TL}.

$$\frac{V_i}{V_\infty} = (1/2)\left[(\cos^2 \alpha_{TL} + T_c)^{1/2} - \cos \alpha_{TL}\right] \tag{23}$$

The inclination of the fully developed slipstream to the free-stream, α_{ss}, is given from Figure 13 as

$$\tan \alpha_{ss} = \frac{V_\infty \sin \alpha_{TL}}{V_\infty \cos \alpha_{TL} + 2V_i} \tag{24}$$

---

* The choice of the area of capture is arbitrary, as long as momentum-type theory is employed. Kuhn (Reference 21) used Sp as the area of capture, but did not correct for the inclination of the slipstream from the shaft axis.

It is convenient to rewrite Eq. (24) in terms of T_c, using Eq. (23).

$$\tan \alpha_{ss} = \frac{\sin \alpha_{TL}}{(T_c + \cos^2 \alpha_{TL})^{1/2}} \tag{25}$$

Eq. (25) provides the basis for calculating the lift and drag developed by the portions of the wing which are immersed in the slipstream as described in the next subsection.

In calculating the descent boundaries, the propeller normal force (i.e., the force normal to the shaft axis) was assumed negligible. The validity of this assumption was checked during the subsequent calculations of stability derivatives, described in Chapter IV. In general, it appears that propeller normal force will not be a significant fraction of the thrust during low speed level flight and descending conditions.

For purposes of computing the forces on the wing, the isolated propeller gross thrust is required. This is defined as the vector sum of the net thrust and the reversed ram drag (See Figure 14). The magnitude of the ram drag is simply mV_∞, where m is the mass flow. Resolving the ram drag into components normal and parallel to the propeller shaft yields a convenient expression for the magnitude of the gross thrust, F_g, as indicated below.

$$\left|F_g\right| = \left[(T + mV_\infty \cos \alpha_{TL})^2 + (mV_\infty \sin \alpha_{TL})^2\right]^{1/2} \tag{26}$$

$$= mV_\infty \left[\left(\frac{T}{mV_\infty}\right)^2 + 2 \left(\frac{T}{mV_\infty}\right) \cos \alpha_{TL} + 1\right]^{1/2} \tag{27}$$

$$= mV_\infty \left[\left(\frac{2V_i}{V_\infty}\right)^2 + 2 \left(\frac{V_i}{V_\infty}\right)^2 + 1 \right]^{1/2} \tag{28}$$

Combining Eq. (22) and Eq. (28) yields the following simple result:

$$\left|F_g\right| = mV_\infty \left[T_c + 1\right]^{1/2} \tag{29}$$

The inclination of the gross thrust to the propeller axis is given from Eq. (29) and Figure 14 as

$$\tan \chi_{ss} = \frac{\sin \alpha_{TL}}{(T_c + \cos^2 \alpha_{TL})^{1/2}} \tag{30}$$

Computation of Wing Forces

It is assumed that the portion of the wing immersed in the slipstream produces lift and drag solely by turning the total 'inner' slipstream mass flow and does not influence the lift and drag associated with the 'outer' flow. This assumption implies a flow model in which the protective sheath of vorticity surrounding the slipstream isolates the velocities inside the slipstream from those outside. This is physically plausible, and corresponds to an assumption usually made in analyses of propeller and helicopter rotor wakes, where it is shown that the assumed distributions of shed vorticity are such that no velocities are induced outside the wakes. A consequence of this assumption is that the flow model for downwash behind a slipstreamed-wing is non-uniform.

The gross thrust is assumed to be rotated through an angle $\chi_{ss} + \theta_{ZLL}$. The angle χ_{ss} is determined from Eq. (24), and θ_{ZLL} can be found either from standard airfoil data or power-on tests at zero forward speed, as explained below.

It is convenient to express θ_{ZLL} in terms of quantities illustrated in Figures 14 and 15, as:

$$\theta_{ZLL} = \left(\frac{\partial \alpha_{OL}}{\partial \delta_F}\right) \delta_F - \left(i_{TL} + \alpha_{OL}\right) \tag{31}$$

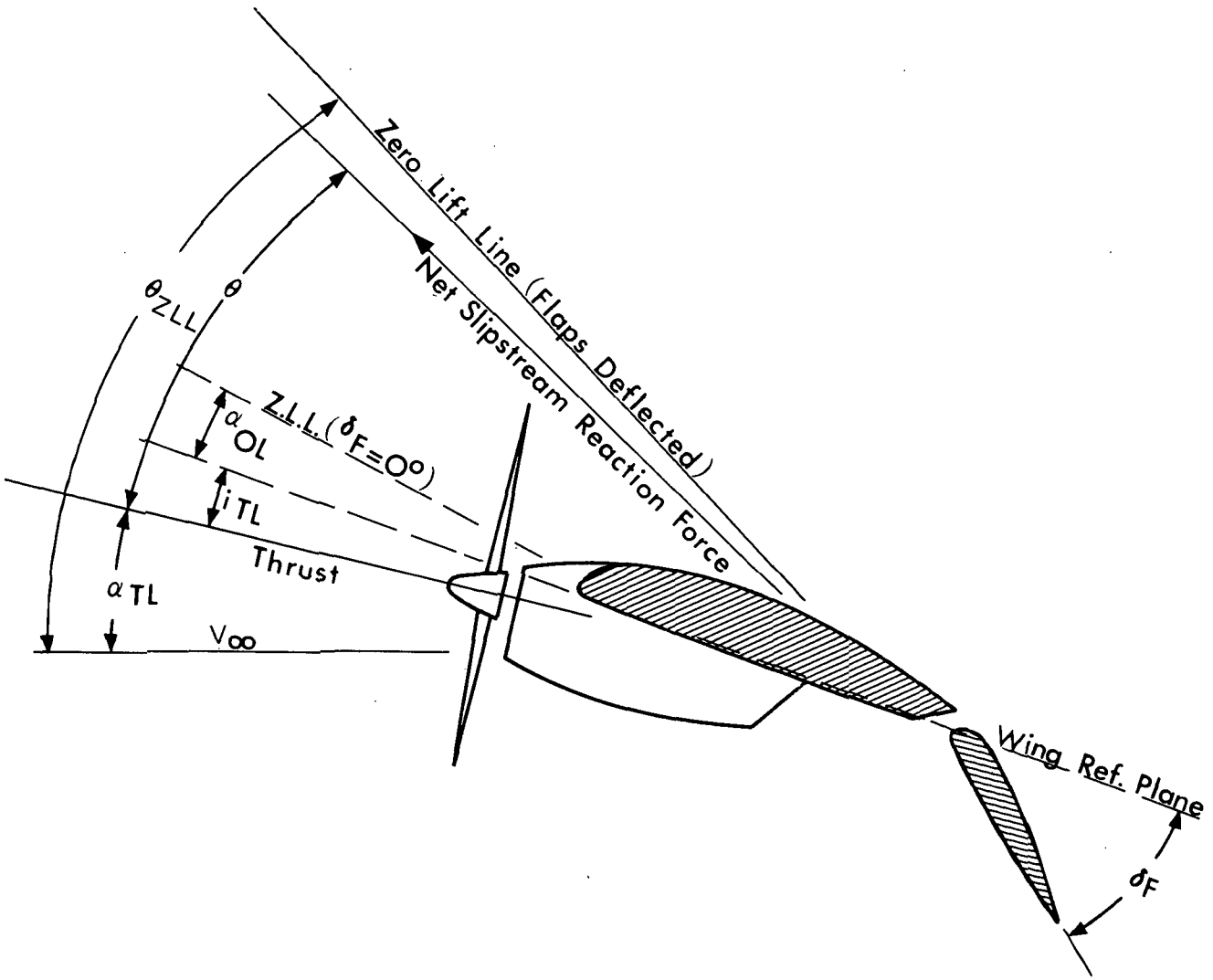

Figure 15. - Angular Relationships of Wing-Propeller Configuration and Slipstream Reaction Forces (Static Case)

The angle $(i_{TL} + \alpha_{OL})$ represents the incidence of the zero-lift line to the shaft axis, at zero flap deflection. By the usual convention, i_{TL} and α_{OL} are negative for the typical arrangement shown in Figure 15. It has been found empirically that, for typical chord/diameter ratios, the flow turning angle at zero forward speed, θ, can be closely approximated by the angle θ_{ZLL} as determined from power-off tests. The theory presented here assumes that the slipstream is turned parallel to the zero lift line at all flight conditions, from hover to cruise.

To obtain the lift and drag due to the slipstream-wing interaction, the initial gross thrust and the final gross thrust are resolved with components normal and parallel to the free-stream direction and the appropriate components are subtracted. Figure 16 shows the required geometric relationships. The result is:

$$L_{FG} = F_G \left[k_1 \sin (\alpha_{TL} + \theta_{ZLL}) - \sin (\alpha_{TL} - \alpha_{ss}) \right] \qquad (32)$$

$$D_{FG} = F_G \left[-k_1 \cos (\alpha_{TL} + \theta_{ZLL}) + \cos (\alpha_{TL} - \alpha_{ss}) \right] \qquad (33)$$

The factor k_1 allows for turning losses in F_G. These have been observed in power-on tests at zero forward speed, where it is found that for extreme flap deflections the resultant force is approximately 90% of the isolated propeller thrust.

Eqs. (32) and (33) express the portion of the wing lift and drag due to the flow within the slipstream. The flow outside the slipstream provides a lift and drag which can be estimated by standard methods for power-off conditions; however, a correction factor must be applied to allow for the part of the total power-off lift and drag that is included in Eqs. (32) and (33), since these equations do not equal zero for zero thrust (because $F_G \neq 0$ for $T = 0$).

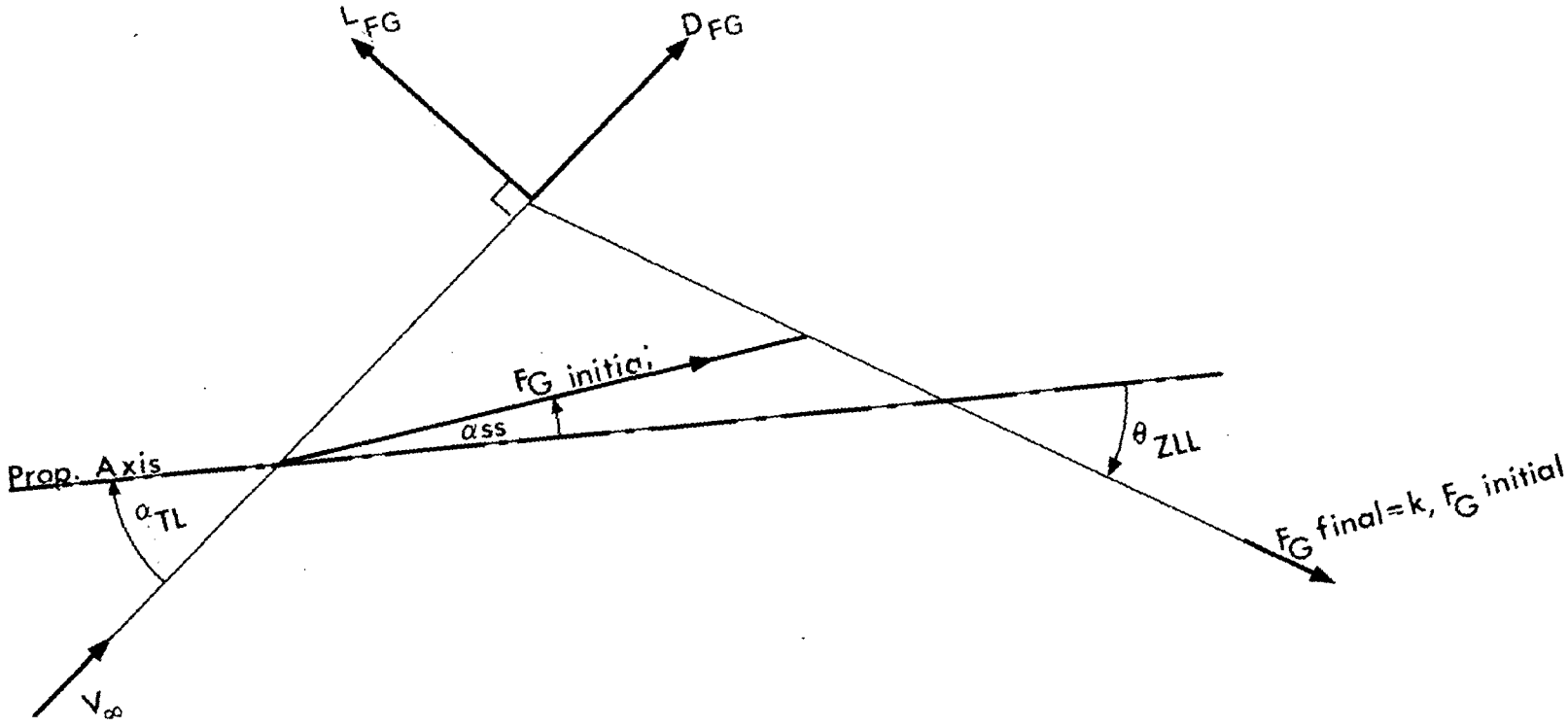

Figure 16. - Initial and Final Gross Thrust Vectors

The correction factor is:

$$1 - \frac{\text{total disc area}}{\frac{\pi}{4} \times (\text{effective span})^2}$$

The effective span is the span of an elliptic wing having the same lift and induced drag as the actual wing, i.e., $b\sqrt{e}$, where b is the actual span and e is the span-efficiency factor. Applying this correction yields

$$L_{\substack{\text{outer} \\ \text{flow}}} = 1/2\ \rho\ V^2 S\left[1 - \frac{N}{e}\left(\frac{D}{b}\right)^2\right] C_{L_{\text{power-off}}} \tag{34}$$

$$D_{\substack{\text{outer} \\ \text{flow}}} = 1/2\ \rho\ V^2 S\left[1 - \frac{N}{e}\left(\frac{D}{b}\right)^2\right] C_{Di\ \text{power-off}}$$

$$+ 1/2\ \rho\ V^2 S C_{D_{o\ \text{power-off}}} \tag{35}$$

Note that the induced drag is subject to the interference correction factor, whereas the profile drag is not, since the total wetted area is relevant for C_{D_o}. In Eqs. (34) and (35), the power-off coefficients may be estimated by standard 'handbook' methods or directly from power-off wind-tunnel tests.

Computation of Total Lift and Drag

The contribution of the propeller thrust to the total lift and drag is

$$L_T = T \sin \alpha_{TL} \tag{36}$$

$$D_T = -T \cos \alpha_{TL} \tag{37}$$

The total lift and drag can be written by summing Eqs. (36), (34), and (32), and Eqs. (37), (35), and (33), thus:

$$L = F_G \left[k_1 \sin(\alpha_{TL} + \theta_{ZLL}) - \sin(\alpha_{TL} - \alpha_{ss})\right]$$

$$+ 1/2\ \rho\ V^2 S\left[1 - \frac{N}{e}\left(\frac{D}{b}\right)^2\right] C_{L_{\text{power-off}}}$$

$$+ T \sin \alpha_{TL} \qquad (38)$$

$$D = F_G \left[-k_1 \cos\ (\alpha_{TL} + \theta_{ZLL}) + \cos\ (\alpha_{TL} - \alpha_{ss})\right]$$

$$+ 1/2\ \rho\ V^2 S \left[1 - \frac{N}{e}\left(\frac{D}{b}\right)^2\right] C_{D_{i\ \text{power-off}}}$$

$$+ 1/2\ \rho\ V^2 S\ C_{D_{o\ \text{power-off}}} - T \cos\alpha_{TL} \qquad (39)$$

To solve these equations for a given T and α_{TL}, use Eq. (22) to determine V_i, solve Eq. (24) for α_{ss}, determine $\overrightarrow{V_D}$ as $\overrightarrow{V_\infty} + \overrightarrow{V_i}$, solve Eq. (21) for m, then solve Eq. (28) for F_G and substitute α_{ss}, and F_G in Eqs. (38) and (39). The remaining quantities can be estimated from standard aerodynamic handbooks or other appropriate data sources.

Correlation with Experiment within the Unstalled Region

The lift and drag equations given above have been checked against widely different configurations with good correlation. Examples of correlation with the experimental data of Reference 22 are shown in Figure 17(a) and 17(b). The airfoils used were symmetrical with double plain flaps. Figures 17(a) and 17(b) show results obtained with the rear flap deflected 30 degrees. Figure 17(a) and 17(b) indicate that the theory predicts the lift and drag with good accuracy in the unstalled region. Further verification of the accuracy of the theory is given in Chapter IV, where calculated stability derivatives for the CL-84 tilt-wing aircraft are shown to give fair agreement with flight test results.

Estimated buffet boundaries may be compared to buffet indications in the experimental data. The estimated buffet boundaries in Figures 17(a) and 17(b) were obtained by using $\alpha_{stall} - \alpha_{oL}$ (as indicated by the power-off data for the configuration) as the value of χ_{ss} and solving for T_c versus α_{TL}. To be consistent with the notation of Reference 22, the data are presented in terms of $T_c'' (=2T/\rho V_{ss}^2 S_p)$, in Figures 17(a) and 17(b).

Calculation of Descent Boundaries for the XC-142A

This section applies the theory developed in the preceding sections to calculate the limiting angle of descent of the XC-142A tilt-wing aircraft at air speeds from 30 to 80 knots. As explained in Chapter I, the problem is equivalent to predicting $(D/L)_{max.}$ The general procedure is described below; the aerodynamic and geometric data used for the XC-142A are then summarized, and finally the calculated descent boundary is compared with boundaries obtained from wind-tunnel and flight test results.

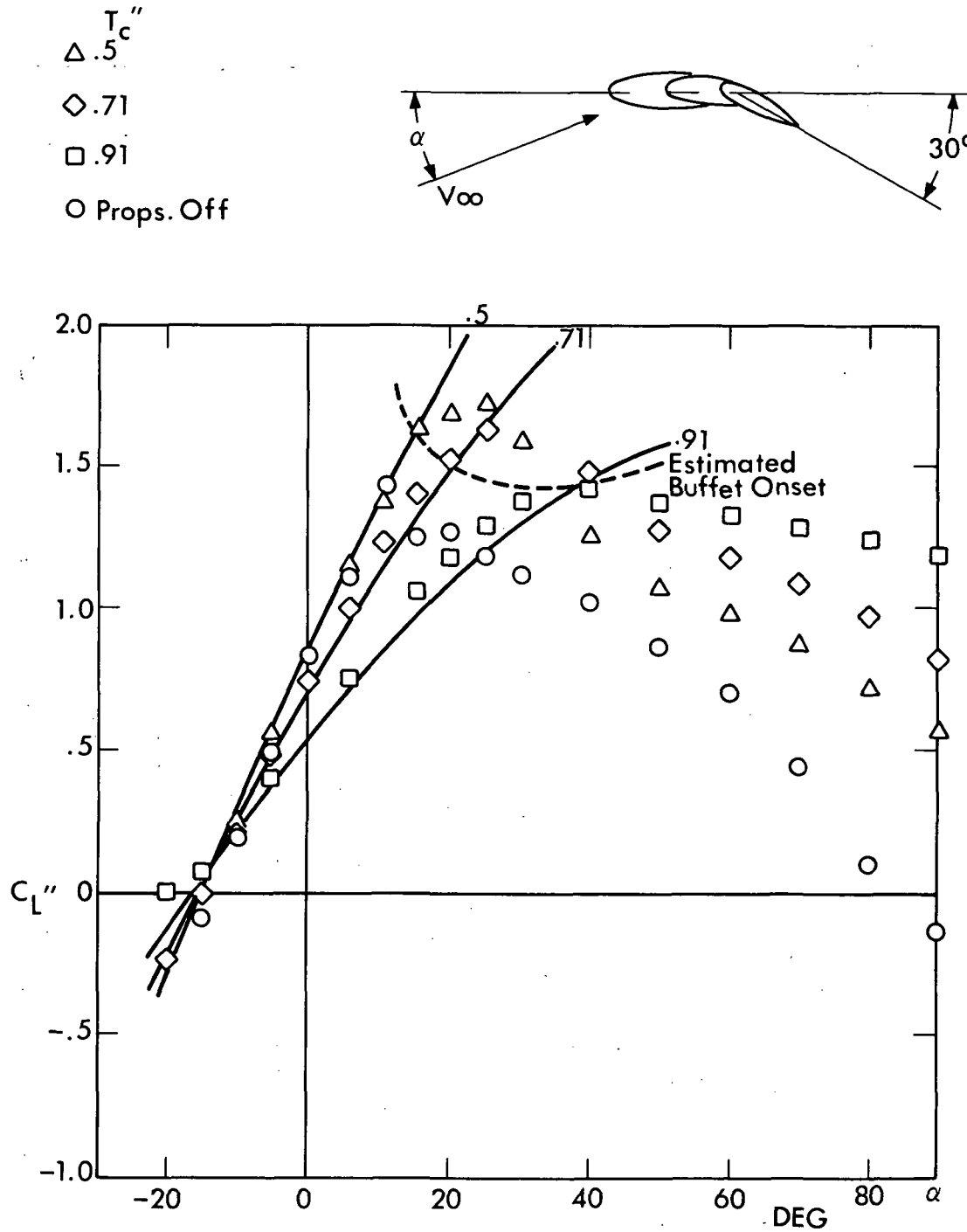

Figure 17(a). - Correlation of Lift and Estimated Buffet Onset with Figure 16, Ref. 22.

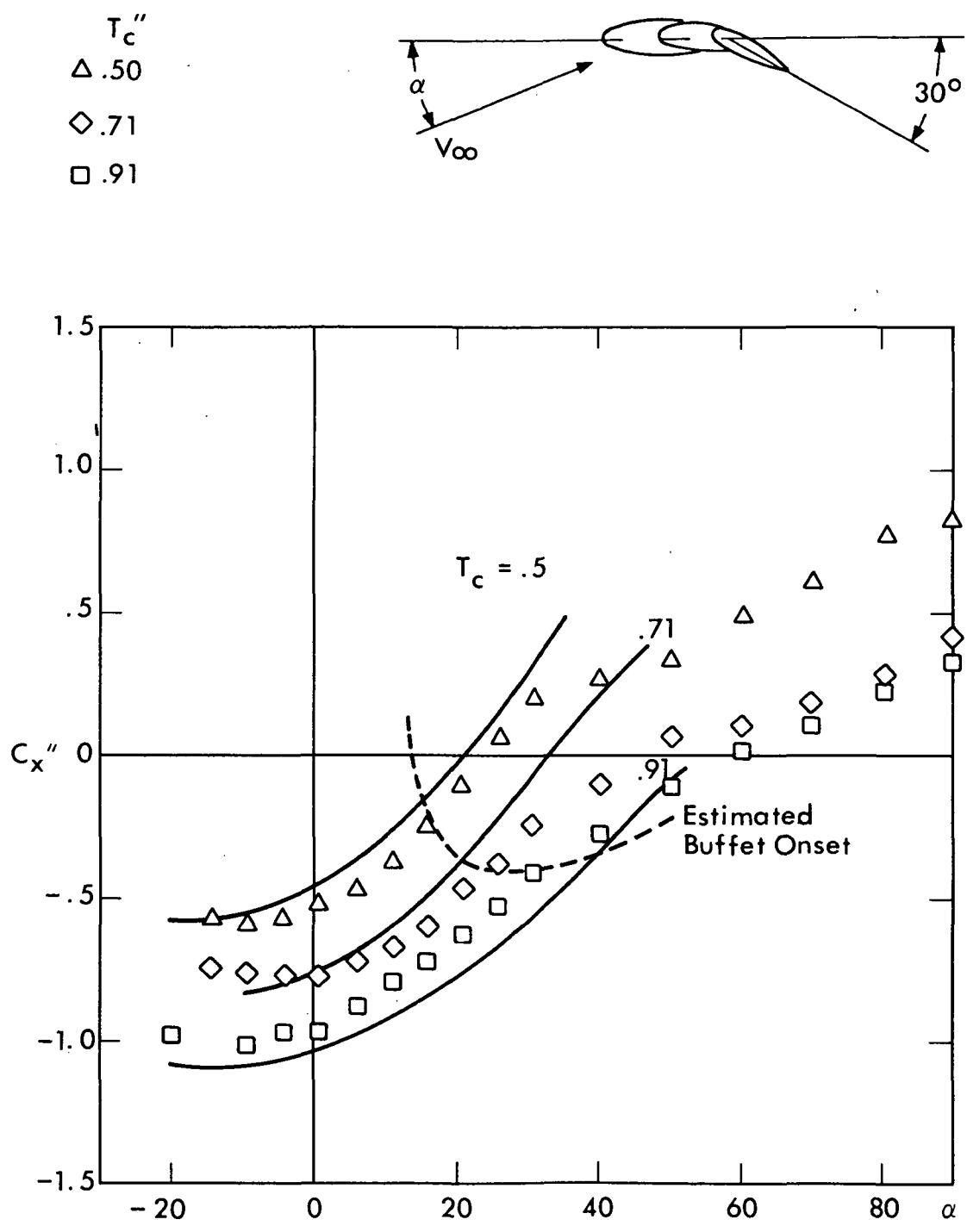

Figure 17(b). - Correlation of Longitudinal Force and Estimated Buffet Onset with Figure 16, Ref. 22.

General Procedure for Calculating Descent Boundaries

In calculating the descent boundaries, the flight condition (V, γ, and W) and an initial value of T_c were assumed; Eq. (25) was then solved iteratively to find a T_c that satisfied either of the following limiting conditions, plus the appropriate overall aircraft lift-drag weight equilibrium relationship of Figure 1.

(1) $\tan (\alpha_{ss} - i_w)$ equals the stall angle of the wing, where i_w is the incidence of the reference wing chord relative to the propeller shaft.

(2) T_c equals the T_c that can be produced by the propeller operating at maximum power, under the given flight conditions. To calculate the power, an efficiency of 87% was assumed. This assumption was not critical, since the descent boundaries were, in fact, set by condition (1).

If the selected flight condition did not produce a T_c satisfying either of the above conditions, it was assumed that the flight condition did not lie on the nominal flight path boundaries. Thus, by a trial-and-error process, the descent boundaries were established.

Geometric and Aerodynamic Characteristics of the XC-142A

The XC-142A airplane is a turbine-engined, tractor propeller, flapped, tilt-wing design for vertical and short takeoff and landing. It has four propellers of diameter and spacing such that the wing is nearly totally immersed in the slipstream. The wing has slight sweep and double-slotted Fowler-type flaps, plus slats. Figure 18 illustrates the general appearance of the aircraft.

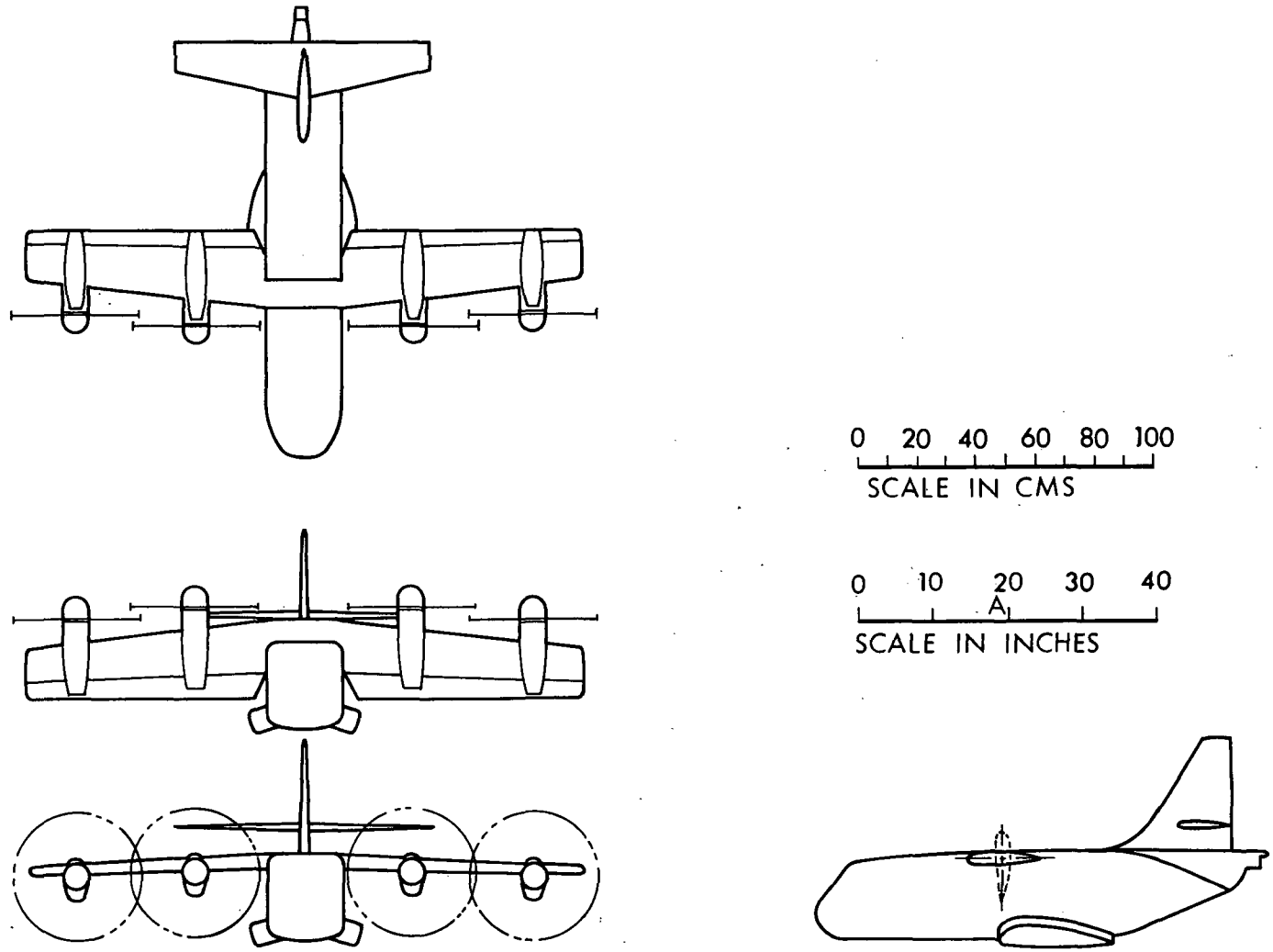

Figure 18. - Three-View Drawing of 1/11 Scale XC-142A Model of Reference 23

General dimensional data required for calculation of the transition descent boundary were taken from References 23 and 24 and are shown on Table 2. Required configuration parameters derived from this data are shown on Table 3.

In addition to the dimensional data, four items of basic aerodynamic data are required for use in calculation of the transition descent boundary. These are the power-off angle of attack of the wing reference chord line at zero lift, α_o; power-off zero lift drag coefficient; flap effectiveness*; and variation of section maximum unstalled angle of attack with flap deflection. The value of α_o is found to be -1.7 degrees, from Figure 7 of Reference 25.

Zero lift drag coefficient data versus thrust coefficient for several model configurations were taken from Figure 12 through 14 of Reference 23 and are shown on Table 4. These data are plotted on Figure 19. Based upon Figure 19, a power-off $C_{D_o} = 0.15$ was taken as representative of the configuration. This value is also in general agreement with Figure 7 of Reference 25.

Data from Reference 23 showing the total angle of attack of the wing, $\alpha_T = (\alpha + i_W)$, at maximum lift coefficient as a function of flap deflection and thrust coefficient are shown in Table 5. Data are shown for flap deflection of 40° and 60° only. Although data for zero flap deflection were available, these did not show a clear $C_{L_{max}}$, and indicated values of α_T at $C_{L_{max}}$ from 20° to beyond 40°.

---

*Flap effectiveness is defined here as the variation of the angle of attack for zero lift with flap deflection. The significance of this parameter is explained later in this chapter.

TABLE 2

XC-142A BASIC DIMENSIONAL DATA

Wing Span	67.5 ft^2
Wing Area	534.0 ft^2
Number of Propellers	4
Propeller Diameter	15.5 ft^2
Engines	(4) GE T64-GE-1
Maximum Power (S.L. Std.) per engine	3080./H.P.
Gross Weight	37,490 lb
Empty Weight	23,016 lb
Angle of Prop. Shaft to Wing Reference Chord	0 degree
Flap: Double Slotted, Fowler Type	
Flap to Chord Ratio (at $\delta = 60^{\circ}$)	$\approx$.28
Airfoil	NACA 63-318

TABLE 3

XC-142A CONFIGURATION PARAMETERS

Wing Area	534.0 ft^2
Aspect Ratio	8.5
Propeller Disc Area	188.7 ft^2/prop
Wing Loading	70.2 lb/ft^2
Disc Loading	49.5 lb/ft^2

TABLE 4

ZERO LIFT DRAG COEFFICIENT DATA, XC-142A

Data from 1/11 Scale Model of Reference 23

(NASA-TN-D-3217)

Figure No. in Ref. 23	δ_F (deg)	C_{T_S} (nominal)	Slat	i_w (deg)	C_D (L=0)	i_T (deg)	Symbol
12	0	.49	none	0	-.46	tail	⊙
	0	.26	none	0	-.21	off	⊙
	0	.03	none	0	.12	off	⊙
	0	-.32	none	0	.42	off	⊙
13a	40	.59	S_1	0	-.67	20	⊡
	40	.41	S_1	0	-.35	20	⊡
	40	.18	S_1	0	-.08	20	⊡
	40	-.04	S_1	0	.20	20	⊡
13b	40	.82	S_1	20	-.93	20	⊡
	40	.64	S_1	20	-.62	20	⊡
	40	.48	S_1	20	-.31	20	⊡
14a	60	.60	S_1	0	-.60	20	◬
	60	.39	S_1	0	-.30	20	◬
	60	.20	S_1	0	-.05	20	◬
14b	60	.80	S_1	10	-.75	20	◬
	60	.60	S_1	10	-.46	20	◬
	60	.42	S_1	10	-.17	20	◬

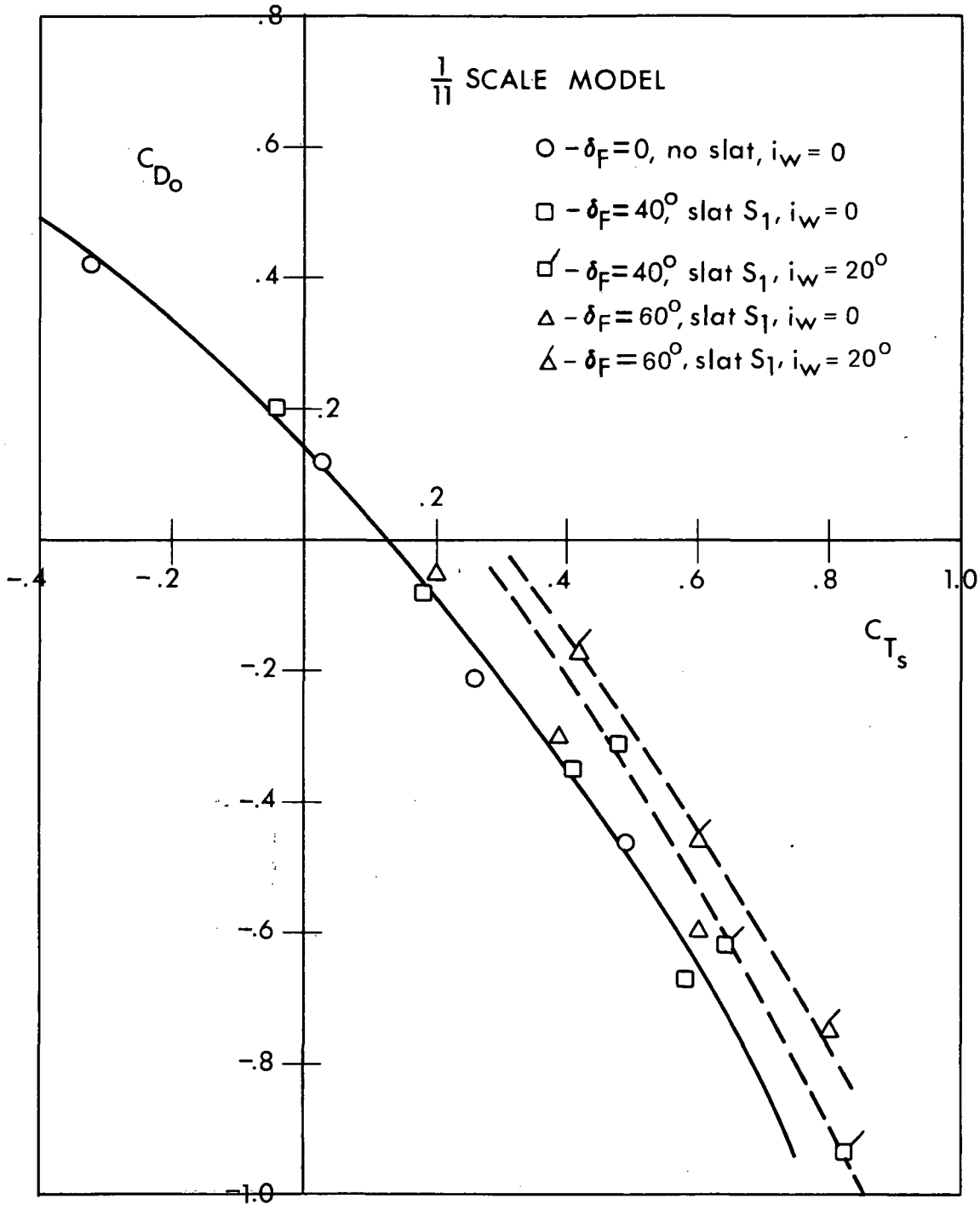

Figure 19. - Zero Lift Drag Data, XC-142A

TABLE 5

ANGLE OF ATTACK AT MAXIMUM LIFT - XC-142A

(Data from Reference 23)

Figure No. in Ref. 23	δ_F (deg)	Slat	C_{T_S} nominal	C_{T_S}	i_W (deg)	$(\alpha+i_W)_{max}$ (deg)	i_T (deg)
13a	40	S_1	all		0	20	20
13b	40	S_1	.82	.83	20	35	20
	40	S_1	.64	.66	20	25	20
	40	S_1	.48	.51	20	25	20
14a	60	S_1	.60	.62	0	18	20
	60	S_1	.39	.42	0	15	20
	60	S_1	.20	.21	0	10	20
14b	60	S_1	1.00		10		20
	60	S_1	.80	.81	10	25	20
	60	S_1	.60	.62	10	16	20
	60	S_1	.42	.44	10	15	20
15a	60	S_1	.40	.42	0	15	20
	60	S_1	.40	.44	10	15	20
15b	60	S_1	.60	.61	0	18	20
	60	S_1	.60	.61	10	17	20
	60	S_1	.60	.62	20	20	20
	60	S_1	.60	.62	30	20	20
15c	60	S_1	.80	.80	10	26	20
	60	S_1	.80	.82	20	26	20
	60	S_1	.80	.81	30	27	20
	60	S_1	.80	.80	40	30	20

The data of Table 5 are plotted in Figure 20(a). This figure indicates the experimental ranges of possible α_T at $C_{L_{max}}$, power-off, for 40^o and 60^o flap deflections. From this and the trends of other airfoil data, the curve of α_T at $C_{L_{max}}$ versus flap deflection δ_F, power-off, of Figure 20(b) is estimated as representative of the XC-142A as indicated by the data of Reference 23. Since this angle is to be used as the angle χ_{max} or buffet-limiting local angle of attack of the fully developed slipstream with respect to the wing reference line, it is so indicated on the ordinate of Figure 20(b). Note that data with slat S, were used for this curve, and that only power-off data are required for use in the descent boundary calculation.

A dashed line representing an arbitrary increment of 10 degrees added to the experimental angles at maximum lift will be noted on Figure 20(b). This was used in a calculation to demonstrate the effect of leading edge devices, as discussed later.

Data showing wing angle of zero lift, $\alpha_{T,L=0}$ versus flap deflection and thrust coefficient, taken from Reference 23 are shown on Table 6. These data are plotted on Figure 21(a), in order to determine the flap effectiveness (power-off), defined as the variation of zero lift angle of attack with flap deflection. The estimated curve of this variation based on the experimental data is shown as the solid line in Figure 21(b). The initial slope of this curve at small δ_F is known from various airfoil tests, as in Figure 96 of Reference 26. However, the experimental data shows the flap to be less effective than expected at high flap deflections; the change in $\alpha_{T,L=0}$ is very small from $\delta_F = 40$ degrees to $\delta_F = 60$ degrees. The ineffectiveness is unexpected, and may perhaps be ascribed to scale or tunnel wall effects.

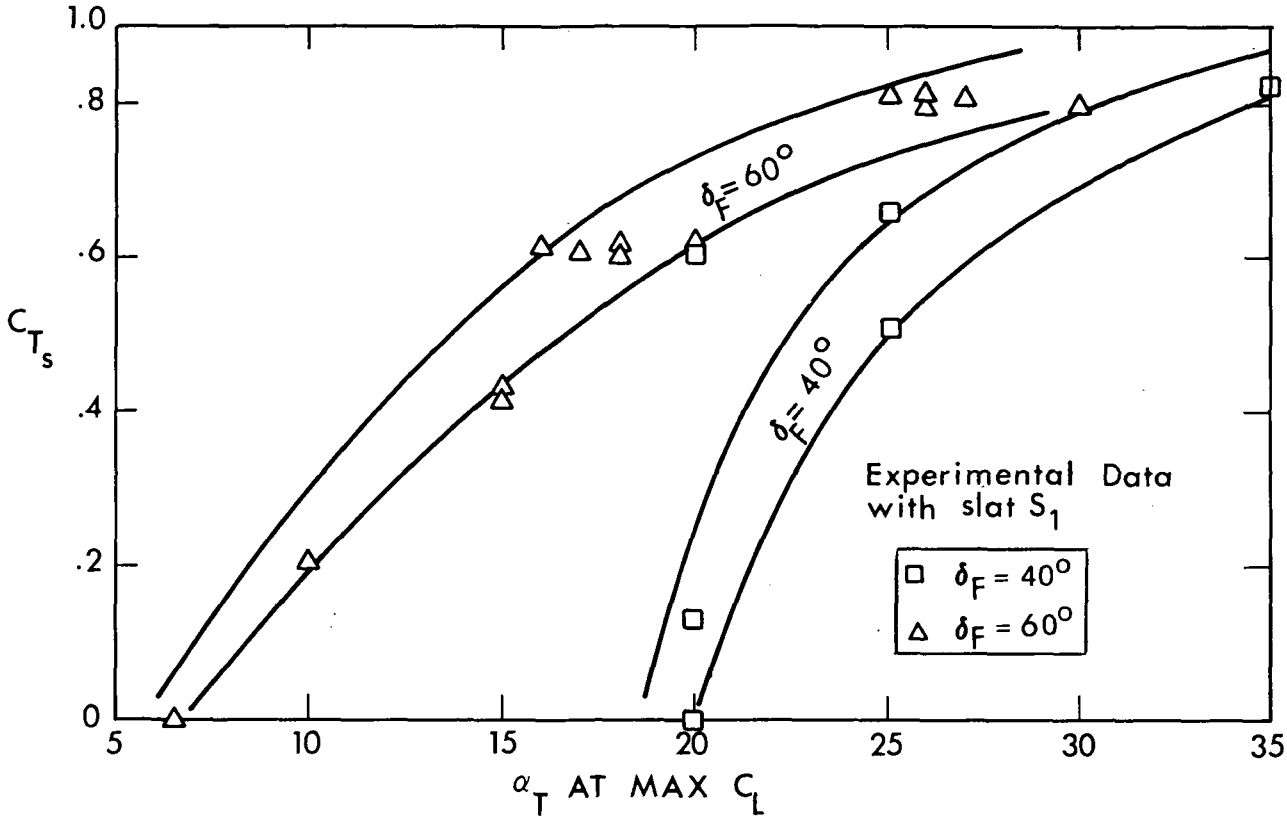

Figure 20(a). - XC-142A 1/11 Scale Model Local Angle of Attack at Maximum Lift

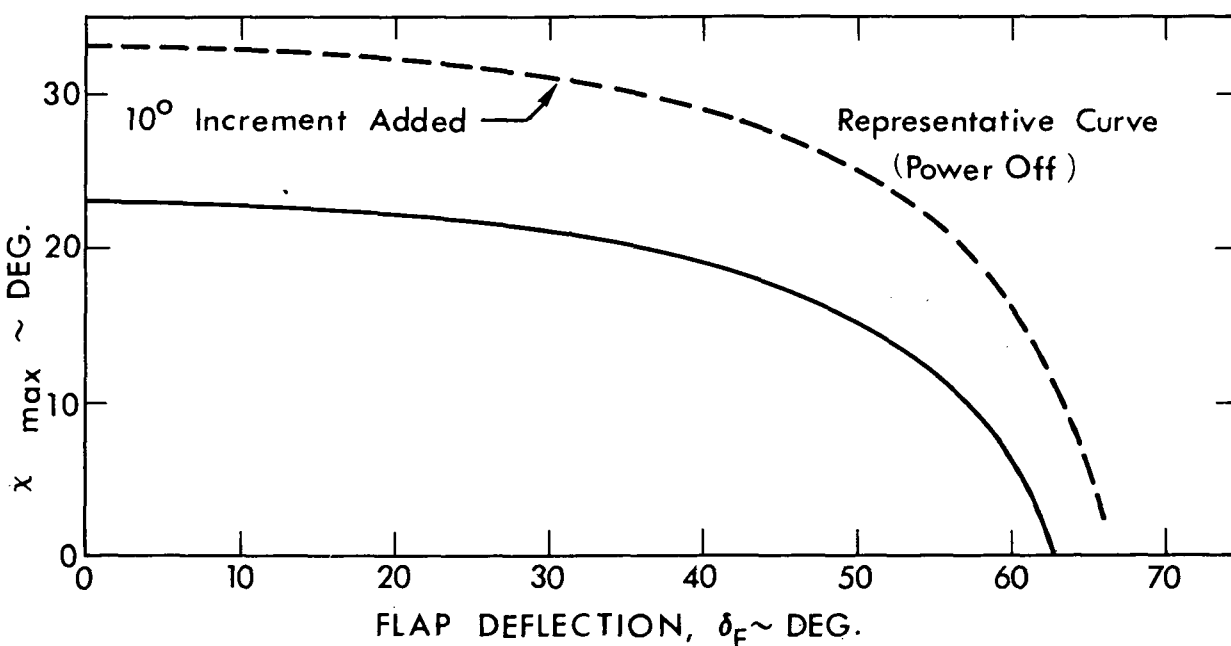

Figure 20(b) - Flap Effectiveness for XC-142A 1/11 Scale Model

TABLE 6

FLAP EFFECTIVENESS DATA - XC-142A

1/11 Scale Model of Reference 23

(NASA TN-D-3217)

Figure No. of Ref. 23	δ_F (deg)	C_{T_S} nominal	Slat	i_W (deg)	$^*(\alpha+i_{W_{L=0}})$ (deg)	C_{T_S}	i_T (deg)	Comments
12	0	.49	none	0	-.50	.49	Tail	
	0	.26	none	0	-.75	.26	Off	
	0	.03	none	0	-1.30	.03	Off	
	0	-.32	none	0	-1.00	-.32	Off	
13a	40	all	S_1	0	-11.5	All	20	
13b	40	.82	S_1	20	-11.0	.81	20	
	40	.64	S_1	20	-9.0	.62	20	
	40	.48	S_1	20	-8.5	.44	20	
14a	60	.60	S_1	0	-15.3	.62	20	
	60	.39	S_1	0	-14.0	.42	20	
	60	.20	S_1	0	-14.2	.26	20	
14b	60	.80	S_1	10	-16.4	.81	20	
	60	.60	S_1	10	-14.8	.62	20	
	60	.42	S_1	10	-13.2	.45	20	
15a	60	.40	S_1	0	-15.0	.43	20	
	60	.40	S_1	10	-13.5	.45	20	
15b	60	.60	S_1	0	-16.0	.61	20	
	60	.60	S_1	10	-15.0	.61	20	
	60	.60	S_1	20	-14.2	.61	20	

TABLE 6
(Continued)

Figure No. of Ref. 23	δ_F (deg)	C_{T_S} nominal	Slat	i_W (deg)	$^*(\alpha+i_{W_{L=0}})$ (deg)	C_{T_S}	i_T (deg)	Comments
17a	0	prop's	none	0	0.0	prop's	tail off	Trim at about i_T = 2.0 deg.
	0	off	none	0	0.0	off	-5	
	0	off	none	0	0.0	off	0	
	0	off	none	0	-1.5	off	10	
	0	off	none	0	-5.0	off	20	
17b	60	off	S_1	0	-12.5	off	off	Trim at about i_T= -1.50 deg.
	60	off	S_1	0	-10.5	off	-5	
	60	off	S_1	0	-11.0	off	0	
	60	off	S_1	0	-12.5	off	10	
18a	40	off	S_1	0	-10.0	off	off	No trim
	40	off	S_1	0	-11.0	off	10	
	40	off	S_1	0	-11.5	off	20	

* $(\alpha+i_W) = \alpha_T$

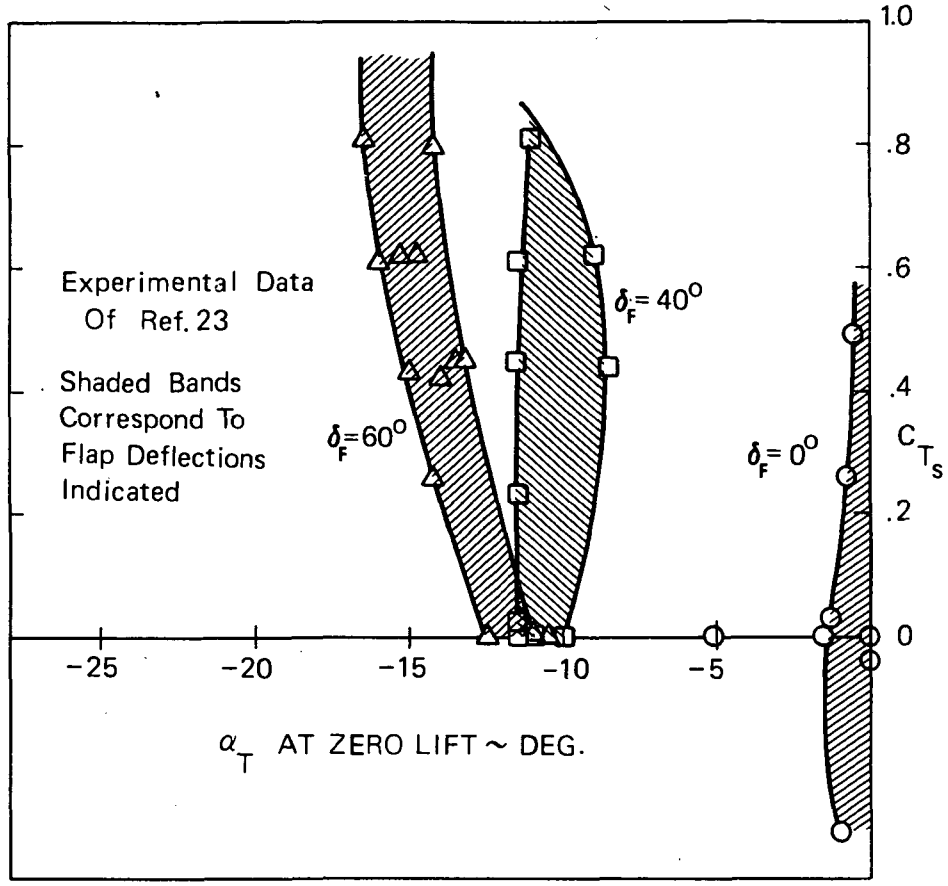

Figure 21(a). - XC-142A Zero Lift Angle Characteristics

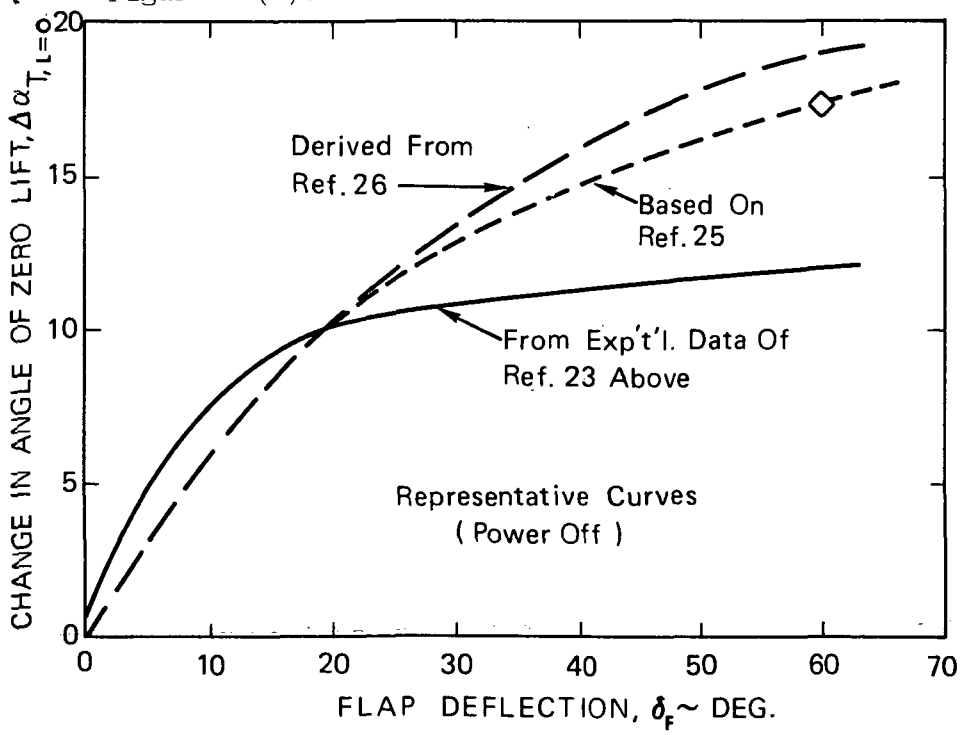

Figure 21(b). - Flap Effectiveness, XC-142A

It is believed that the flap effectiveness of the full scale XC-142A is greater than indicated by the experimental data of Reference 23. Therefore, the dashed curve on Figure 21(b) was estimated from section test data of Reference 26, and the flap effectiveness data at low flap deflections of Figure 96, Reference 26. This curve indicates the degree of flap effectiveness which could be expected under full scale conditions.

The data of Reference 25 offer flap effectiveness for a single deflection, $\delta_F = 60^\circ$, as shown on Figure 21(b). The tests of Reference 25 used surface roughness treatment for control of boundary layer transition. The curve of effectiveness versus deflection shown on Figure 21(b) as based on Reference 25 used the single point at $\delta_F = 60^\circ$, faired into the curve based on Reference 26 at lower flap deflections. The curve was used to calculate the descent boundaries.

Calculated and Experimental Descent Boundaries

Descent boundaries taken from the wind tunnel test data of References 23 and 25, and the flight test data of Reference 14 are shown on Figure 22. The wind tunnel boundaries are shown for two values of flap deflection. These show the flight path angle corresponding to the lift to drag ratio measured at the value of wing incidence (with fuselage level) at which flow breakdown on the wing was indicated by observation of tufts. These curves are based on untrimmed data.

Boundaries based on the flight test data of Reference 14 are shown as the solid curves on Figure 22. These data were obtained by flying a configuration having constant wing incidence and flap deflection, gradually reducing power to increase rate of sink, and controlling air speed by fuselage incidence. The boundaries correspond to

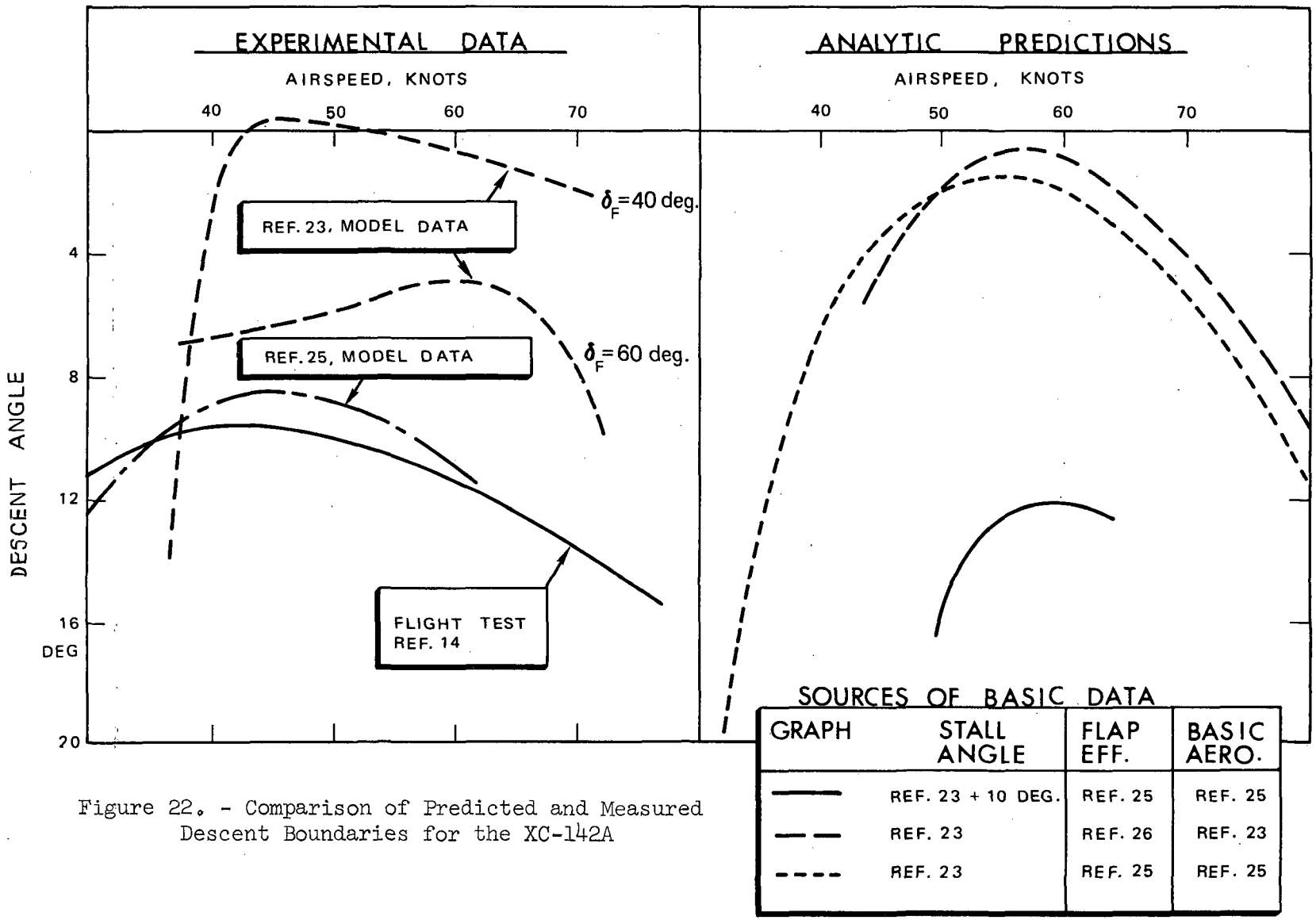

Figure 22. - Comparison of Predicted and Measured Descent Boundaries for the XC-142A

the low frequency buffet characteristics. These boundaries are the same as those shown in Figure 10.

Descent boundaries calculated by the analytic method are also shown on Figure 22. The dotted line represents results using best estimates of basic aerodynamic data from Reference 23, 25, and 26. The dashed curve was calculated using the curve of slightly higher flap effectiveness derived from Reference 26, but other basic aerodynamic data from Reference 23, i.e., a lift curve slope of 4.30 instead of 4.91 as from Reference 25, and an angle of zero lift of -1.0° at zero flap deflection.

Steeper descent angles are realized in flight testing than are predictable by the theoretical method. The theoretical method indicates that the boundary should be very sensitive to the angle of attack at maximum C_L, as this angle, χ_{max}, is the index to the maximum deflection of the slipstream by the wing. Leading edge devices are especially effective in extending the value of this angle. To define the effect of χ_{max} on the descent boundary, the boundary was calculated for speeds in the vicinity of minimum allowable angle of descent, using values of χ_{max} from Reference 23 to which an arbitrary increment of 10° had been added. The curve of $(\chi_{max} + 10^{\circ})$ is shown on Figure 20(b). The resulting segment of descent boundary is shown as the solid curve of Figure 22. Although the increase of χ_{max} without accounting for accompanying losses is to some extent arbitrary, the results indicate the power of this parameter in affecting the descent boundary.

The angles of descent resulting from the extension of χ_{max} are in reasonable agreement with those obtained in flight testing. This result indicates the probable importance of scale effects and tunnel wall corrections at the limiting flow deflection conditions, especially regarding the effectiveness of leading edge devices.

CHAPTER IV

EFFECT OF DESCENT ON TRANSFER FUNCTIONS OF TILT-WING AND TILT-DUCT V/STOL AIRCRAFT

Introduction

The preceding chapters have discussed the restrictions imposed on descent capabilities of V/STOL aircraft by $(D/L)_{max}$. This restriction is an important one for establishing nominal flight paths. However, it does not necessarily follow that a nominal flight path is flyable. Factors such as poor handling qualities, unsatisfactory gust response, improper coupling to ground-based guidance equipment, etc., may render a given nominal flight path impractical. These factors are associated with the small-perturbation dynamics of the aircraft. Accordingly it is desirable to study the effect of descent on the small-perturbation dynamics of typical V/STOL aircraft, in order to detect any trends that may limit the accuracy with which the aircraft can follow a given nominal flight path. Particular interest centers on characteristics which are innocuous in level flight but which become adverse in descent.

To achieve this objective, transfer functions have been calculated for the Canadair CL-84 tilt-wing aircraft, and for the Bell X-22A tilt-duct aircraft, for a range of low speed conditions, including level flight, shallow descents, and descents as steep as the aircraft's $(D/L)_{max}$ limitations will permit. This chapter is mainly concerned with the calculation and verification of the transfer functions, and the aircraft response to step control inputs. It is shown that for the tilt-wing configuration, with stability augmenter system off (S.A.S.-off) a marked deterioration in the height response to throttle or collective pitch occurs in steep low-speed descents. This change is associated with the appearance of a right-half-plane zero in the appropriate transfer function.

In Chapter V the consequences of this change in the transfer function on the accuracy of terminal guidance are calculated. It is shown that, even with optimum control, the ability of the aircraft to follow a given nominal flight path is severely degraded when the magnitude of the right-half-plane zero lies within a certain critical region.

Calculation and Validation of CL-84 Stability Derivatives

The CL-84 is shown in Figure 23, which is based on data from Reference 27. This reference describes flight tests on the CL-84, and contains the basic dimensional data used in the calculation of stability derivatives. Accordingly, the dimensional data is not repeated here. Reference 27 does not present inertial data; manufacturers' estimates were therefore used.

The CL-84 is equipped with a three-axis stability augmentation system (S.A.S.). This produces additional rate damping of 1.8, 2.4, and 3.6 rad/sec^2 per rad/sec about the yaw, roll, and pitch axes, plus an artificial pitch attitude stiffness of 1.8 rad/sec^2 per rad. The term "S.A.S.-on" is used here to denote conditions where all of the above augmentation functions are operating.

The stability and control derivatives were calculated by the MOSTAB modular stability derivative program described in Reference 1, for the nineteen flight conditions listed in Table 7. These flight conditions cover the airspeed range from hover to 100 knots, with rates of descent varying from level flight to the descent buffet boundary, as estimated in Reference 28. Because the forward speed tests of Reference 27 were performed at 85 percent of nominal RPM, this was used for derivative calculations, to facilitate comparisons between flight test data and the predicted aircraft response characteristics. Some cases were re-run at 95 percent RPM to detect any significant effects of propeller speed on the derivatives.

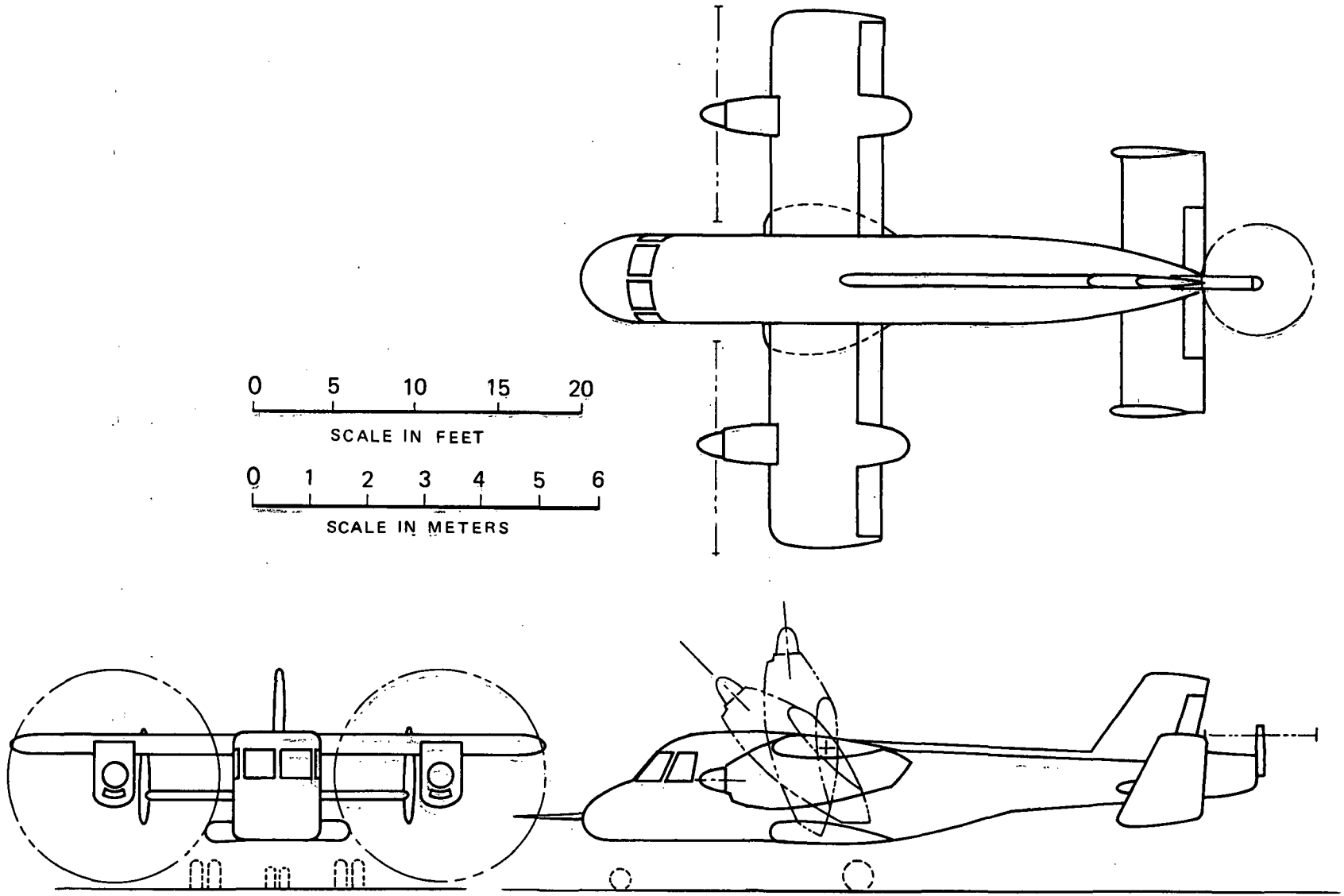

Figure 23. - Three-View Drawing of CL-84 Tilt-Wing Aircraft

TABLE 7.

FLIGHT CONDITIONS STUDIED FOR CL-84

Case	Airspeed	Rate of Descent Ft/Sec	RPM % Max
1.	Hover	0	95
2.	Vertical Descent	10	95
3.	20 Knots	0	85
4.	20 Knots	5	85
5.	20 Knots	10	85
6.	42 Knots	0	85
7.	42 Knots	16	95
8.	42 Knots	8	85
9.	42 Knots	16	85
10.	60 Knots	0	85
11.	60 Knots	12	85
12.	60 Knots	24	85
13.	80 Knots	0	85
14.	80 Knots	15	85
15.	80 Knots	30	85
16.	100 Knots	0	85
17.	100 Knots	30	95
18.	100 Knots	15	85
19.	100 Knots	30	85

Derivatives were calculated for all the flight conditions listed in Table 7, and the derivatives for Cases 1, 6, 9, 13 and 15 are presented in Appendix A together with appropriate inertias. To check the accuracy of these derivatives they were used to compute time histories of responses to specified control inputs. The calculated responses were then compared with flight test responses given in Reference 27. A typical comparison of longitudinal responses is shown in Figure 24. The calculated response was obtained by direct integration of the equations of motion using the derivatives given in Appendix A, and the same stick deflection time history as recorded in flight. It will be seen from Figure 24 that the agreement between the calculated and actual longitudinal responses is very good, for the flight conditions examined in Figure 24 (42 knots level flight attitude S.A.S. off). Similar comparisons of lateral responses were made for the following level flight conditions; 100 knots, roll S.A.S. on; 42 knots, yaw S.A.S. off; and 42 knots, roll S.A.S. off. All of these comparisons showed satisfactory agreement between the calculated and actual flight test time histories. Thus, the derivatives and the calculated transfer functions discussed below appear to be of good accuracy.

The Effect of Descent Angle on the CL-84 Longitudinal Transfer Functions

Appendix A presents longitudinal and lateral transfer functions for each of the cases listed in Table 7, both with S.A.S. on and with S.A.S. off. In general, the effect of descent angle on the transfer function is slight; however, there are some important exceptions to this generalization, as noted below. A brief summary of the major effects of descent on each transfer function is given below. Appendix A presents the transfer functions which form the basis for this summary.

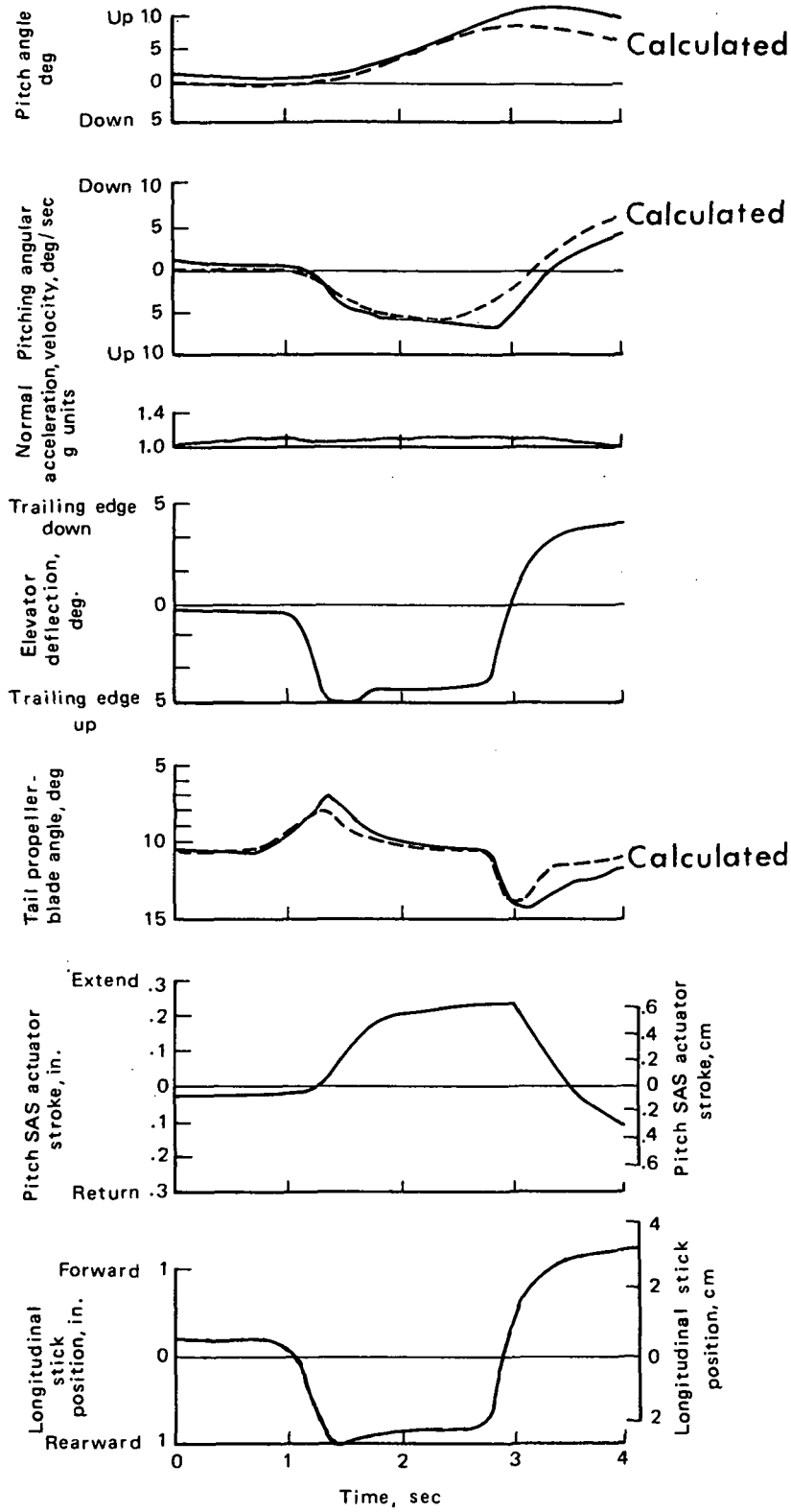

Figure 24. - Time History of Longitudinal-Control Step Pull-and-Hold Maneuver with Pitch-Attitude SAS off and Pitch-Rate SAS on Airspeed of 42 Knots; Wing Incidence of 40°; Flap Incidence of 24°
CL-84

Longitudinal transfer function denominators. - With S.A.S. off the CL-84 displays typical characteristics of tilt-wing V/STOL aircraft as summarized in Reference 29. At hover there exist two stable aperiodic roots and one markedly unstable oscillation. As forward speed is increased to 100 knots these roots merge to form the conventional phugoid and short-period roots, as described in Reference 29. At a given airspeed, the effect of descent angle on these roots is generally negligible. In most cases the change in the roots from level flight to maximum descent is less than 10 percent.

With S.A.S. on, there is a marked increase in the stability of the hovering oscillation (the roots change from $+0.156 \pm 0.526j$ to $-0.334 \pm 0.214j$). This increase in stability is maintained throughout transition, and at 100 knots the S.A.S. almost doubles the phugoid damping ratio and increases the short-period damping ratio by approximately 25 percent. As in the 'S.A.S. Off' case, the effect of descent angle on the roots at a given airspeed is generally negligible.

Pitch attitude/longitudinal stick deflection transfer function. - At a given flight condition the numerators of these transfer functions are the same 'S.A.S. on' and 'S.A.S. off.' There is very little change with descent angle, at a given airspeed. As noted above, the denominator change is negligible; therefore, pilot opinion of attitude control should be unaffected by descent.

Speed/longitudinal stick deflection transfer function. - The control of stability-axis speed perturbations (u) is of importance for stationkeeping and for establishing the desired approach speed. The numerator of this transfer function is virtually unchanged by the S.A.S. Descent angle does induce some change at speeds below 100 knots. For example, at 42 knots the relevant transfer functions for the S.A.S. off, 85 percent RPM condition, are:

$$\frac{u}{\delta_E} = \frac{1.03\ (s + .24)\ (s - 9.94)\ (s + 9.81)}{(s + .0122 \pm .217j)\ (s + .525 \pm .936j)}$$

Level Flight

$$\frac{u}{\delta_E} = \frac{2.09\ (s + .182)\ (s - 6.23)\ (s + 6.58)}{(s + .0177 + .244j)\ (s + .504 + .941j)}$$

960 fpm
Descent

This change is probably not significant for human or automatic control, since the D.C. gain of the transfer function remains unchanged and the right-half-plane zero is too large to be critical, as will be explained in Chapter V.

Height error/longitudinal stick deflection transfer function. - First it is necessary to define the term "height error" as used in this report. The definition is illustrated in Figure 25. The height error, h_e, is defined as the distance of the airplane c.g. above the unperturbed flight path, measured normal to the unperturbed flight path. Thus, if the nominal flight path is level, the height error is simply the altitude of the aircraft above the datum altitude, i.e., $h_e = h$. If the aircraft is descending at an angle γ_o in the unperturbed state, the height error, h_e, equals the altitude perturbation multiplied by cosine γ_o. The quantity h_e is used here, in preference to altitude, because it is more directly related to the pilot's control task in attempting to follow a steep flight path. For example, perturbations in speed, (u) could induce an altitude rate ($\dot{h}$) error with the aircraft continuing to follow the desired spatial flight path. It is felt that the problem of controlling speed along the desired flight path should be treated separately from the problem of controlling the aircraft to follow the desired flight path. Thus, the r.m.s. deviation of h_e is a significant measure of the accuracy of a given guidance system. In terms of stability axis quantities, h_e, can be obtained from:

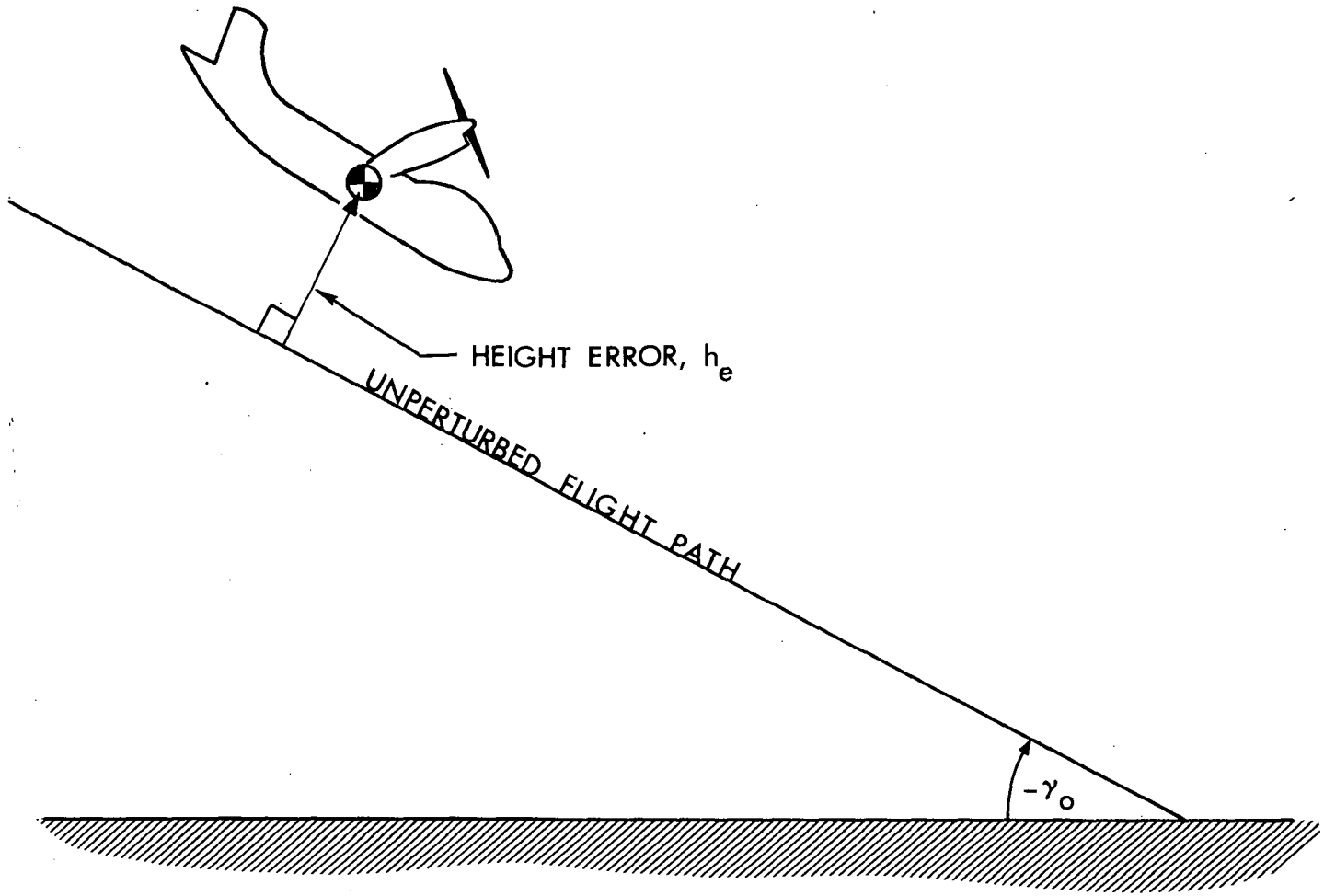

Figure 25. - Definition of Height Error

$$\frac{dh_e}{dt} = - w + U_o \int q \, dt \qquad (40)$$

It is well-known that for conventional aircraft below the minimum drag speed, it becomes difficult to control height (h) by elevator alone in small perturbations from level flight. In Reference 30 the cause is traced to a right-half-plane zero in the h/δ_E transfer function.* The zero is in the left-half-plane at speeds above the minimum airspeed. This characteristic appears in the CL-84 level flight h/δ_E numerators which are:

At 100 knots; $9.43 (s + .011) (s + 7.47) (s - 7.39)$
At 60 knots; $8.85 (s - .080) (s + 4.15) (s - 3.77)$

It is interesting to see how the right-half-plane zero at $s = + .080$ is affected by descent. We, therefore, compare the above transfer function numerators with the corresponding h_e/δ_E numerators for descent. For the maximum descent rates, at the above airspeeds, the h_e/δ_E numerators are:

At 100 knots; 1800 f.p.m. descent $9.77 (s - .024) (s + 7.14) (s - 7.05)$

At 60 knots; 1440 f.p.m. descent $7.98 (s - .361) (s + 3.3) (s - 2.16)$

The above examples show that descent angle produces a significant increase in the magnitude of the smaller right-half-plane zero, and a decrease in the magnitude of the larger right-half-plane zero.

*The h/δ_E transfer function normally contains one large right-half-plane zero. This zero causes the initial 'drop' of the c.g. in response to up-elevator. This drop is, of course, of very short duration and causes no control problems. The zero discussed here is additional.

As explained in Chapter V, both these effects are adverse, since they tend to move the zeros into a critical region. Thus, the difficulties experienced in controlling the flight path by elevator will worsen in steep descents.

Height error/collective transfer function. - Because of the above-mentioned difficulties experienced in controlling height with elevator, it is usual to control height by thrust in low-speed flight. The h_e/θ_o transfer functions tabulated in Appendix A describe the response of the CL-84 to changes in collective propeller pitch, θ_o, at constant r.p.m. These transfer functions show some significant changes between level flight and descent for the S.A.S. off condition. For example, at 42 knots and 85 percent rpm the h_e/θ_o numerators are:

In level flight: $-107.8\ (s + .015)\ (s + .443 \pm 1.09j)$

At 960 fpm descent: $-112.0\ (s - .092)\ (s + .477 + 1.03j)$

The appearance of the right-half-plane zero causes a drastic change in the nature of the response to a collective step input. This is illustrated in Figure 26. In level flight the response is always in the "right" direction, i.e., an increase of collective causes the aircraft to climb. By contrast, in descent h_e increases only for the first 9 seconds, and actually reverses sign after 16 seconds.

The sign reversal is a direct consequence of the change in the small zero from $s = + .015$ to $s = - .092$. It can be shown by the Laplace Transform Final Value Theorem that a stable transfer function with one right-half-plane zero has a step response which initially is of the opposite sign to the final response. This "wrong-way" characteristic may explain a control deficiency noted in Reference 27 (p. 16) which describes difficulties experienced in establishing a steady 300 fpm descent rate at 42 knots. In Reference 27 it is suggested that low plunge damping, $-Z_w$, may have been the cause; however, the calculated derivatives given in Appendix A do not show a significant decrease in $|Z_w|$ with increase in rate of descent. Further, it is noted in Reference 27

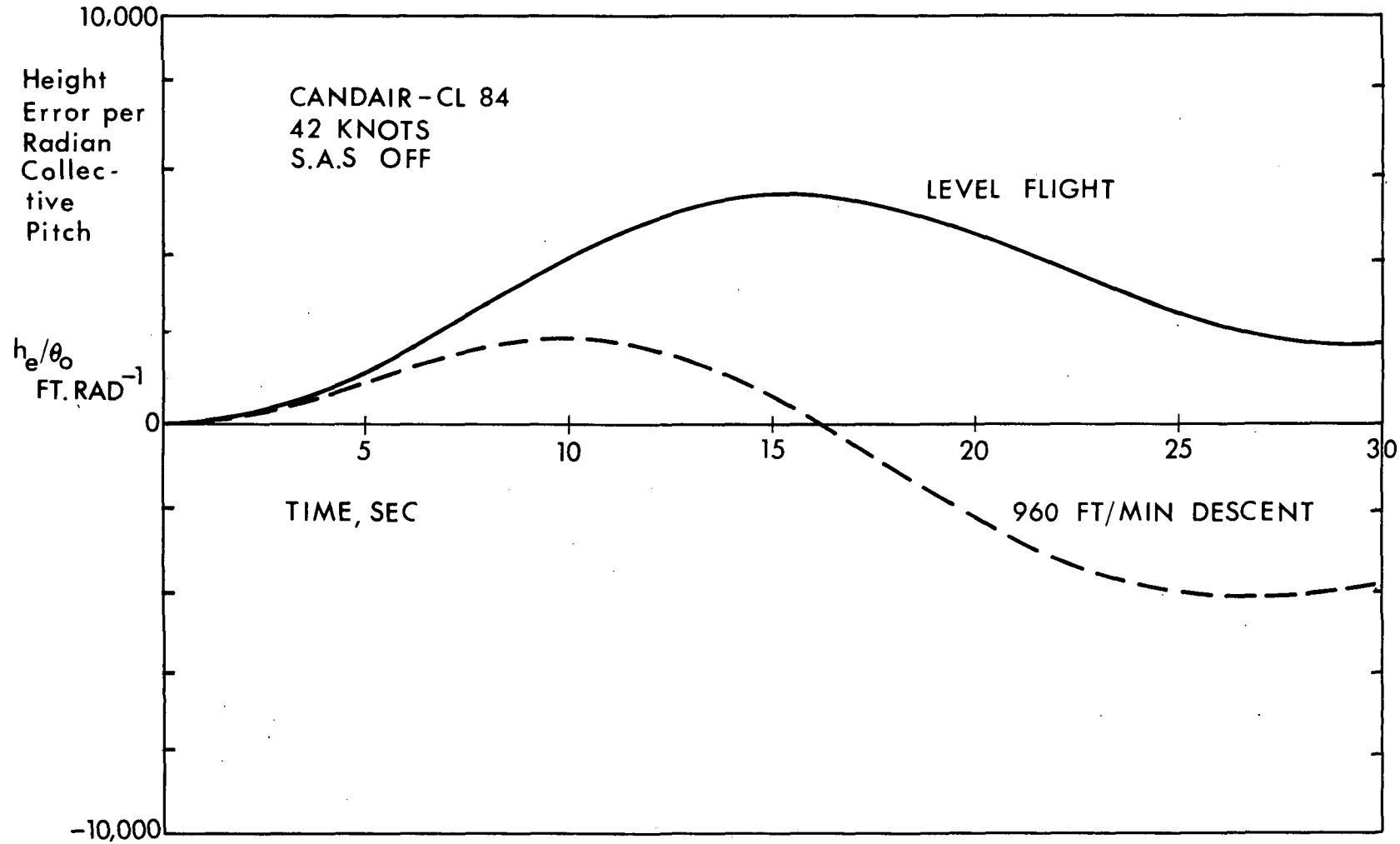

Figure 26. - Effect of Descent Angle on Height Error Response for CL-84 at 42 Knots Airspeed with S.A.S. Off

that 'an indicated rate of descent could be maintained between 300 and 700 fpm if frequent adjustments to the power lever were made.' This would be expected from the step response characteristics shown in Figure 26.

The S.A.S. removes the offending zero and thus eliminates the wrong-way final step response. This is illustrated in Figure 27(a). The appropriate h_e/θ_o transfer function numerators, with S.A.S. on, are:

In level flight: $-107.8\ (s + .124)\ (s + 1.44 \pm .798j)$

At 960 fpm descent: $-112.0\ (s + .050)\ (s + 1.37 \pm .802j)$

Although the descent case transfer function is free of right-half-plane zeros, the tendency for the response to be smaller than the level flight case remains. It is possible that the rather low magnitude of the h_e/θ_o step response in descending flight (compared to the level flight response) might be objectionable to the pilot. An extensive discussion of the effect of right-half-plane zeros on the minimum possible r.m.s. tracking error, with special reference to CL-84 height error control, is given in Chapter V.

The pitch responses associated with the height error responses of Figures 26 and 27(a) were calculated to check whether the "wrong-way" characteristic appears in the pitch attitude response. These responses are shown in Figure 27(b). This figure shows that there is not much effect of descent angle on the pitch attitude response to collective, both with S.A.S. on and with S.A.S. off. The S.A.S. reduces the magnitude of the pitch response to collective but the peak response remains relatively large, even with S.A.S. on.

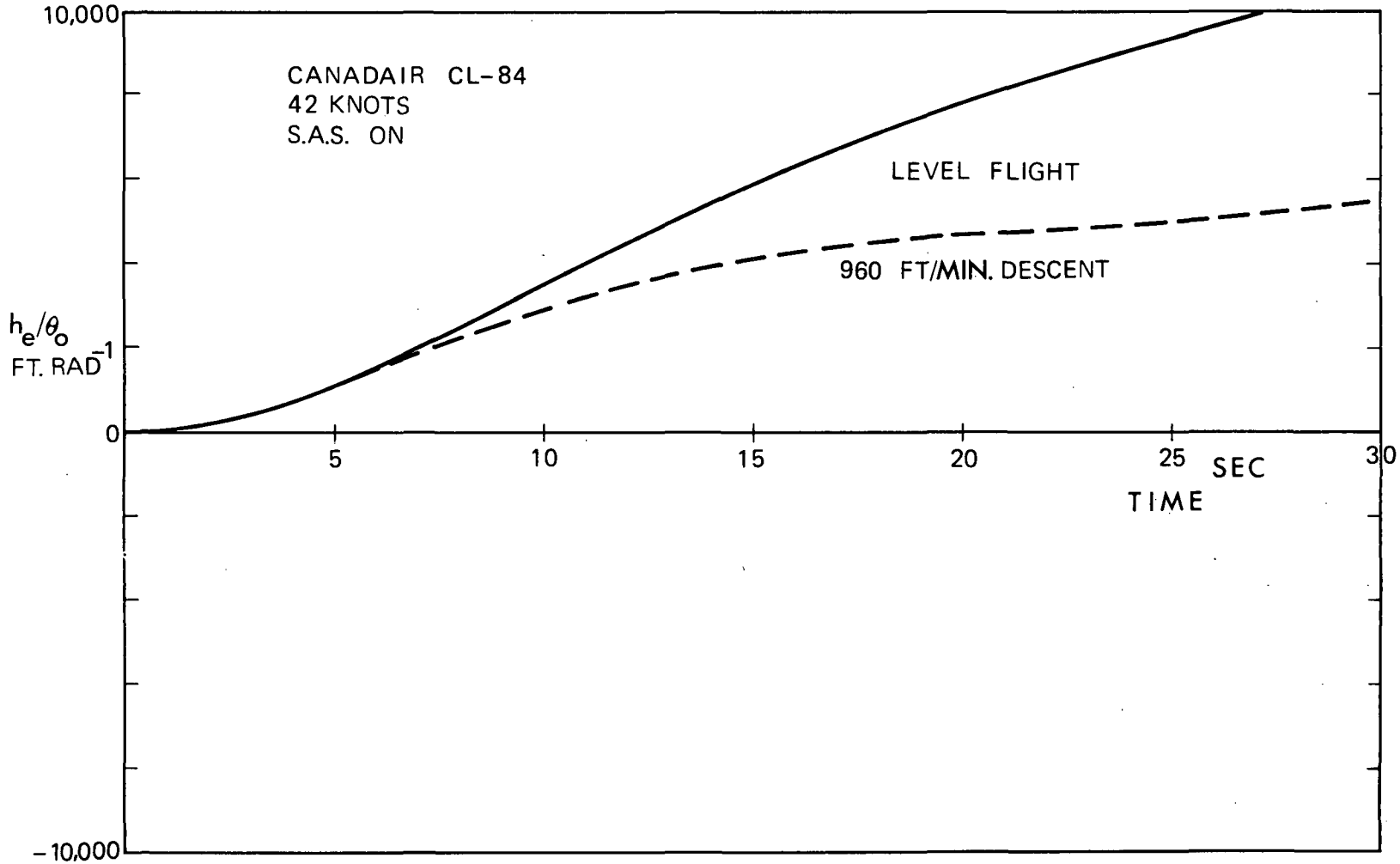

Figure 27(a). - Effect of Descent Angle on Height Error Response for CL-84 at 42 Knots Airspeed with S.A.S. On

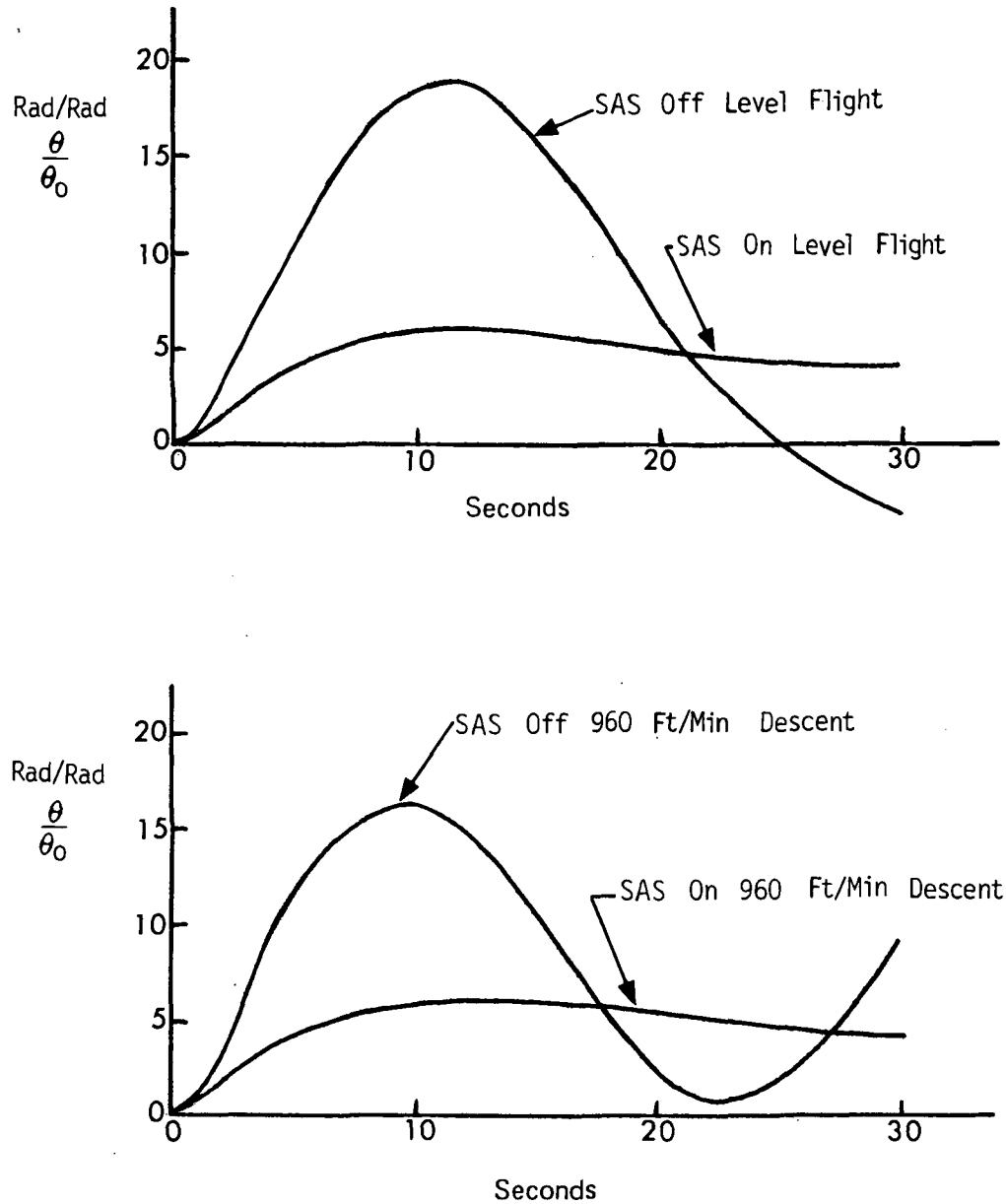

Figure 27(b). - Effect of Descent and Stability Augmenter System on Pitch Attitude Response to Unit Step Input in Collective Pitch for CL-84 at 42 Knots Airspeed at Sea Level

The Effect of Descent Angle on the CL-84 Lateral Transfer Functions

Appendix A presents transfer functions relating roll control, (δ_A) to bank angle and also relating roll and yaw control (δ_R) to lateral deviation from the unperturbed flight path. This quantity, denoted as y, is a measure of the lateral drift of the c.g. from the desired position, and is significant for terminal guidance since it equals the offset from the center of the runway. In general, there are few significant effects of descent on the lateral transfer functions, and hence only a brief summary is given below.

Lateral transfer function denominators. - With S.A.S. off the CL-84 displays typical tilt-wing characteristics, changing from an unstable hover oscillation plus two stable subsidences at hover, to the usual dutch roll, spiral, roll subsidence combination at 100 knots. The roll subsidence root is unusually small, being of the same magnitude as the dutch roll root, because of the high roll inertia/damping of the CL-84. In the speed range 0 to 100 knots the effect of descent angle upon the denominator roots is negligible.

With S.A.S. on, the hovering oscillation becomes slightly stable, and there is a marked increase in the stability of the hovering roll-subsidence root. At higher speeds these trends continue: the dutch roll becomes well stabilized and the roll-subsidence root increases from approximately -1.5 S.A.S. off, to approximately -6.6. These characteristics are only very slightly affected by descent angle for all the speeds considered.

Bank angle/lateral stick deflection transfer function numerators. These are the same S.A.S. on and S.A.S. off. The effect of descent angle is negligible.

Lateral ground velocity/pedal deflection transfer function numerators. - With S.A.S. off, in level flight this numerator is characterized by a moderately large right-half-plane root, a left-half-plane root of about 50 to 100 percent of the magnitude of the first root, and a stable complex pair. Some changes do occur between level flight and descent, however, the general character of the roots remains the same. For example, at 80 knots, the y/δ_R numerator is:

Level flight: $-3.43\ (s - 3.17)\ (s + 1.37)\ (s + .059 \pm 3.94j)$

1800 fpm descent: $-3.44\ (s - 4.81)\ (s + 2.73)\ (s + .522 \pm 2.26j)$

No adverse effects are apparent in this change. The behavior with S.A.S. on is generally similar except that the oscillatory roots become more stable.

Lateral ground velocity/lateral stick deflection transfer function numerators. - With S.A.S. off this important transfer function is characterized by a numerator with four roots. Two of these form an oscillatory pair which is approximately cancelled by the dutch roll pair in the denominator. This cancellation occurs in both level flight and descent; it assures a non-oscillatory step response, which is desirable for good handling qualities. The remaining roots comprise one which is of either sign but very small, and can be regarded as zero, and one which is exceedingly large (>100 rad/sec) which has no influence on handling qualities. The above characteristics are unchanged by descent. One would expect, therefore, that the lateral positioning of the aircraft would be no more difficult in descent than in level flight.

With S.A.S. on, the very small root becomes large (>30 rad/sec) and stable. The other characteristics remain as described above, and no significant effect of descent on handling qualities related to the y/δ_A transfer function is indicated.

Calculation and Validation of X-22A Derivatives and Transfer Functions

The Bell X-22A is a V/STOL research aircraft equipped with four ducted fans. Figure 28, taken from Reference 15, illustrates the general arrangement of the vehicle. Manufacturer's estimates of stability derivatives for the X-22A are given in Reference 31 for various level flight conditions, mostly with a deceleration a_x 'g's. These are equivalent to the derivatives for steady descent at an angle $\gamma_o = \sin^{-1} a_x$. Interpreting the derivatives in this fashion yields derivatives for the flight conditions listed in Table 8. These descending cases correspond to the buffet boundary of the X-22A as estimated in Reference 31. The derivatives are tabulated in Appendix B. For reasons explained below, only lateral data are included in Appendix B.

TABLE 8.

FLIGHT CONDITIONS STUDIED FOR THE X-22A

Run No.	Airspeed fps	Flight Path Angle deg	S.A.S.
1	10	-12.1	ON and OFF
3	67.5	- 7.1	" "
5	101.2	-10.0	" "
7	168.9	-13.5	" "
9	219.5	0	" "
12	0	0	" "

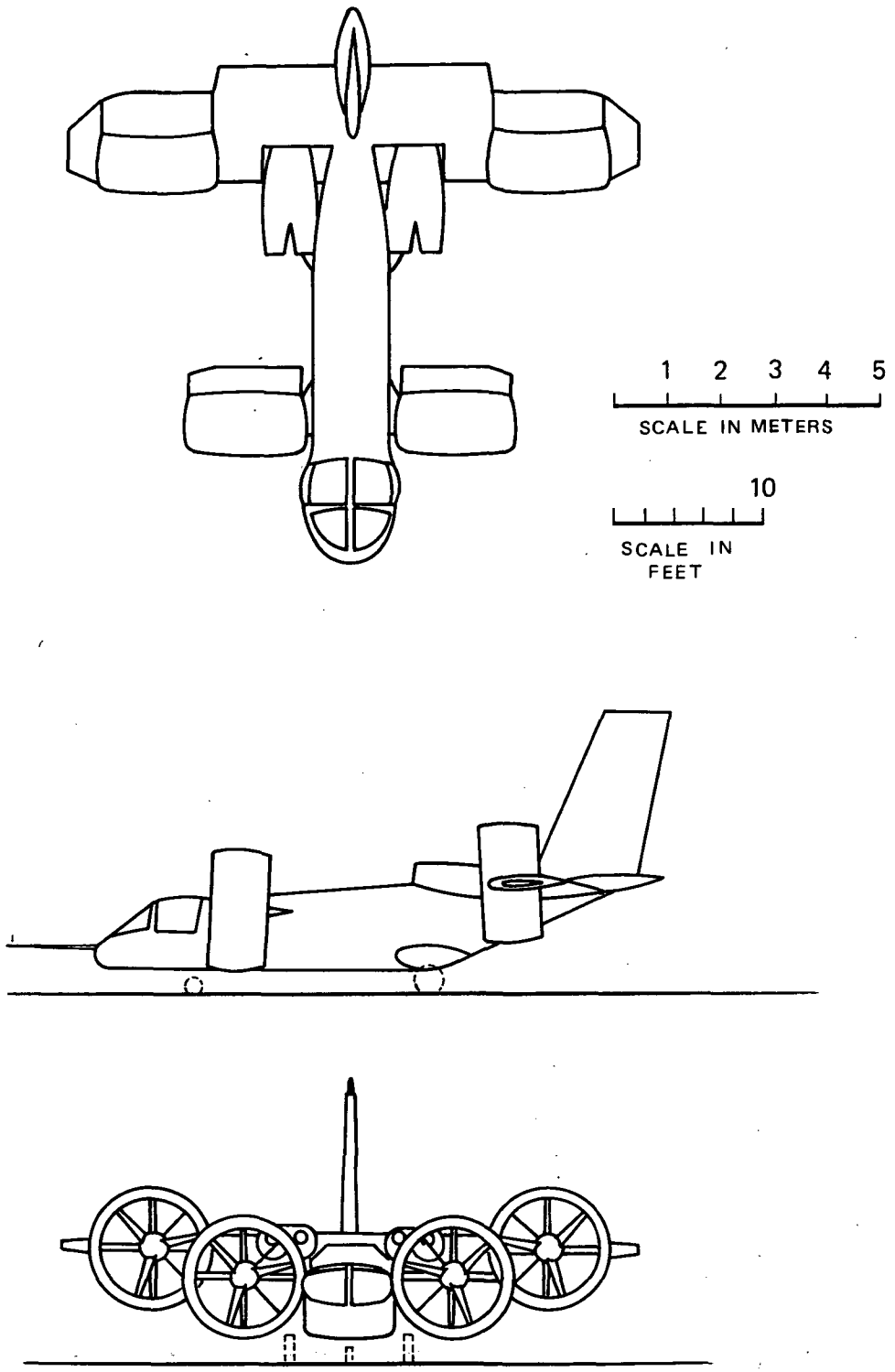

Figure 28. - Three-View Drawing of Bell X-22A Tilt-Duct V/STOL Aircraft

Reference 15 presents data on the pitch roll and yaw rate damping provided by the S.A.S. As indicated in Appendix B, for the 'S.A.S. on' cases, the derivatives were augmented by factors proportional to the rate feedbacks so that the calculated transfer functions include the effects of the S.A.S. Appendix B presents derivatives for 'S.A.S. on' and 'S.A.S. off' conditions.

To validate the derivatives, the measured periods, damping, and dutch roll φ/β ratio given in the flight test data of Reference 15 were compared with the values obtained from the transfer functions. The results are indicated in Figure 29, which shows reasonable agreement between the predicted and measured characteristics. It would have been preferable to compare the predicted and measured characteristics at identical flight conditions. This was not possible, because Reference 15 only includes data for perturbations from steady level flight, whereas the derivatives of Reference 31 are applicable to steady descent, except at 130 knots and hover. A further difference between References 15 and 31 is that the data of Reference 31 are calculated for sea level, whereas the flight tests of Reference 15 were made at altitudes between 3,800 and 5,000 feet. Longitudinal periods and damping ratios computed using the data of Reference 31 did not agree with the flight test data of Reference 15. It is possible that this discrepancy is merely the result of the difference in flight conditions; however, it was decided not to include the longitudinal data in Appendix B because of the possibility that these data may be inaccurate.

Reference 31 does not present derivatives for level flight at the same airspeeds used in descent, and such data were not available from other sources. Hence, no systematic comparison of the effect of descent on the transfer functions was made. The implications of the X-22A transfer functions for terminal guidance are described in the next chapter.

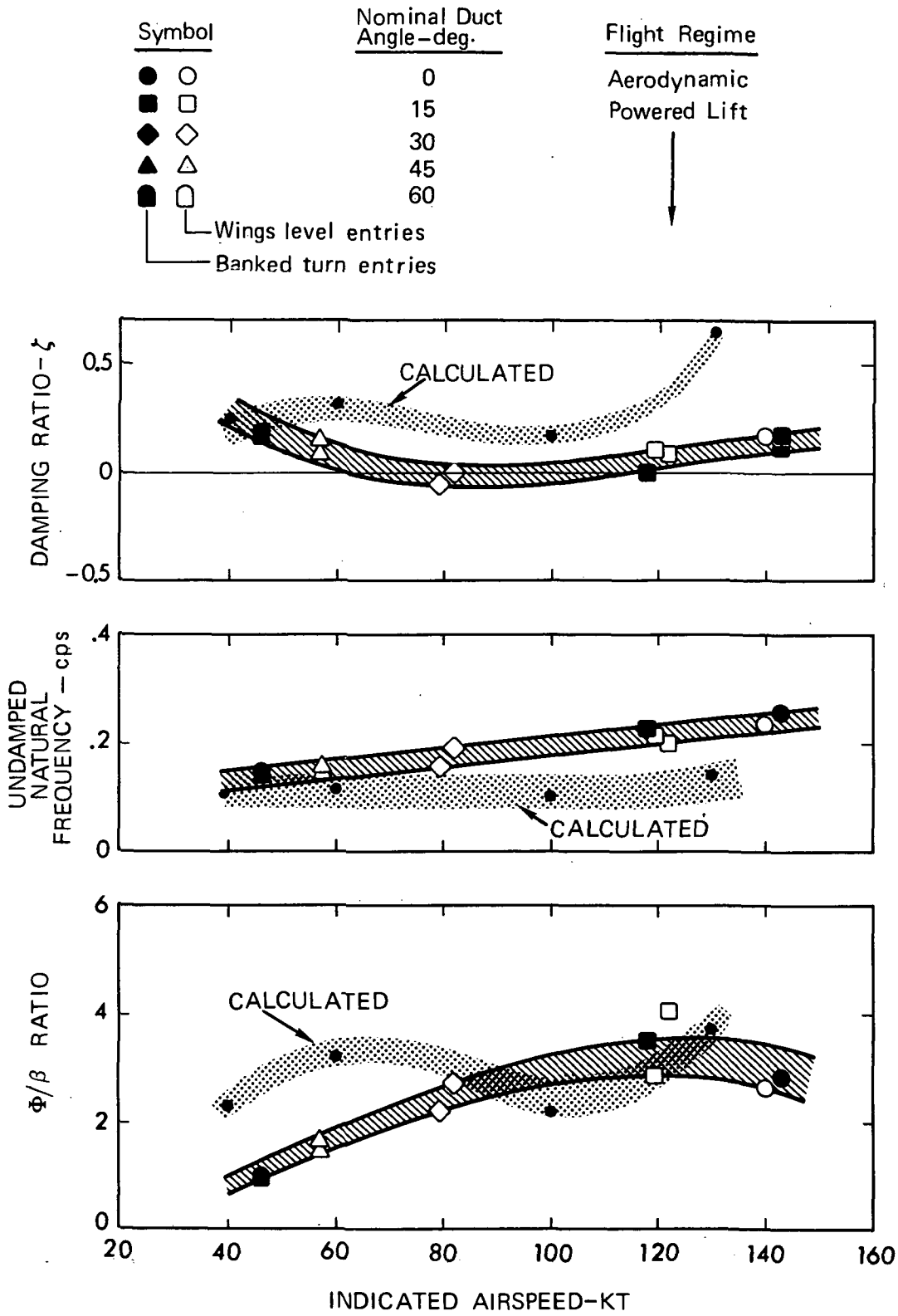

Figure 29. - Dynamic Lateral-Directional Stability (Dutch Roll) For X-22A with S.A.S. On. Gross Weight Range 14,500 to 15,000 lb. Presure Altitude Range 3,800 to 5,000 ft.

CHAPTER V

PREDICTION OF THE BEST ACCURACY ACHIEVABLE FOR V/STOL TERMINAL GUIDANCE

Introduction and Summary

The problem of controlling an aircraft to fly as closely as possible to some desired flight path, in the presence of gusts, is analogous to the problem of designing a filter network which reproduces a signal as closely as possible in the presence of noise. The latter problem was solved by N. Wiener (Reference 32) for the case of stationany random signal and noise, with subsequent extensions by J. F. Newton and R. E. Kalman for deterministic inputs, and time-varying signal and noise (References 33, 34). In this section, we apply Wiener's results to the V/STOL terminal guidance problem. We show that a key factor governing the accuracy with which a given nominal flight profile can be followed is the presence of right-half-plane zeros in the numerator of the appropriate transfer function. Such "nonminimum phase" zeros can seriously degrade the accuracy of the vehicle-plus-guidance system.

With a pilot in the loop, additional nonminimum phase effects are introduced by the pilot's effective time delay τ_e, which can be approximated by a nonminimum phase Pade' expression, $(-s + 2/\tau_e)/(s + 2/\tau_e)$, in the Laplace transform domain.

In this Chapter we first present some results derived from optimal control theory. These are:

(1) a formula for the optimum controller transfer function, for a given airplane and given gust characteristics

(2) a simple expression for the mean square gust response of the airplane-plus-optimum controller combination. This

is the minimum possible gust response achievable with the given airplane in the specified gust environment.

Next a simple example is given to illustrate the use of these formulas. The applicability of optimal control theory to a typical V/STOL aircraft terminal guidance situation is then discussed. Some examples of the optimum gust response obtainable with the CL-84 and X-22A are then presented to illustrate the effects of nonminimum phase and time delay characteristics on the accuracy obtainable in various gust environments. It is shown that, unless special precautions are taken in S.A.S. design, the accuracy obtainable in V/STOL terminal guidance systems may be unsatisfactory.

Transfer Function and Mean Square Error of an Optimal Regulator

Figure 30 illustrates the regulator* configuration considered here. In Figure 30, a "plant" or "vehicle" having a transfer function $P\bar{Q}$ is controlled by a single control, δ. The plant transfer function is assumed to be stable, and P includes the gain, all the numerator factors with left-half-plane roots, and all the denominator factors. $\bar{Q}$ is the product of all the numerator factors with right-half-plane roots. For a minimum phase plant, $\bar{Q} = 1$. For example, for a plant with a transfer function $P\bar{Q} = 5(s - 1)(s + 3)/(s + 2)(s + 4)(s + 7)$, the factors P and $\bar{Q}$ are: $\bar{Q} = s - 1$, $P = 5(s + 3)/(s + 2)(s + 4)(s + 7)$.

---

*"Regulator" is standard control system terminology for a system in which the only inputs are 'unwanted' inputs, such as gusts. If a command input were added, as in tracking a maneuvering target, the system would be called a 'tracking' or 'following' system.

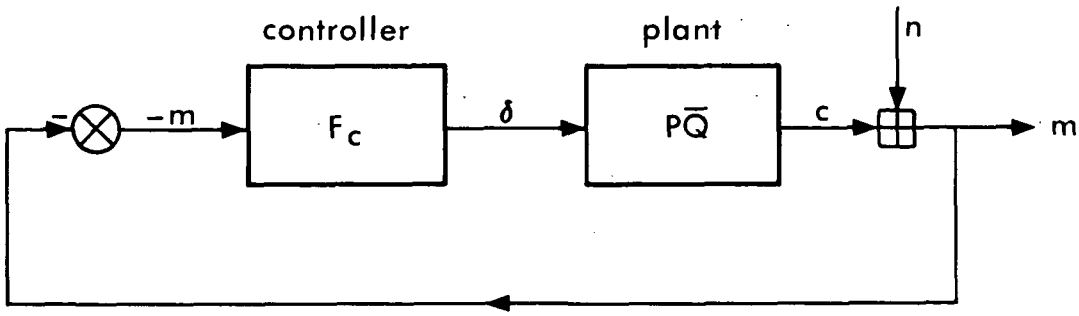

Figure 30. - Regulator Block Diagram

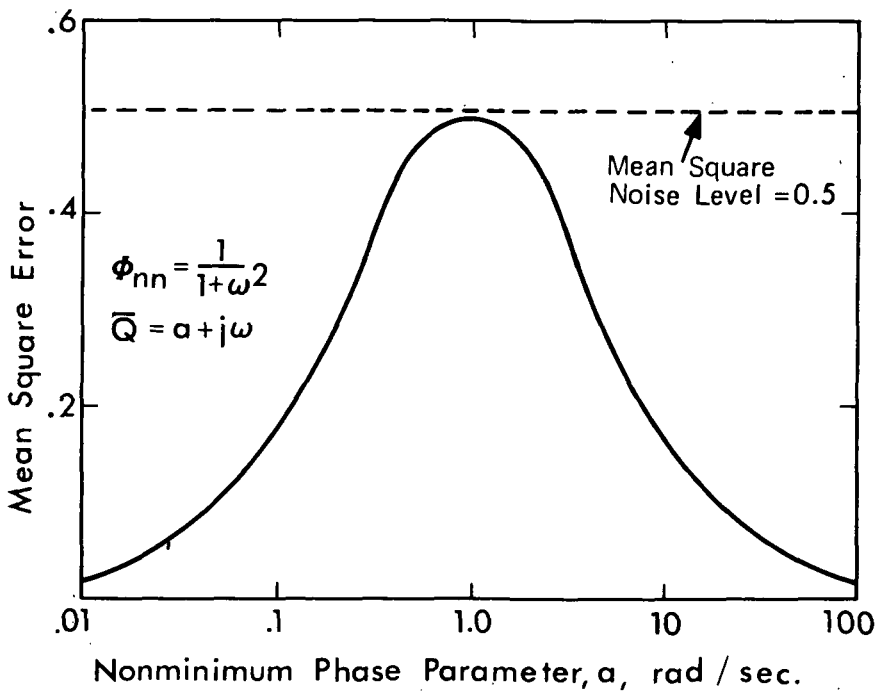

Figure 31. - Effect of Nonminimum Phase Transfer Function on Mean Square Error

In Figure 30 the system is forced by a noise n, and responds by producing an output c, which sums with n to give a total system "error" m. This quantity is called the "error" because it represents the deviation of the system from the desired unperturbed state. The problem is to find the transfer function of the feedback controller F_c which will produce a δ yielding the minimum value of some specified performance index, which is a function of m. Here we shall assume that n is a stationary random noise,* and the appropriate quantity to be minimized is the mean square value of m, denoted by $\overline{m^2}$.

It is important to note that the performance criterion chosen here places no penalty on the magnitude of the controller deflection, δ. This is in contrast to previous studies of the application of optimal regulator theory to aircraft, e.g., References 31, 36 and 37. These references employ a performance criterion of the form: minimum $(\overline{m^2} + k\overline{\delta^2})$, where k is a positive weighting constant. It is frequently asserted that k must be included to obtain a meaningful optimum system, i.e., if k is allowed to go to zero the optimum regulator will be an ultra-fast-responding system with infinite feedback gain, requiring infinitely large control deflections, and producing zero error. This assertion is true only if the plant contains no nonminimum phase or time delay elements. For V/STOL aircraft such elements are always present, either in the aircraft transfer function or in the dynamics of the control system. As will be shown, the simpler performance criterion, minimum $\overline{m^2}$, gives meaningful results and, by definition, yields a system which has a smaller mean square error then any other system.

---

*The solution for a deterministic n can be obtained simply from the solution presented here, through the use of the "transient analog" (Reference 35). For the deterministic case the performance index is $\int_0^\infty m^2 dt$.

For the system of Figure 30; from Reference 2, the transfer function giving minimum mean square response $\tilde{m}^2$ to a stationary random noise, n, is:

$$\frac{M(j\omega)}{N(j\omega)} = 1 - \frac{\bar{Q}}{Q} \cdot \frac{1}{\Phi_{nn}^{+}} \left[\frac{Q}{\bar{Q}} \Phi_{nn}^{+} \right]_{+} \tag{41}$$

where $M(j\omega)/N(j\omega)$ denotes the transfer function written as a function of $j\omega$ rather than the more general Laplace transform complex variable $s = \sigma + j\omega$.

Φ_{nn} is the noise power spectrum

Φ_{nn}^{+} is the factor of Φ_{nn} containing all the left-half plane complex poles and zeros

$\left[\cdot \right]_{+}$ denotes the expansion in partial fractions of the quantity within the braces omitting partial fractions with right-half plane poles

Q is the complex conjugate of $\bar{Q}$, the product of the nonminimum phase factors of the plant transfer function.

Example of calculation of optimum regulator transfer function.

For the system of Figure 30, let the noise power spectrum be

$$\Phi_{nn} = \frac{1}{1 + \omega^2} = \frac{1}{(1 + j\omega)(1 - j\omega)} \tag{42}$$

Let the nonminimum phase factor be

$$\bar{Q} = a - j\omega \tag{43}$$

where, for the purpose of this example, a is variable. From Eq. (42) the left-half plane factor of Φ_{nn} is;

$$\Phi_{nn}^{+} = \frac{1}{1 + j\omega} \tag{44}$$

Combining Eqs. (43) and (44)

$$\frac{Q}{\bar{Q}} \Phi_{nn}^{+} = \frac{a + j\omega}{(1 + j\omega)(a - j\omega)} = \frac{a - 1}{a + 1} \cdot \frac{1}{1 + j\omega} + \frac{2a}{1 + a} \cdot \frac{1}{a - j\omega} \tag{45}$$

Expanding into partial fractions and retaining only the left-half-plane factors

$$\left[\frac{Q}{\bar{Q}} \Phi_{nn}^{+}\right]_{+} = \frac{a - 1}{a + 1} \cdot \frac{1}{1 + j\omega} \tag{46}$$

Substituting from Eqs. (45) and (46) in Eq. (41) the optimum transfer function reduces to

$$\frac{M(j\omega)}{N(j\omega)} = 1 - \frac{a - 1}{a + 1} \cdot \frac{a - j\omega}{a + j\omega} \tag{47}$$

It is of interest to interpret Eq. (47), the overall system transfer function, in terms of F_c the optimum controller. From Figure 30, the system output, c, is related to the error, m by:

$$\frac{C(j\omega)}{M(j\omega)} = 1 - \frac{N(j\omega)}{M(j\omega)} \tag{48}$$

Hence the optimum controller transfer function is:

$$F_c = \frac{1}{P} \cdot \frac{1 - a}{1 + a} \cdot \frac{1}{a + j\omega} \tag{49}$$

In practice, P must have more poles than zeros. To make F_c satisfy this practical requirement it is necessary to introduce arbitrary high frequency poles. Provided these are located beyond the noise bandwidth, the increase in mean square error is negligible. Thus Eq. (47) can be used to find a lower bound on system mean square error which can be very closely approached by practical systems.

Example of calculation of mean square error. - It is instructive to calculate the performance of the optimum system, varying the non-minimum phase characteristics of the plant. The mean square error is given by the integral of the error power spectrum as:

$$\widetilde{m^2} = \frac{1}{2\pi j} \int_{-j\infty}^{j\infty} \Phi_{mm}\, dj\omega = \frac{1}{2\pi j} \int_{-j\infty}^{j\infty} \frac{M(j\omega)}{N(j\omega)} \frac{M(-j\omega)}{N(-j\omega)} \Phi_{nn}(\omega)\, dj\omega \tag{50}$$

For the above example, from Eq. (47)

$$\frac{M(j\omega)\, M(-j\omega)}{N(j\omega)\, N(-j\omega)} = 1 + \frac{1 - a}{1 + a} \left\{ \frac{a - j\omega}{a + j\omega} + \frac{a + j\omega}{a - j\omega} \right\} + \frac{(1 - a)^2}{(1 + a)^2}$$

$$= \frac{4a^2 + 4a^2\omega^2}{(1 + a)^2 (a^2 + \omega^2)} \tag{51}$$

Hence,

$$\widetilde{\widetilde{m^2}} = \frac{1}{2\pi j} \int_{-j\infty}^{j\infty} \frac{4\,a^2}{(1+a)^2} \cdot \frac{1}{a^2+\omega^2}\, d(j\omega) \qquad (52)$$

Integrals of the above kind can be readily evaluated from the tables given in Appendix E of Reference 33, or by summing the left-half-plane residues of Φ_{mm}. The result is:

$$\widetilde{\widetilde{m^2}} = \frac{2a}{(1+a)^2} \qquad (53)$$

Eq. (53) is graphed in Figure 31. Note the remarkable degradation in performance that occurs as the magnitude of the nonminimum phase zero approaches the input break frequency. By contrast, when the zero is either very 'close-in' or very 'far-out' the performance loss is less significant.

The mechanism of the performance loss can be understood by considering Figure 32. This illustrates the step response of a simple system with a nonminimum phase zero compared with the same system with the sign of the zero switched, (i.e., made minimum phase). The transfer function of the system is

$$\frac{C(s)}{R(s)} = \frac{1 + s/\lambda}{1 + s^2} \quad \text{where } \lambda = +1, \text{ or } -1 \qquad (54)$$

For the nonminimum phase condition $\lambda = -1$, and the transient response moves in the "wrong" direction for the first 1.5 seconds. One can see intuitively that a random signal made up of a series of steps of equal magnitude, but switching sign with an average frequency of about 1.5 seconds, would be difficult to follow because of the nonminimum phase zero causing the initial response to be "wrong-way".

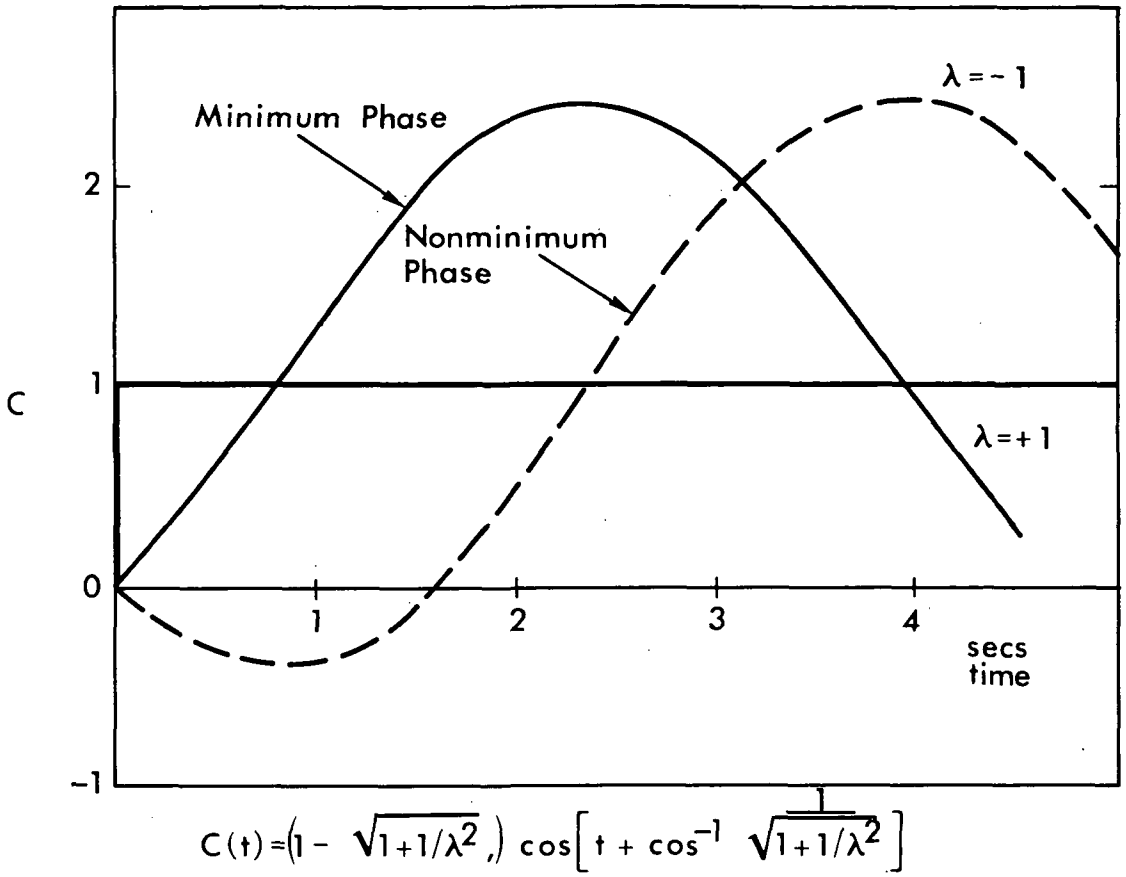

Figure 32. - Effect of Nonminimum Phase Characteristics on Step Response of a Second Order System

The above reasoning explains the "worst case" situation in Figure 31, where, with a = 1, the mean square error is equal to the mean square noise. This implies that the optimum feedback is zero! This astonishing result can be explained as follows. For low frequency noise, the optimum F_c has positive DC gain. For high frequency noise, the optimum F_c has negative DC gain because of the initial "wrong-way" response (e.g., Figure 32). For some intermediate noise, the optimum F_c gain is zero.

A Simple Formula for the Mean Square Error of an Optimal Regulator

The calculation of the mean square error of optimal regulator systems becomes very simple through the use of the formula derived below. As will be shown later, the formula indicates how the minimum achievable mean square error is affected by aircraft characteristics such as short-period and phugoid frequency and damping, dutch roll root locations, etc.

From Eqs. (41) and (50), the ratio of error and noise power spectra is:

$$\frac{\Phi_{mm}}{\Phi_{nn}} = \left\{1 - \frac{\bar{Q}}{Q}\frac{1}{\Phi_{nn}^{+}}\left[\frac{Q}{\bar{Q}}\Phi_{nn}^{+}\right]_{+}\right\}\left\{1 - \frac{Q}{\bar{Q}}\frac{1}{\Phi_{nn}^{-}}\left[\frac{\bar{Q}}{Q}\Phi_{nn}^{-}\right]_{-}\right\} \tag{55}$$

where $\left[\ \ \right]_{-}$ denotes the expansion in partial fractions of the term within the braces omitting partial fractions with left-half-plane poles. Note that in Eq. (55), the second term in $\{\ \}$ is merely the complex conjugate of the first.

Rearranging Eq. (54),

$$\frac{\Phi_{mm}}{\Phi_{nn}} = \left\{ \frac{\frac{Q}{\bar{Q}} \Phi_{nn}^{+} - \left[\frac{Q}{\bar{Q}} \Phi_{nn}^{+} \right]_{+}}{\frac{Q}{\bar{Q}} \Phi_{nn}^{+}} \right\} \left\{ \frac{\frac{\bar{Q}}{Q} \Phi_{nn}^{-} - \left[\frac{\bar{Q}}{Q} \Phi_{nn}^{-} \right]_{-}}{\frac{\bar{Q}}{Q} \Phi_{nn}^{-}} \right\}$$

$$= \left\{ \frac{\left[\frac{Q}{\bar{Q}} \Phi_{nn}^{+} \right]_{-}}{\frac{Q}{\bar{Q}} \Phi_{nn}^{+}} \right\} \quad \left\{ \frac{\left[\frac{\bar{Q}}{Q} \Phi_{nn}^{-} \right]_{+}}{\frac{\bar{Q}}{Q} \Phi_{nn}^{-}} \right\} \tag{56}$$

Writing $\Phi_{nn} = \Phi_{nn}^{+} \Phi_{nn}^{-} \frac{Q}{\bar{Q}} \frac{\bar{Q}}{Q}$, and integrating Eq. (56) yields the desired formula

$$\overline{\tilde{m}^2} = \frac{1}{2\pi j} \int_{-j\infty}^{j\infty} \Phi_{mm} \, dj\omega = \frac{1}{2\pi j} \int_{-j\infty}^{j\infty} \left[\frac{Q}{\bar{Q}} \Phi_{nn}^{+} \right]_{-} \left[\frac{\bar{Q}}{Q} \Phi_{nn}^{-} \right]_{+} dj\omega \tag{57}$$

In most applications $\bar{Q}$ consists of only a single nonminimum phase factor, hence the evaluation of $\left[\frac{Q}{\bar{Q}} \Phi_{nn}^{+} \right]_{-}$ requires only the calculation of a single residue.

Example of the use of Eq. (67).- To swiftly calculate the mean square error of the simple example given above, note that in Eq. (45),

$$\left[\frac{Q}{\bar{Q}} \Phi_{nn}^{+} \right]_{-} = \frac{2a}{1 + a} \cdot \frac{1}{a - j\omega} \tag{58}$$

Hence the error power spectrum is immediately found as:

$$\Phi_{mm} = \frac{4\,a^2}{(1+a)^2} = \frac{1}{(a-j\omega)(a+j\omega)} \qquad (59)$$

The mean square error can be found as before from the integral tables of Reference 33 or by summing left-half-plane residues of Φ_{mm}.

Applicability of Wiener Regulator Theory to V/STOL Control

From the above discussion, it appears plausible that nonminimum phase may cause significant inaccuracy in V/STOL aircraft control. To explore this in more detail, it is necessary to check that the underlying assumptions of Wiener optimization are valid for the V/STOL control problem. Let us therefore review the points of difference between the regulator and an actual aircraft.

It is immediately apparent that a number of features distinguish the V/STOL airplane in a gust environment from the Wiener optimum regulator outlined above. These include

(1) The aircraft transfer function and the gust input spectra may be time-varying as the aircraft decelerates through transition.

(2) The aircraft may be unstable.

(3) The aircraft dynamics may contain nonlinearities.

(4) More than one noise may be applied (e.g., horizontal and vertical gust components).

(5) The aircraft has several degrees of freedom and two or more lateral and longitudinal controls.

As will be shown below, none of these features invalidates the use of Wiener theory, though some mathematical complications may arise.

Nonstationary inputs and aircraft dynamics. - Nonstationary inputs can be handled by an extension of Wiener's theory due to Kalman (Reference 34). For the stationary case, with constant airplane dynamics, the Kalman optimal system is equivalent to the Wiener system. Here, we shall consider stationary conditions only, assuming that the gust spectra are not functions of time. Furthermore, the "frozen-point" representations of aircraft dynamics will be employed. To justify these assumptions, note that

(1) The forms of gust spectrum commonly used have frequency characteristics which depend on the ratio of h_g/V. Thus, as height and speed are lost during an approach, the frequency characteristics of the spectrum remain approximately constant.

(2) The frozen-point (constant coefficient) approximation to time-varying airplane dynamics is valid provided the deceleration is small. For V/STOL aircraft, the combined descent plus deceleration capability is limited to small values by limits on drag, since, from Eq. (1)

$$\frac{dV}{dt} = g \sin(-\gamma) - \left(\frac{D}{L}\right) g \cos(-\gamma) \qquad (60)$$

Typically, for V/STOL approach conditions, $(D/L)_{max} = 0.25$ Thus, particularly for descending flight, the available deceleration is small, and it is legitimate to use the frozen-point approximation.

Instability of the aircraft. - At low speeds most V/STOL aircraft are unstable without stability augmentation. To apply Wiener theory to either a human or an automatic controller, one must assume that the controller is capable of stabilizing the aircraft. Note however, that although the controller stabilizes the aircraft, it may also degrade the performance of the overall system through the introduction of nonminimum phase effects or transportation lags in the controller.

Nonlinearities. - For stationary Gaussian inputs, the Wiener system gives a closer approximation to the desired response than any other system, linear or nonlinear.* Therefore, no advantage is gained by deliberately introducing nonlinearities. Linear representation of the basic airframe dynamics is standard practice for V/STOL aircraft, though it can only be strictly justified by appealing to test data on the specific configuration under consideration. An examination of the validity of linear representation for the Vertol VZ-2 tilt-wing aircraft and the Doak VZ-4 tilt-duct aircraft is given in Reference 7. For the CL-84 and X-22A considered here, the flight test correlations presented in Chapter IV indicate that the linear representations are of adequate accuracy for small perturbations.

Different points of application of signal and noise. - The system block diagram used in Figure 32 was intentionally simple, in order to present the Wiener formulas clearly. "Real-life" flight control systems require more complicated block diagrams, but the Wiener formulas can still be applied, after performing suitable block diagram algebra. In many instances, this has already been done in the literature (e.g., Reference 2). With such manipulations one could consider internal system noise, such as human pilot remnant, in addition to u-gusts and w-gusts.

---

* For a proof of this, see Reference 35.

Multiloop control. - Historically, Wiener optimization has been used for single-loop control, with Kalman optimization reserved for multi-loop situations. The two approaches are compared in Reference 38, where it is shown that the Kalman and Wiener systems are identical for stationary inputs. Whitbeck (Reference 37) has shown that the Wiener formulation can readily be extended to the multiloop case. This approach is attractive for our purposes, since it uses aircraft transfer functions rather than the state-variable equations required by the Kalman formulation hence, nonminimum phase effects can be more readily detected.

Optimal Control of the CL-84

This section presents calculations of the minimum achievable mean square height error of the CL-84 performing a steep approach under gusty conditions. The purpose of these calculations is:

(1) to demonstrate the application of the Wiener optimal regulator theory to a practical situation

(2) to determine the best performance obtainable with single-axis control

(3) to explore possible improvements through multiloop control

The assumed gust spectrum consists of u and w components, uncorrelated with each other, each having a power spectrum of the form suggested in Reference 39, slightly modified to remove steady-state gust components.

$$\Phi_{w_g w_g} = \frac{\overbrace{(w_g^2)}\, 2\,\omega_b}{(j\omega + \omega_b)(-j\omega + \omega_b)} \left\{ \frac{(j\omega)(-j\omega)}{(j\omega + .001)(-j\omega + .001)} \right\} \qquad (61)$$

where $\overbrace{w_g^2}$ is the mean square gust intensity

ω_b is the gust break frequency in rad/sec.

The choice of $\widetilde{w_g^2}$ is arbitrary here, since the mean square height error, $\widetilde{h_e^2}$, will be normalized by division by $\widetilde{w_g^2}$. The gust break frequency ω_b will be varied parametrically to show the effect of ω_b on $\widetilde{h_e^2}$. Note, however, that Reference 39 suggests that $\omega_b = (3/2)(V_A/h_g)$ where h_g is the altitude. This relationship is graphed in Figure 33 to illustrate the tendency for ω_b to remain relatively constant during the approach, as speed and height are both lost.

Initially, choose a r.m.s. gust intensity of 3.0 fps, $V_A = 42$ knots, and a gust break frequency of 0.204 rad/sec, which corresponds to an altitude of approximately 500 feet. The CL-84 gust response transfer function at 42 knots and 960 fpm rate of descent, with S.A.S. off, is

$$\frac{h_e}{w_g} = \frac{-.202\ (s + .0965 \pm .7014j)\ (s + .6751)}{s\,(s + .0177 \pm .244j)\ (s + .504 \pm .9407j)} \qquad (62)$$

The transfer function relating height error to collective pitch is tabulated in Appendix A as

$$\frac{h_e}{\theta_o} = \frac{-112.0\ (s - .0916)\ (s + .477 \pm 1.03j)}{s(s + .0177 \pm .244j)\ (s + .504 \pm .9407j)} \qquad (63)$$

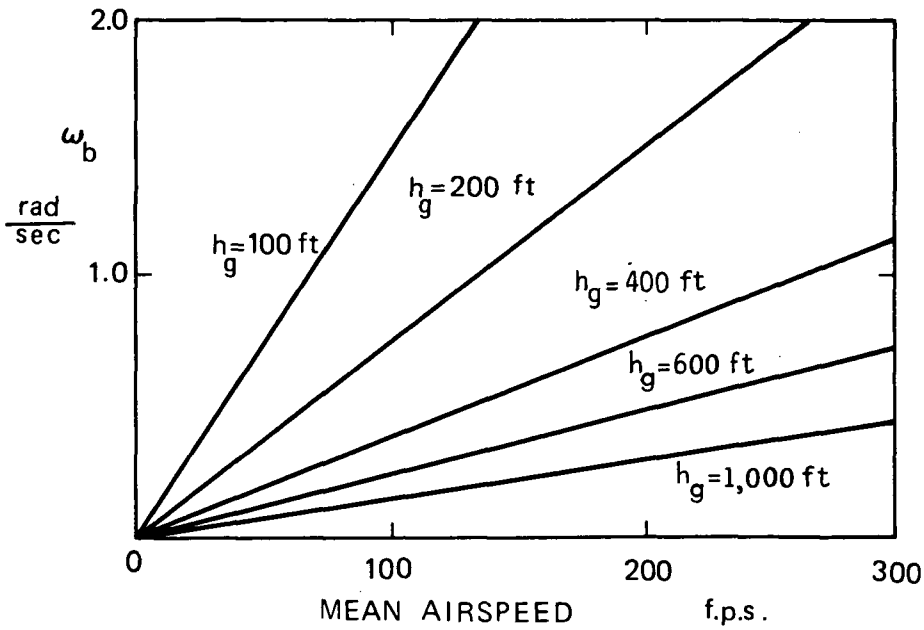

Figure 33. - Gust Spectrum Break Frequency as a Function of Airspeed and Altitude

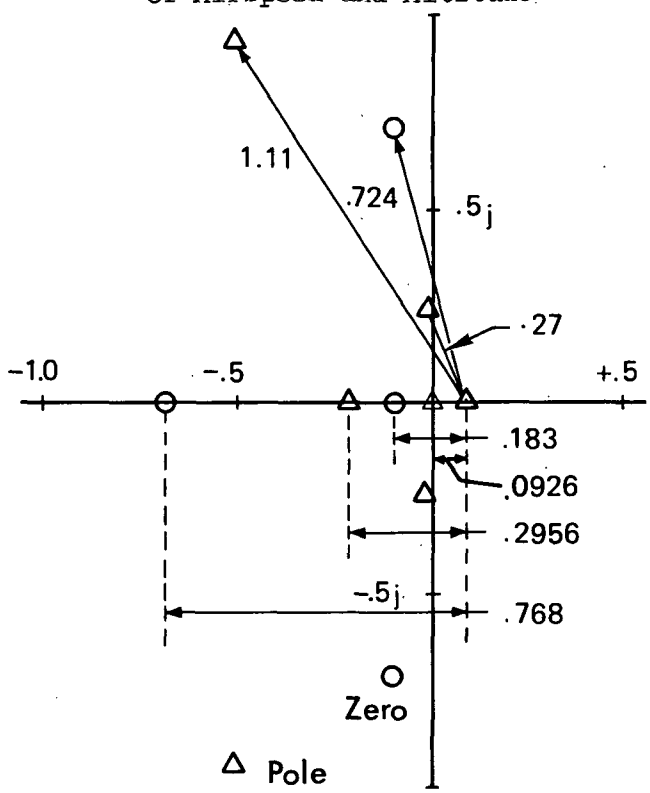

Figure 34. - Graphical Representation of Evaluation of Right-Half Plane Residue

Substituting in Eq. (57),

$$\frac{Q}{\bar{Q}}\,\Phi_{nn}^{+} = \left(\frac{j\omega + .0916}{j\omega - .0916}\right)\left(\frac{3\sqrt{.408}}{j\omega + .204}\right)\left(\frac{1}{j\omega + .001}\right)$$

$$\times \frac{(-.202)\,(j\omega + .0965 \pm .7014j)\,(j\omega + .6751)}{(j\omega + .0177 \pm .244j)\,(j\omega + .504 + .9407j)} \qquad (64)$$

$$\left[\frac{Q}{\bar{Q}}\,\Phi_{nn}^{+}\right]_{-} = \frac{-.385\,(j\omega + .0916)\,(j\omega + .0965 \pm .7014j)\,(j\omega + .6751)}{(j\omega + .204)\,(j\omega + .0177 \pm .244j)\,(j\omega + .504 + .9407j)(j\omega + .001)}$$

evaluated at $j\omega = +.0916$

$$\times \frac{1}{j\omega - .0916} \qquad (65)$$

It is instructive to evaluate Eq. (65) graphically by drawing vectors from each pole and zero to the $\bar{Q}$ zero, as shown in Figure 34. This indicates the relative contribution of each pole and zero to the total response.

$$\left[\frac{Q}{\bar{Q}}\,\Phi_{nn}^{+}\right]_{-} = \frac{(.385)\,(.724)^2\,(.768)\,(.183)}{(.0926)(.27)^2\,(1.11)^2\,(.2956)(j\omega - .0916)} = \frac{11.8}{(j\omega - .0916)} \qquad (66)$$

The mean square height error is evaluated either from the integral tables of Reference 33, or by calculating the sum of the left-half-plane residues of the height error spectrum.

$$\Phi_{h_e h_e} = \frac{(11.8)^2}{(j\omega - .0916)\,(-j\omega - .0916)} = \frac{(11.8)^2/(2)(.0916)}{j\omega + .0916} + \frac{(11.8)^2/(2)(.0916)}{-j\omega + .0916} \qquad (67)$$

$$\widetilde{\widetilde{h_e^2}} = (11.8)^2/(2)(.0916) = 768 \text{ ft}^2 \qquad (68)$$

The above optimum response calculation has been reworked for a range of gust break frequencies, keeping the same r.m.s. gust amplitude, 3.0 fps, and the results are shown in Figure 35. This figure shows that for the expected range of gust break frequencies, the r.m.s. height error cannot be reduced much below 25 feet. Thus, even the optimal control is relatively ineffective, because of the nonminimum phase aircraft transfer function.

It is instructive to compare the optimum gust response with that of the uncontrolled aircraft. The latter can be calculated from Equations 61 and 62, and is also graphed in Figure 35. Because of the large low frequency component of the gust spectrum, the height error response is very large. It would be infinite, if the spectrum did not include the terms enclosed in $\{\}$ in Equation (61). Thus, comparison of the height error responses of the optimum and uncontrolled systems is not too meaningful. It is better to compare the corresponding r.m.s. values of dh_e/dt, the height error rate. This is done in the lower half of Figure 35. Note that $(dh_e/dt)_{r.m.s.}$ for the optimum system is typically about 40 percent of the control-fixed $(dh_e/dt)_{r.m.s.}$ This percentage shows that only limited improvement in the gust response is possible through the use of collective pitch alone.

It is of interest to compare the effects of u-gusts with the w-gust effects calculated above. The transfer function relating height-error to u-gusts for the CL-84 at 42 knots and 960 f.p.m. descent is:

$$\frac{h_e}{u_g} = \frac{-.2439\ (s + .2927 \pm .7577j)}{(s + .0177 \pm .244j)\ (s + .504 \pm .9407j)} \qquad (69)$$

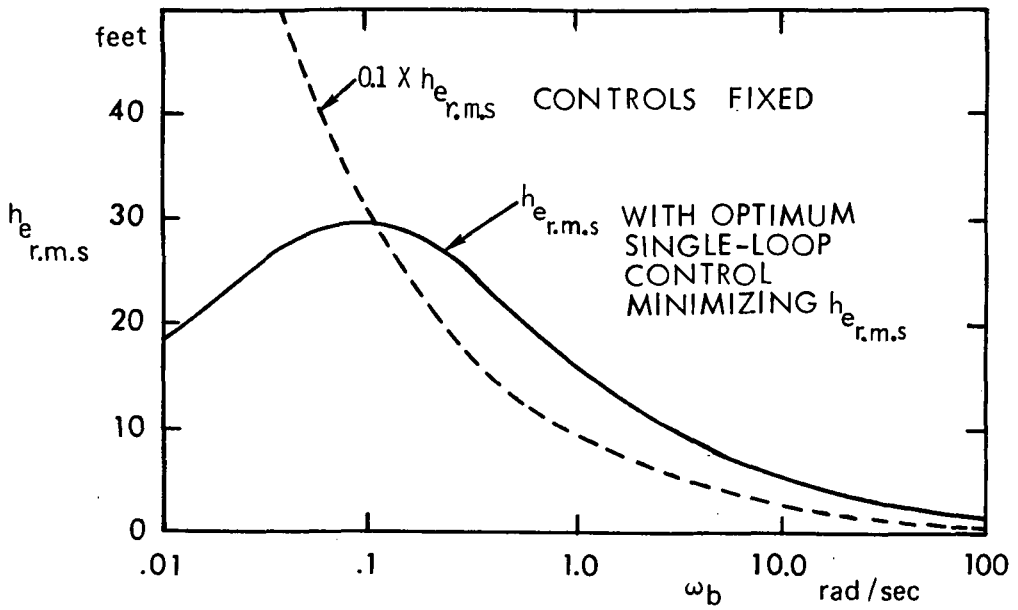

NOTE: r.m.s GUST AMPLITUDE = 3.0 fps FOR ALL BREAK FREQUENCIES

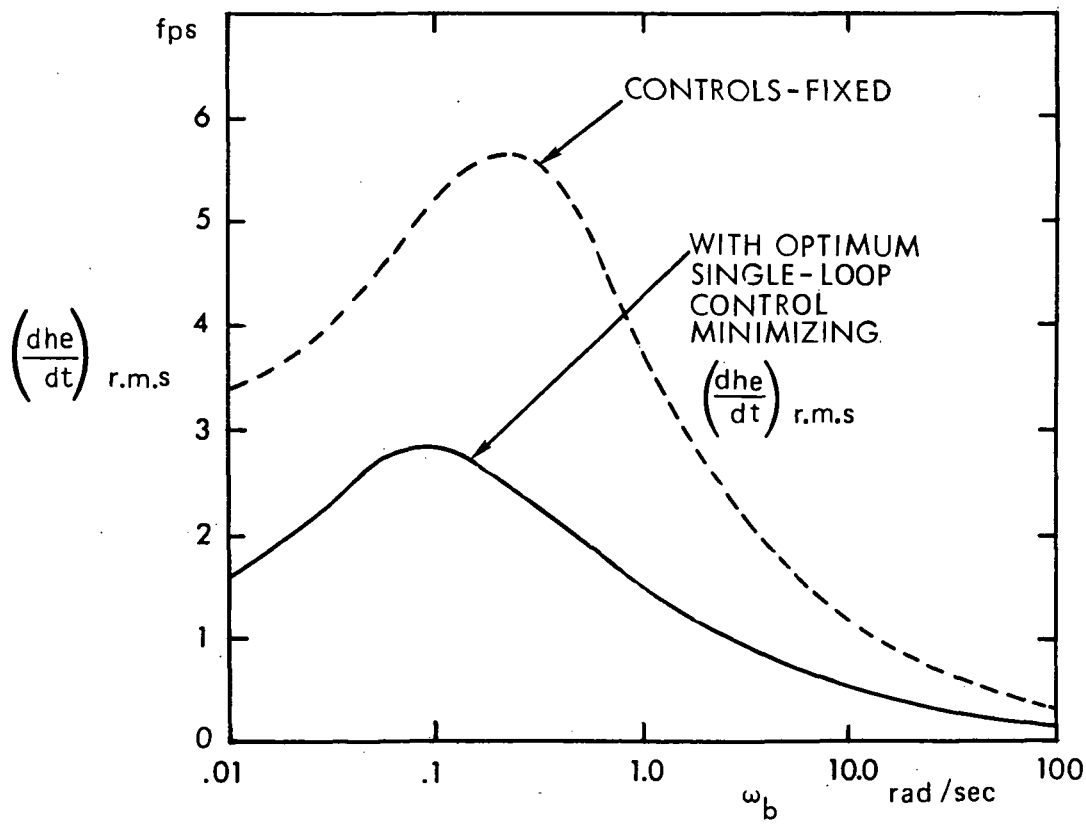

Figure 35. Effect of Gust Break Frequency on Minimum Achievable Gust Response with Optimum Single-Loop Control

With zero feedback, and a u-gust spectrum identical to the w-gust spectrum, the r.m.s. height error is 13.2 feet, as compared with 211.0 feet due to w-gusts of the same 3.0 fps r.m.s. intensity. With optimal feedback the r.m.s. height error reduces to 5.4 feet. These numbers apply for a gust break frequency of 0.204 rad/sec. With this break frequency the aircraft, therefore, responds less to u-gusts than w-gusts.

Alternative control techniques. - The height error levels indicated above may be unacceptable for approaches in a gusty environment, i.e., large r.m.s. values of u-gust and w-gusts. Hence, consideration must be given to alternative methods of control. Two possible alternatives are

(1) control of height error through feedbacks to pitch attitude control

(2) multiloop feedbacks involving pitch attitude and collective propeller pitch control.

The first alternative appears unattractive because of the presence of some badly placed right-half-plane zeros in the h/δ_e transfer function. These zeros are present even in level flight, because the aircraft is flying below its minimum drag speed. For example, at 42 knots in level flight, from Appendix A

$$\frac{h_e}{\delta_e} = \frac{7.28\,(s - 0.219)\,(s - 2.23)\,(s + 3.12)}{s(s + .0122 \pm .217j)\,(s + .525 \pm .936j)} \qquad (70)$$

The zero at 0.219 rad/sec is virtually coincident with the assumed gust break frequency at 0.204 rad/sec. As shown in Figures 31 and 35 this represents the worst possible situation.

Turning to multiloop control, one would expect that, since the excessive height error stems from the right-half-plane zero in the

h_e/θ_o transfer function, it would be advantageous to use a S.A.S. feedback to pitch attitude control that would remove this zero. This can be done with the CL-84 S.A.S. system, which incorporates both attitude and rate feedback to the pitch attitude control (which is comprised of elevator and horizontal tail propeller collective pitch). At 42 knots and 960 fpm descent, the height error/collective transfer function with S.A.S. on is:

$$\frac{h_e}{\theta_o} = \frac{-112.0\ (s + .05)\ (s + 1.37 \pm .802j)}{s(s + .095 \pm .200j)\ (s + 1.35 \pm .734j)} \qquad (71)$$

Since this is minimum phase it might appear that the height error of the optimum system would be zero. In practice, this is not so, since some allowance must be made for sensor and actuator lags, plus the time delay of the human pilot, if he is in the loop. For example, adding a 'system' delay of 0.3 seconds, would require the above transfer function to be multiplied by the Pade approximation $(6.67 - s)(6.67 + s)$. This would induce appreciable height error for high frequency gust inputs (e.g., self-induced turbulence due to buffeting). However the system performance will be improved over the single-loop case.

Gust Models. - In this chapter, atmospheric turbulence has been assumed to be stationary and random. The theory developed here shows that the minimum achievable error in following the desired flight path depends as much upon the turbulence spectrum as upon the dynamic characteristics of the aircraft. This indicates the importance of obtaining an accurate model of low altitude turbulence. Data are also needed on self-induced turbulence, due to buffeting, which may be significant in steep descents, and on vortices trailing from nearby aircraft.

The situation regarding available low altitude turbulence data and analytic models is far from satisfactory. The power spectrum in this report is taken from Reference 34, and dates back to the early 1960's. It was hoped to use a more up-to-date representation of atmospheric turbulence including nonstationary effects. However, the review of recent low altitude turbulence data given in Reference 1 indicates a dearth of reliable experimental data to substantiate more sophisticated models. Until more data are gathered it seems advisable to use one of the older analytic representations of turbulence, such as that of Reference 34, varying the break frequency parametrically to cover a reasonable range of atmospheric conditions. Random wind-shears can be approximated by allowing the break frequency to become small.

Optimal Control of the X-22A Tilt-Duct Aircraft

As has been demonstrated for the CL-84, optimal control theory can be used to pinpoint flight conditions which will pose difficulties for human or automatic control. A right-half-plane zero of similar magnitude to the gust input break frequency, or close to the frequency or inverse time constant of one of the aircraft's characteristic modes, causes an increase in the mean square deviation from the desired flight path. The corollary follows that nonminimum phase zeros that are distant from these critical regions are innocuous. This is well exemplified by the Bell X-22A. The calculated longitudinal and lateral transfer functions are remarkably free of critically located right-half-plane zeros.

For example, at an airspeed of 67.5 fps and a descent angle of 7.1 degrees, the transfer function relating lateral stick deflection to lateral deviation from the unperturbed flight path is:

$$\frac{y}{\delta_A} = \frac{-2.626\ (s + .153)\ (s + 1.915)\ (s - 25.05)}{s\ (s + .167 \pm .659j)\ (s + 1.916)\ (s + 4.318)} \qquad (72)$$

Although this contains a right-half-plane zero, it is located well beyond the break frequency of any plausible atmospheric turbulence. From this consideration one would predict that the X-22A would be capable of accurate lateral tracking, despite the high gust sensitivity due to its large Y_v. This is confirmed by the pilot comments reported in Reference 15.

The reason for the general absence of right-half-plane zeros appears to be connected with the "pure moment" controls used on the X-22A. Because it is supported by four ducts symmetrically located about the c.g., moments can be generated without associated net forces. For example the X-22A can be pitched-up without requiring a net down-load acting on the tail of the aircraft. Thus there is no 'wrong-way' response in controlling height error with longitudinal stick deflection.

Implications of Optimal Control Theory for Other V/STOL Configurations

It has been shown in Reference 40, that aircraft with aft-mounted elevators, flying below the minimum drag speed must have a height/elevator transfer function with two right-half-plane zeros. One zero is of relatively high frequency and does not cause difficulties of control. The other is of low frequency and may be in a critical region, as discussed previously. For V/STOL aircraft it is usual, therefore, to control height by thrust. If the thrust line acts above the c.g., a nose-down pitching moment will occur which may cause a response which ultimately goes in the wrong direction. The CL-84 demonstrates this, as described. This also occurs on the Breguet 941 when the "transparency" method of flight path control is used, whereby the pitch of the outer propellers is decreased to steepen the flight path. The flight tests described in Reference 13 show that, for a few seconds after application of transparency, the flight path angle of the Breguet 941 becomes <u>less</u> steep.

Other nonminimum phase effects have been noted in Reference 1 on single-rotor helicopters, and certain of these effects may also be applicable to tilt-wing configurations. Where these effects exist, application of the optimal control theory described here will be useful in determining the maximum accuracy obtainable in following a given nominal flight path.

CHAPTER VI

CONCLUSIONS AND RECOMMENDATIONS

Conclusions

1. The possible terminal flight paths of most types of V/STOL aircraft are limited by the aircraft's inability to generate the steady aerodynamic forces required for low-speed deceleration and steep descent. Increased drag/lift ratio, without sacrifice of low-speed lifting capability, is required to overcome this limitation.

2. Stability derivatives, and maximum drag/lift ratios for tilt-wing and deflected slipstream aircraft can be predicted if the full-scale power-off characteristics are known. A new method for predicting the maximum drag/lift ratio of general slipstreamed-wing aircraft configurations is presented in this report. The method uses momentum theory, plus power-off data. The method has been applied to the XC-142A tilt-wing aircraft, and gives results which are in reasonable agreement with measured descent boundaries.

3. Descent angle has only a small effect on most of the transfer functions of typical tilt-wing and tilt-duct aircraft, as exemplified by the CL-84 and X-22A. However, there is an important exception to this generalization for the tilt-wing aircraft, relating to control of flight path angle by thrust, at low speeds. For steep descents, a right-half-plane zero appears in this transfer function. This causes the response to move in the wrong direction, after a few seconds. This phenomenon is believed to be a major cause of the difficulty encountered in controlling tilt-wing aircraft to fly steep approaches. The zero can be moved back into the left-half-plane by feeding back pitch rate and pitch angle to the pitch control.

4. The accuracy with which an aircraft can follow a given steep approach path is seriously degraded when the above right-half-plane zero is located near the break frequency of the input gust spectrum. This is demonstrated in this report by calculating the gust response characteristics of the CL-84 in a steep approach at 42 knots airspeed, using thrust control only. For this condition the aircraft is stable, even with the stability augmenter system switched off. It is shown that even with the optimal feedback, the r.m.s. velocity normal to the desired flight path can be reduced only to approximately 40 percent of its value with controls fixed. The effect can be partially removed by stability augmentation using pitch attitude as well as pitch rate feedbacks.

5. A simple formula has been derived for calculating the minimum achievable gust response of a given configuration. This formula gives the r.m.s. deviation from the desired flight path in terms of gust descriptors and parameters relating to lags in the control system and right-half-plane zeros in the aircraft transfer function.

6. The limitations described in this report may seriously restrict the usefulness of certain V/STOL configurations in operating in wind-shears and gusts. Therefore, such limitations should be considered in assessing the performance of V/STOL terminal guidance systems.

Recommendations

1. The results derived in this report have been obtained by considering a limited number of specific aircraft. It is believed that the results are generally applicable to the appropriate configurations, but further work is required to determine whether the results are typical.

2. The method for calculating the descent boundaries of slipstreamed-wing configurations should be extended to provide a parametric study of the effect of configuration geometric parameters on descent/deceleration capability. The possible improvement in maximum drag/lift ratio obtainable through the use of stall-delaying devices such as drooped leading edges, blown flaps, etc., should be assessed.

3. The path-following accuracy obtainable with various practical feedback systems should be studied, using transfer functions specifically calculated for steep descents, plus a representative variety of gust spectra. Investigations should be made of the feasibility of approaching the optimum path-following accuracy, and handling qualities should be predicted, using analytic models of the human pilot.

4. The objectionable right-half-plane zero which occurs in the example tilt-wing aircraft in steep descents should be traced to the geometric and aerodynamic parameters from which it originates. The feasibility of removing this zero through configuration modifications should be explored.

5. Analytic methods of predicting descent boundaries of ducted-fan configurations in terms of power-off characteristics should be developed. This would facilitate rational design to obtain the best possible descent characteristics.

APPENDIX A

CL-84 TRANSFER FUNCTIONS AND DERIVATIVES

Introduction

This Appendix presents calculated stability derivatives and transfer functions for the CL-84. The flight conditions considered are listed in Table 7 of the main text. Transfer functions are presented for all these flight conditions. For brevity, derivatives are given only for flight conditions 1, 6, 9, 13, and 15. The main text also presents dimensional data on the CL-84 and explains the procedure used to calculate the derivatives. For further details of the procedure, see the description of the MOSTAB program in Reference 1. The MOSTAB program was used to calculate the derivatives.

Note that the derivatives presented here are referred to stability axes. The hover condition is approximated by level flight at 1.0 fps. The effect of the stability augmenter system is represented by appropriate changes in the derivatives. The printout of derivatives contains some superfluous information (e.g., Mach number) which is arbitrarily set to zero, without affecting the accuracy of the calculated derivatives. The "primed" derivatives, listed in the printout of lateral derivatives are derivatives which have been combined so as to remove the product of inertia from explicit appearance in the equations of motion (see Reference 40). Thus, the general primed rolling derivative is

$$L_i' = L_i + (I_{xz}/I_x)\, N_i \Big/ \left[1 - (I_{xz})^2 / I_x I_z\right]$$

and the general primed yawing derivative is

$$N_i' = N_i + (I_{xz}/I_z)\, L_i \Big/ \left[1 - (I_{xz})^2 / I_x I_z\right]$$

The blending of the control surfaces on the CL-84 has been taken into account in calculating the control derivatives. These are referred to the stick and rudder pedals, not to the individual control surfaces.

TABLE A.1.

CL-84 LONGITUDINAL TRANSFER FUNCTION DENOMINATORS

Case	V. Knots TAS	Rate of Descent Ft/Min	RPM % Max	SAS Off, Roots, Rad/Sec			SAS On, Roots, Rad/Sec		
Hover (1 Ft/Sec)									
1		0	95	.1563 ± .526j	-.1323	-.7963	-.334 ± .214j	-.129	-3.35
Vertical Descent									
2		600.	85	.1316 ± .581j	-.143	-.797	-.348 ± .229j	-.137	-3.36
3	20	0	85	.016 ± .267j	-.400 ± .487j		-.121 ± .136j	-.764	-2.45
4	20	300.	85	.042 ± .221j	-.419 ± .506j		-.109 ± .126j	-.781	-2.4
5	20	600.	85	.074 ± .139j	-.44 ± .495j		-.101 ± .103j	-.771	-2.37
6	42	0	85	-.0122 ± .217j	-.525 ± .936j		-.104 ± .182j	-1.45 ± .645j	
7	42	960.	95	-.0191 ± .243j	-.516 ± .961j		-.102 ± .195j	-1.58 ± .452j	
8	42	480.	85	-.0176 ± .232j	-.514 ± .950j		-.101 ± .192j	-1.40 ± .704j	
9	42	960.	85	-.0177 ± .244j	-.504 ± .941j		-.095 ± .200j	-1.35 ± .734j	
10	60	0	85	-.064 ± .261j	-.949 ± 1.84j		-.098 ± .235j	-1.96 ± 1.46j	
11	60	720.	85	-.082 ± .279j	-.934 ± 1.88j		-.109 ± .251j	-1.96 ± 1.48j	
12	60	1440.	85	-.114 ± .294j	-.567 ± 1.36j		-.139 ± .242j	-1.57 ± 1.09j	
13	80	0	85	-.049 ± .309j	-1.21 ± 1.86j		-.087 ± .276j	-2.05 ± 1.55j	
14	80	900.	85	-.069 ± .266j	-1.18 ± 2.37j		-.088 ± .244j	-2.02 ± 2.11j	
15	80	1800.	85	-.082 ± .281j	-1.16 ± 2.39j		-.097 ± .258j	-2.01 ± 2.13j	
16	100	0	85	-.032 ± .238j	-1.5 ± 2.23j		-.059 ± .224j	-2.06 ± 2.07j	
17	100	1800.	95	-.033 ± .253j	-1.5 ± 2.33j		-.06 ± .233j	-2.21 ± 2.1j	
18	100	900.	85	-.033 ± .245j	-1.49 ± 2.25j		-.058 ± .229j	-2.04 ± 2.1j	
19	100	1800.	85	-.033 ± .251j	-1.47 ± 2.27j		-.056 ± .234j	-2.03 ± 2.12j	

TABLE A.2.

CL-84 PITCH/STICK DEFLECTION TRANSFER FUNCTION NUMERATOR

Case	V. Knots TAS	Rate of Descent Ft/Min	RPM % Max	Root Locus Gain	SAS Off, Roots, Rad/Sec	SAS On, Roots, Rad/Sec
Hover (1 Ft/Sec)						
1		0	95	4.81	-.116 -.177	-.116 -.177
Vertical Descent						
2		600.	95	4.8	-.116 -.196	-.117 -.196
3	20	0	85	3.77	-.113 -.222	-.113 -.222
4	20	300.	85	3.73	-.101 -.226	-.101 -.226
5	20	600.	85	3.69	-.087 -.236	-.087 -.236
6	42	0	85	3.24	$-.226 \pm .063j$	$-.226 \pm .063j$
7	42	960.	95	3.60	$-.208 \pm .09j$	$-.208 \pm .090j$
8	42	480.	85	3.15	$-.218 \pm .083j$	$-.218 \pm .083j$
9	42	960.	85	3.01	$-.209 \pm .090j$	$-.209 \pm .090j$
10	60	0	85	3.95	-.217 -.335	-.217 -.335
11	60	720.	85	3.82	$-.268 \pm .077j$	$-.268 \pm .077j$
12	60	1440.	85	3.58	$-.249 \pm .054j$	$-.249 \pm .054j$
13	80	0	85	4.39	-.151 -.560	-.151 -.560
14	80	900.	85	4.51	-.105 -.501	-.105 -.501
15	80	1800.	85	4.36	-.117 -.471	-.117 -.471
16	100	0	85	3.96	-.098 -.756	-.098 -.756
17	100	1800.	95	4.59	-.078 -.716	-.078 -.716
18	100	900.	85	4.04	-.090 -.740	-.090 -.737
19	100	1800.	85	4.11	-.079 -.717	-.079 -.717

TABLE A.3.

CL-84 u /STICK DEFLECTION TRANSFER FUNCTION NUMERATOR

Case	V. Knots TAS	Rate of Descent Ft/Min	RPM % Max	Root Locus Gain	SAS Off, Roots, Rad/Sec			SAS Off, Roots, Rad/Sec		
Hover (1 Ft/Sec)										
1		0	95	.379	-.122	17.8	-23.0	-.122	17.8	-23
Vertical Descent										
2		600.	95	11.1	.218 ±	.692j	-.822	.218 ±	.692j	-.822
3	20	0	85	.306	-.147	19.3	-21.03	-.147	19.2	-21.2
4	20	300.	85	1.48	-.129	8.68	-9.48	-.129	8.68	-9.47
5	20	600.	85	2.62	-.114	6.38	-6.99	-.114	6.42	-6.96
6	42	0	85	1.03	-.24	9.94	-9.81	-.24	9.77	-9.96
7	42	960.	95	2.48	-.182	6.25	-6.59	-.182	6.25	-6.58
8	42	480.	85	1.57	-.215	7.61	-7.85	-.215	7.55	-7.90
9	42	960.	85	2.09	-.182	6.23	-6.58	-.182	6.23	-6.57
10	60	0	85	0.55	-.35	13.67	-16.8	-.35	12.93	-17.7
11	60	720.	85	0.91	-.335	9.99	-12.5	-.335	9.68	-12.9
12	60	1440.	85	1.51	-.25	8.87	-8.09	-.25	8.8	-8.14
13	80	0	85	1.35	-.75	9.13	-9.18	-.75	8.05	-10.3
14	80	900.	85	0.572	-.373	16.62	-18.4	-.37	16.1	-18.9
15	80	1800.	85	0.75	-.365	13.8	-15.6	-.37	13.5	-15.9
16	100	0	85	1.25	-.978	8.57	-9.45	-.976	7.85	-10.3
17	100	1800.	95	1.45	-.943	8.49	-9.19	-.941	7.63	-10.2
18	100	900.	85	1.35	-.963	8.26	-9.09	-.962	7.57	-9.86
19	100	1800.	85	1.45	-.948	7.97	-8.75	-.946	7.3	-9.49

TABLE A.4.

CL-84 HEIGHT ERROR/STICK DEFLECTION TRANSFER FUNCTION NUMERATOR

Case	V. Knots TAS	Rate of Descent Ft/Min	RPM % Max	Root Locus Gain	SAS Off, Roots, Rad/Sec	SAS On, Roots, Rad/Sec
Hover (1 Ft/Sec)						
1		0	95	11.13	.34 ± .332j -1.05	.34 ± .332j -1.05
Vertical Descent						
2		600.	95	.296	3.2 ± 21.9j -.126	3.24 ± 21.9j -.126
3	20	0	85	8.65	.718 ± .387j -1.97	.711 ± .398j -1.98
4	20	300.	85	8.45	.395 ± 1.06j -1.32	.383 ± 1.06j -1.32
5	20	600.	85	8.07	.097 ± 1.69j -.711	.078 ± 1.69j -.712
6	42	0	85	7.28	.219 2.23 -3.12	.222 2.18 -3.16
7	42	960.	95	7.73	.763 ± .704j -2.2	.729 ± .73j -2.24
8	42	480.	85	6.98	.457 1.57 -2.7	.473 1.50 -2.74
9	42	960.	85	6.53	.761 ± .711j -2.19	.728 ± .74j -2.23
10	60	0	85	8.85	.080 3.77 -4.15	.080 3.71 -4.2
11	60	720.	85	8.46	.139 3.36 -3.78	.139 3.3 -3.82
12	60	1440.	85	7.98	.361 2.16 -3.3	.371 2.08 -3.36
13	80	0	85	10.2	.017 5.8 -6.02	.016 5.72 -6.10
14	80	900.	85	10.4	.091 4.83 -5.10	.091 4.74 -5.18
15	80	1800.	85	10.0	.133 4.49 -4.80	.133 4.40 -4.87
16	100	0	85	9.43	-.011 7.39 -7.47	-.012 7.32 -7.54
17	100	1800.	95	10.81	.026 7.08 -7.17	.025 7.00 -7.25
18	100	900.	85	9.61	.005 7.22 -7.31	.005 7.15 -7.38
19	100	1800.	85	9.77	.024 7.05 -7.14	.024 6.98 -7.21

TABLE A.5.

CL-84 u/STICK DEFLECTION TRANSFER FUNCTION NUMERATOR

Case	V. Knots TAS	Rate of Descent Ft/Min	RPM % Max	Root Locus Gain	SAS Off, Roots, Rad/Sec	SAS On, Roots, Rad/Sec
Hover (1 Ft/Sec) 1		0	95	.332	-.2515 15.0 -27.2	-.236 14.5 -26.6
Vertical Descent 2		600.	95	-142.1	.122 ± .573j -.795	-.355 ± .218j -3.6
3	20	0	85	11.76	-.469 2.64 -3.01	1.52 -.47 -4.53
4	20	300.	85	-4.57	-.403 .31 ± 4.62j	-.39 -1.36 ± 4.33j
5	20	600.	85	-21.1	-.309 -.01 ± 2.15j	-.267 -1.47 ± 1.74j
6	42	0	85	36.5	1.125 -.961 ± .729j	.569 -1.16 -2.2
7	42	960.	95	9.74	-1.32 3.04 -1.98	2.44 -.971 -3.58
8	42	480.	85	22.8	1.58 -1.12 ± .662j	.979 -1.09 -2.43
9	42	960.	85	7.65	-1.17 3.06 -2.13	2.56 -.948 -3.34
10	60	0	85	64.9	.333 -.419 ± .896j	.263 -2.08 ± 1.45j
11	60	720.	85	54.0	.535 -1.16 ± 1.85j	.341 -2.16 ± 1.46j
12	60	1440.	85	40.1	.792 -.935 ± 1.24j	.431 -1.76 ± .899j
13	80	0	85	94.3	.158 -1.27 ± 1.89j	.045 -2.09 ± 1.58j
14	80	900.	85	83.5	.213 -1.30 ± 2.36j	.123 -2.12 ± 2.12j
15	80	1800.	85	76.8	.223 -1.30 ± 2.38j	.135 -2.12 ± 2.14j
16	100	0	85	112.3	.062 -1.52 ± 2.26j	.001 -2.07 ± 2.11j
17	100	1800.	95	137.1	.047 -1.52 ± 2.37j	-.017 -2.22 ± 2.14j
18	100	900.	85	109.6	.055 -1.51 ± 2.29j	-.003 -2.06 ± 2.13j
19	100	1800.	85	106.8	.048 -1.49 ± 2.31j	-.008 -2.05 ± 2.15j

TABLE A.6.

CL-84 HEIGHT ERROR/COLLECTIVE TRANSFER FUNCTION NUMERATOR

Case	V. Knots TAS	Rate of Descent Ft/Min	RPM % Max	Root Locus Gain	SAS Off, Roots, Rad/Sec	SAS On, Roots, Rad/Sec
Hover (1 Ft/Sec				(SAS Off & SAS On)		
1		0	95	-142.7	.143 ± .542j -.78	-.344 ± .2j -3.57
Vertical Descent						
2		600.	95	-8.63	-.306 -.4.25 3.48	-.296 -6.34 1.932
3	20	0	85	-108.6	-.347 ± .664j .0764	-.841 -.111 -2.51
4	20	300.	85	-108.8	-.434 ± .608j .2603	-.816 -.06 -2.54
5	20	600.	85	-106.5	-.514 ± .537j .436	-.765 -.013 -2.58
6	42	0	85	-107.8	-.443 ± 1.09j -.015	-1.44 ± .798j -.124
7	42	960.	95	-145.2	-.487 ± 1.05j .085	-1.6 ± .52j -.066
8	42	480.	85	-111.0	-.458 ± 1.07j .029	-1.41 ± .812j -.091
9	42	960.	85	-112.0	-.477 ± 1.03j .092	-1.37 ± .802j -.050
10	60	0	85	-97.9	-.792 ± 1.96j -.272	-1.85 ± 1.53j -.286
11	60	720.	85	-103.0	-.806 ± 1.99j -.253	-1.89 ± 1.55j -.268
12	60	1440.	85	-109.0	-.492 ± 1.48j -.221	-1.53 ± 1.17j -.249
13	80	0	85	-69.9	-.838 ± 1.96j -.726	-1.72 ± 1.51j -.737
14	80	900.	85	-86.5	-.963 ± 2.48j -.411	-1.85 ± 2.17j -.413
15	80	1800.	85	-90.5	-.971 ± 2.52j -.400	-1.86 ± 2.21j -.402
16	100	0	85	-53.6	-.925 ± 1.98j -1.05	-1.48 ± 1.67j -1.11
17	100	1800.	95	-72.3	-1.05 ± 2.17j -.932	-1.73 ± 1.78j -.956
18	100	900.	85	-55.1	-.965 ± 2.06j -.971	-1.53 ± 1.77j -.999
19	100	1800.	85	-56.3	-.996 ± 2.13j -.906	-1.57 ± 1.86j -.921

TABLE A.7.

CL-84 LATERAL TRANSFER FUNCTION DENOMINATORS

Case	V. Knots TAS	Rate of Descent Ft/Min	RPM % Max	SAS Off, Roots, Raa/Sec		SAS On, Roots, Rad/Sec	
Hover (1 Ft/Sec)							
1		0	95	.128 ± .387j	-.262 -.616	-.009 ± .167j	-1.45 -3.53
Vertical Descent							
2		600.	95	.112 ± .413j	-.223 -.623	-.018 ± .141j	-1.53 -3.12
3	20	0	85	.07 ± .6j	-.159 -.702	-.085 ± .307j	-1.19 -2.59
4	20	300.	85	.047 ± .618j	-.147 -.682	-.095 ± .304j	-1.21 -2.6
5	20	600.	85	.03 ± .633j	-.134 -.67	-.101 ± .299j	-1.2 -2.63
6	42	0	85	-.05 ± .971j	-.101 -.712	-.273 ± .648j	-.931 -2.09
7	42	960.	95	-.104 ± 1.1j	-.069 -.65	-.387 ± .831j	-.571 -2.61
8	42	480.	85	-.077 ± 1.03j	-.086 -.673	-.339 ± .724j	-.739 -2.06
9	42	960.	85	-.103 ± 1.09j	-.072 -.638	-.389 ± .822j	-.57 -2.06
10	60	0	85	-.127 ± 1.08j	-.051 -.761	-.334 ± .464j	-1.69 -1.86
11	60	720.	85	-.138 ± 1.15j	-.04 -.725	-.454 ± .533j	-1.15 -1.9
12	60	1440.	85	-.153 ± 1.24j	-.037 -.664	-.617 ± .742j	-.617 -1.91
13	80	0	85	-.182 ± 1.3j	-.032 -1.21	-1.01 ± .578j	-.154 -4.51
14	80	900.	85	-.198 ± 1.35j	-.017 -.874	-1.00 ± .668j	-.267 -2.61
15	80	1800.	85	-.195 ± 1.4j	-.012 -.844	-0.946 ± .836j	-.297 -2.35
16	100	0	85	-.238 ± 1.52j	-.042 -1.51	-1.02 ± 1.13j	-.0266 -6.6
17	100	1800.	95	-.22 ± 1.58j	-.043 -1.45	-1.15 ± 1.06j	-.0855 -6.02
18	100	900.	85	-.229 ± 1.55j	-.042 -1.48	-.995 ± 1.16j	-.039 -6.31
19	100	1800.	85	-.218 ± 1.57j	-.043 -1.45	-.968 ± 1.19j	-.053 -6.02

TABLE A.8.

CL-84 BANK/LATERAL STICK DEFLECTION TRANSFER FUNCTION NUMERATOR

Case	V. Knots TAS	Rate of Descent Ft/Min	RPM % Max	Root Locus Gain	SAS OFF, Roots, Rad/Sec	Root Locus Gain	SAS On, Roots, Rad/Sec
Hover (1 Ft/Sec)							
1		0	95	5.21	-.0295 -.264	5.21	-.0264 -1.6
Vertical Descent							
2		600.	95	5.89	-.0248 -.227	5.89	-.0248 -1.3
3	20	0	85	4.03	-.175 $\pm$ .42j	4.03	-.234 -1.14
4	20	300.	85	4.05	-.175 $\pm$ .427j	4.05	-.236 -1.15
5	20	600.	85	4.09	-.172 $\pm$ .419j	4.09	-.226 -1.16
6	42	0	85	3.06	-.235 $\pm$ .882j	3.06	-.702 $\pm$ .652j
7	42	960.	95	3.84	-.228 $\pm$ .917j	3.84	-.652 $\pm$ .734j
8	42	480.	85	3.03	-.231 $\pm$ .895j	3.03	-.67 $\pm$ .695j
9	42	960.	85	3.01	-.225 $\pm$ .897j	3.01	-.636 $\pm$ .721j
10	60	0	85	2.94	-.267 $\pm$ 1.03j	2.94	-1.04 $\pm$ .49j
11	60	720.	85	2.79	-.264 $\pm$ 1.05j	2.79	-.956 $\pm$ .657j
12	60	1440.	85	2.71	-.259 $\pm$ 1.07j	2.71	-.899 $\pm$ .745j
13	80	0	85	5.24	-.274 $\pm$ 1.24j	5.23	-1.23 $\pm$ .641j
14	80	900.	85	3.35	-.283 $\pm$ 1.26j	3.35	-1.13 $\pm$ .81j
15	80	1800.	85	3.04	-.278 $\pm$ 1.29j	3.04	-1.03 $\pm$ .922j
16	100	0	85	8.15	-.303 $\pm$ 1.46j	8.15	-1.14 $\pm$ 1.12j
17	100	1800.	95	7.5	-.287 $\pm$ 1.55j	7.5	-1.28 $\pm$ 1.11j
18	100	900.	85	7.79	-.291 $\pm$ 1.48j	7.79	-1.10 $\pm$ 1.17j
19	100	1800.	85	7.37	-.278 $\pm$ 1.49j	7.37	-1.06 $\pm$ 1.22j

TABLE A.9.

CL-84 LATERAL GROUND VELOCITY/PEDAL DEFLECTION TRANSFER FUNCTION NUMERATOR

Case	V. Knots TAS	Rate of Descent Ft/Min	RPM % Max	Root Locus Gain	SAS Off, Roots, Rad/Sec				Root Locus Gain	SAS On, Roots, Rad/Sec			
Hover (1 Ft/Sec)													
1		0	95	.00046	.0264	-.2511	130.7	-422.3	.00046	.0863	-.077	131.8	-418.2
Vertical Descent													
2		600.	95	.00029	0	-.200	177.1	-661.8	.00029	0	1.66	178.4	-658.4
3	20	0	85	-.215	-.521	± 1.12j	-4.71	8.66	-.215	-.75	± .85j	-6.39	
4	20	300.	85	-.212	-.586	± 1.15j	-4.41	8.61	-.212	-.798	± .862j	-6.14	
5	20	600.	85	-.2	-.685	± 1.19j	-4.02	8.53	-.2	-.94	± .797j	-5.73	
6	42	0	85	-.95	-.29	± 1.17j	-8.01	9.17	-.95	-.367	± 1.13j	-9.4	8.07
7	42	960.	95	-.88	-.261	± 1.13j	-10.2	10.92	-.88	-.297	± 1.11j	-11.9	9.64
8	42	480.	85	-.93	-.285	± 1.18j	-8.16	9.19	-.93	-.343	± 1.15j	-9.52	8.12
9	42	960.	85	-.88	-.28	± 1.18j	-8.48	9.38	-.88	-.328	± 1.15j	-9.82	8.33
10	60	0	85	-1.95	-.451	± 1.6j	-4.51	6.61	-1.95	-.789	± 1.4j	-5.84	5.47
11	60	720.	85	-1.94	-.43	± 1.59j	-4.73	6.59	-1.94	-.627	± 1.47j	-6.12	5.46
12	60	1440.	85	-1.9	-.399	± 1.6j	-4.94	6.63	-1.9	-.523	± 1.51j	-6.33	5.51
13	80	0	85	-3.43	-.059	± 3.94j	-1.37	3.17	-3.43	-2.99	± 4.64j	-.674	3.27
14	80	900.	85	-3.46	-.55	± 2.26j	-2.59	4.86	-3.46	-2.27	± 1.9j	-1.92	4.04
15	80	1800.	85	-3.44	-.522	± 2.26j	-2.73	4.81	-3.44	-1.49	± 1.84j	-3.2	3.93
16	100	0	85	-5.39	-.132	± 4.12j	-1.06	2.54	-5.39	-4.24	± 5.12j	-.306	3.37
17	100	1800.	95	-5.39	-.227	± 3.83j	-1.45	3.19	-5.39	-4.01	± 4.61j	-.54	3.37
18	100	900.	85	-5.39	-.107	± 4.13j	-1.10	2.48	-5.39	-4.02	± 4.99j	-.356	3.2
19	100	1800.	85	-5.39	-.086	± 4.13j	-1.14	2.42	-5.39	-3.79	± 4.84j	-.415	3.02

TABLE A.10.

CL-84 LATERAL GROUND VELOCITY/LATERAL STICK DELFECTION TRANSFER FUNCTION NUMERATOR

Case	V. Knots TAS	Rate of Descent Ft/Min	RPM % Max	Root Locus Gain	SAS Off, Roots, Rad/Sec	Root Locus Gain	SAS On, Roots, Rad/Sec
Hover (1 Ft/Sec)							
1		0	95	-.008	-.003 -.264 102.7 -204.8	-.008	-.0006 -1.6 102.7 -205.
Vertical Descent							
2		600	95	-.003	0 -.227 144.6 -417.	-.003	0 -1.3 144.6 -417.
3	20	0	85	.0063	-.149 ± .415j 98.9 ± 103j	.0063	-.168 -1.15 98.9 ± 103.2
4	20	300.	85	.0036	-.151 ± .425j 179.4 ± 60.5j	.0036	-.173 -1.17 179.4 ± 61.6
5	20	600.	85	.00034	-.148 ± .419j 99. 3848.	.0003	-.167 -1.17 99.4 3847.
6	42	0	85	.0016	-.198 ± .885j 141. 422.	.0016	-.663 ± .62j 141. 422.
7	42	960.	95	-.0003	-.197 ± .942j 109. -3074.	-.00035	-.619 ± .738j 109.1 -3074.
8	42	480.	85	-.004	-.196 ± .91j 76.6 -303.6	-.004	-.634 ± .682j 76.5 -303.5
9	42	960.	85	.0011	-.193 ± .924j 113. 712.	.0011	-.604 ± .725j 113. 712.
10	60	0	85	.0014	-.222 ± 1.03j 76.3 852.	.0014	-.993 ± .347j 76.5 852.
11	60	720.	85	.0007	-.22 ± 1.07j 76.6 1660.	.0007	-.911 ± .603j 76.6 1660.
12	60	1440.	85	-.0045	-.216 ± 1.11j 58.8 -301.	-.0045	-.857 ± .74j 58.8 -301.
13	80	0	85	.0008	-.235 ± 1.24j 40. 5278.	.0008	-1.23 ± .231j 40.7 5276.
14	80	900.	85	-.0021	-.234 ± 1.29j 45.9 -1082.	-.0021	-1.1 ± .698j 46.2 -1083.
15	80	1800.	85	-.0003	-.229 ± 1.33j 50.2 -6029.	-.0003	-1.03 ± .866j 50.5 -6030.
16	100	0	85	-.0021	-.258 ± 1.47j 32.0 -3787.	-.0021	-1.16 ± .918j 32.6 -3790.
17	100	1800.	95	-.001	-.25 ± 1.55j 35.8 -6622.	-.001	-1.29 ± .874j 36.3 -6625.
18	100	900.	85	-.0013	-.246 ± 1.49j 32.3 -5846.	-.0013	-1.12 ± .999j 32.9 -5848.
19	100	1800.	85	-.0003	-.233 ± 1.51j 32.5 -22360.	-.0003	-1.07 ± 1.073j 33.1 -22370.

Table A.11 RUN NO. 1

CANADAIR CL-84 HOVER SAS ON

INPUT DATA Stability Derivatives

UNITS ARE 1 PER RADIAN
DIMENSIONAL DERIVATIVES TIMES INERTIA
(STABILITY AXES)

DXDU	=	-.5907+02	DZDU	=	-.2041+01	DMDU	=	.1681+03
DXDW	=	-.5348+01	DZDW	=	-.4549+02	DMDW	=	-.7971+02
DXDQ	=	.5016+02	DZDQ	=	-.2930+04	DMDQ	=	-.8529+05
DXDUD	=	-.0000	DZDUD	=	-.0000	DMDUD	=	-.0000
DXDWD	=	-.0000	DZDWD	=	-.0000	DMDWD	=	-.0000
DXDQD	=	-.0000	DZDQD	=	.0000	DMDQD	=	.0000
DXDE	=	.1317+03	DZDE	=	.3871+04	DMDE	=	.1068+06
DXDT	=	.1156+03	DZDT	=	-.4963+05	DMDT	=	.9394+05

U	=	.1000+01	UZ	=	.0000	GAMA	=	.1913+01
MACH	=	.8953-03	RHO	=	.2380-02	S	=	.2333+03
MAC	=	.7000+01	IXZ	=	-.9041+04	IY	=	.2220+05
HT	=	-.0000	XJ	=	-.0000	TGT	=	-.0000
LX	=	-.0000	LY	=	-.0000	LZ	=	-.0000
CL	=	.0000	CD	=	.0000	W	=	.1120+05
IX	=	.2089+05	IZ	=	.3351+05	R	=	.3220+02

DIMENSIONAL STABILITY DERIVATIVES, PER RADIAN,
STABILITY AXES

YV	=	-.1698-00	ZV	=	-.5866-02	MV	=	.7572-02
YW	=	-.1536-01	ZW	=	-.1304-00	MW	=	-.3591-02
YP	=	.1442-00	ZP	=	-.8424+01	MP	=	-.3842+01
YVD	=	.0000	ZVD	=	.0000	MVD	=	.0000
YWD	=	.0000	ZWD	=	.0000	MWD	=	.0000
YPD	=	.0000	ZPD	=	.0000	MPD	=	.0000
YD	=	.3786-00	ZD	=	.1113+02	MD	=	.4881+01
YT	=	.3324-00	ZT	=	-.1427+03	MT	=	.4232+01

IN STABILITY AXES, U = .1000+01 AND W = 0.0
ZIY = .2220+05 AND ZIXZ = -.9041+04

Table A.12 RUN NO. 1

CANADAIR CL-84 HOVER SAS OFF

INPUT DATA Stability Derivatives

UNITS ARE 1 PER RADIAN
DIMENSIONAL DERIVATIVES TIMES INERTIA
(STABILITY AXES)

DXDU	=	-.5907+02	DZDU	=	-.2041+01	DMDU	= .1681+03
DXDW	=	-.5348+01	DZDW	=	-.4549+02	DMDW	= -.7971+02
DXDQ	=	.1467+03	DZDQ	=	-.9245+02	DMDQ	= -.7002+04
DXDUD	=	-.0000	DZDUD	=	-.0000	DMDUD	= -.0000
DXDWD	=	-.0000	DZDWD	=	-.0000	DMDWD	= -.0000
DXDQD	=	-.0000	DZDQD	=	.0000	DMDQD	= .0000
DXDE	=	.1317+03	DZDE	=	.3871+04	DMDE	= .1068+06
DXDT	=	.1156+03	DZDT	=	-.4963+05	DMDT	= .9394+05

U	=	.1000+01	UZ	=	.0000	GAMA	= .1913+01
MACH	=	.0000	RHO	=	.2380-02	S	= .2333+03
MAC	=	.7000+01	IXZ	=	-.9041+04	IY	= .2220+05
HT	=	-.0000	XI	=	-.0000	TDT	= -.0000
LX	=	-.0000	LY	=	-.0000	LZ	= -.0000
CL	=	.0000	CD	=	.0000	W	= .1120+05
IX	=	.2069+05	IZ	=	.3351+05	G	= .3220+02

DIMENSIONAL STABILITY DERIVATIVES, PER RADIAN,
STABILITY AXES

XU	=	-.1697-00	ZU	=	-.5868-02	MU	= .7572-02
XW	=	-.1536-01	ZW	=	-.1308-00	MW	= -.3591-02
XQ	=	-.4217-02	ZQ	=	-.2658-00	MQ	= -.3154-00
XUD	=	.0000	ZUD	=	.0000	MUD	= .0000
XWD	=	.0000	ZWD	=	.0000	MWD	= .0000
XQD	=	.0000	ZQD	=	.0000	MQD	= .0000
XD	=	.3786-03	ZD	=	.1113+02	MD	= .4811+01
XT	=	.3324-00	ZT	=	-.1427+03	MT	= .4232+01

IN STABILITY AXES, U = .1000+01 AND W = 0.0
ZIY = .2220+05 AND ZIXZ = -.9041+04

Table A.13 RUN NO. 1

CANADAIR CL-84 HOVER SAS ON

INPUT DATA Stability Derivatives

DIMENSIONAL DERIVATIVES TIMES INERTIA
UNITS ARE 1 PER RADIAN
(STABILITY AXES)

DYDV =	-.8971+01	DLDV =	-.5440+02	DNDV =	.1903+02
DYDP =	-.5210+02	DLDP =	-.6148+05	DNDP =	-.5915+04
DYDR =	.1298-00	DLDR =	-.6926+03	DNDR =	-.4564+05
DYDVD =	-.0000	DLDVD =	-.0000	DNDVD =	-.0000
DYDPD =	-.0000	DLDPD =	-.0000	DNDPD =	-.0000
DYDRD =	-.0000	DLDRD =	.0000	DNDRD =	.0000
DYDA =	-.2773+01	DLDA =	.1000+06	DNDA =	.1122+05
DYDR =	.1598-00	DLDR =	-.1553+04	DNDR =	.5294+05

U =	.1000+01	UZ =	.0000	GAMA =	.1913+01
MACH =	.8953-03	RHO =	.2380-02	S =	.2333+03
MAC =	.7000+01	IXZ =	-.9041+04	IY =	.2220+05
HT =	-.0000	XI =	-.0000	TDT =	-.0000
LX =	-.0000	LY =	-.0000	LZ =	-.0000
CL =	.0000	CD =	.0000	W =	.1120+05
IX =	.2089+05	IZ =	.3351+05	G =	.3220+02
SPAN =	.3330+02				

DIMENSIONAL STABILITY DERIVATIVES, PER RADIAN,
STABILITY AXES

YV =	-.2579-01	LV =	-.2604-02	NV =	.5679-03
YP =	-.1498-00	LP =	-.2943+01	NP =	-.1765-00
YR =	.3732-03	LR =	-.3315-01	NR =	-.1362+01
YVD =	.0000	LVD =	.0000	NVD =	.0000
YPD =	.0000	LPD =	.0000	NPD =	.0000
YRD =	.0000	LRD =	.0000	NRD =	.0000
YA =	-.7972-02	LA =	.4787+01	NA =	.3348-00
YDR=	.4594-03	LDR=	-.7434-01	NDR=	.1580+01

DIMENSIONAL DERIVATIVES, PRIMED

YV =	-.2579-01	LV =	-.3227-02	NV =	.1629-02
YP =	-.1498-00	LP =	-.3246+01	NP =	.7916-00
YR =	.3732-03	LR =	.6290-00	NR =	-.1734+01
YVD =	.0000	LVD =	.0000	NVD =	.0000
YPD =	.0000	LPD =	.0000	NPD =	.0000
YRD =	.0000	LRD =	.0000	NRD =	.0000
YA =	-.7972-02	LA =	.5256+01	NA =	-.1226+01
YDR=	.4594-03	LDR=	-.8583-00	NDR=	.2051+01

IN STABILITY AXES, U= .1000+01
,IXX= .2089+05 IZZ= .3351+05 IXZ=-.9041+04

Table A.14 RUN NO. 1

CANADAIR CL-84 HOVER SAS OFF

INPUT DATA Stability Derivatives

DIMENSIONAL DERIVATIVES TIMES INERTIA
UNITS ARE 1 PER RADIAN
(STABILITY AXES)

DYDV =	-.8971+01	DLDV =	-.5440+02	DNDV =	.1903+02
DYDP =	-.5364+02	DLDP =	-.5978+04	DNDP =	.3125+03
DYDR =	.2441-00	DLDR =	-.1303+04	DNDR =	-.7789+04
DYDVD =	-.0000	DLDVD =	-.0000	DNDVD =	-.0000
DYDPD =	-.0000	DLDPD =	-.0000	DNDPD =	-.0000
DYDRD =	-.0000	DLDRD =	.0000	DNDRD =	.0000
DYDA =	-.2773+01	DLDA =	.1000+06	DNDA =	.1122+05
DYDR =	.1596-00	DLDR =	-.1553+04	DNDR =	.5294+05

U =	.1000+01	UZ =	.0000	GAMA =	.1913+01
MACH =	.0000	RHO =	.2380-02	S =	.2333+03
MAC =	.7000+01	IXZ =	-.9041+04	IY =	.2220+05
HT =	-.0000	XJ =	-.0000	TDT =	-.0000
LX =	-.0000	LY =	-.0000	LZ =	-.0000
CL =	.0000	CD =	.0000	W =	.1120+05
IX =	.2069+05	IZ =	.3351+05	G =	.3220+02
SPAN =	.3330+02				

DIMENSIONAL STABILITY DERIVATIVES, PER RADIAN,
STABILITY AXES

YV =	-.2579-01	LV =	-.2604-02	NV =	.5679-03
YP =	-.1542-00	LP =	-.2862-00	NP =	.9326-02
YR =	.7018-03	LR =	-.8631-01	NR =	-.2324-00
YVD =	.0000	LVD =	.0000	NVD =	.0000
YPD =	.0000	LPD =	.0000	NPD =	.0000
YRD =	.0000	LRD =	.0000	NRD =	.0000
YA =	-.7972-02	LA =	.4707+01	NA =	.3348-00
YDR=	.4594-03	LDR=	-.7434-01	NDR=	.1580+01

DIMENSIONAL DERIVATIVES, PRIMED

YV =	-.2579-01	LV =	-.3227-02	NV =	.1629-02
YP =	-.1542-00	LP =	-.3286-00	NP =	.1109+00
YR =	.7018-03	LR =	.1618-01	NR =	-.2681-00
YVD =	.0000	LVD =	.0000	NVD =	.0000
YPD =	.0000	LPD =	.0000	NPD =	.0000
YRD =	.0000	LRD =	.0000	NRD =	.0000
YA =	-.7972-02	LA =	.5256+01	NA =	-.1226+01
YDR=	.4594-03	LDR=	-.8583-00	NDR=	.2051+01

IN STABILITY AXES, U= .1000+01
IXX= .2069+05 IZZ= .3351+05 IXZ=-.9041+04

Table A.15 RUN NO. 6

CANADAIR CL-84 42.KNOTS LEVEL FLIGHT GAS ON

INPUT DATA Stability Derivatives

UNITS ARE 1 PER RADIAN
DIMENSIONAL DERIVATIVES TIMES INERTIA
(STABILITY AXES)

DXDU =	-.7758+02	DZDU =	-.2309+02	DMDU =	-.1051+03
DXDW =	.4726+01	DZDW =	-.9941+02	DMDW =	-.2634+03
DXDQ =	-.2311+03	DZDQ =	-.1603+04	DMDQ =	-.5565+05
DXDUD =	-.0000	DZDUD =	-.0007	DMDUD =	-.0000
DXDWD =	-.0000	DZDWD =	-.0000	DMDWD =	-.0000
DXDQD =	-.0000	DZDQD =	.0007	DMDQD =	.0000
DXDE =	.3575+05	DZDE =	.2531+04	DMDE =	.6865+05
DXDT =	.1268+05	DZDT =	-.3750+05	DMDT =	.4214+05

U =	.7071+02	UZ =	.4358+01	GAMA =	-.3097-03
MACH =	.6356-01	RHO =	.2380-02	S =	.2333+03
MAC =	.7000+01	IXZ =	-.4450+04	IY =	.2120+05
HT =	-.0000	CL =	-.0000	TDT =	-.0000
LX =	-.0000	LY =	-.0000	LZ =	-.0000
CL =	.0000	CD =	.0000	W =	.1120+05
IX =	.1837+05	IZ =	.3383+05	G =	.3220+02

DIMENSIONAL STABILITY DERIVATIVES, PER RADIAN,
STABILITY AXES

XU =	-.2230-00	ZU =	-.2309-00	MU =	-.4958-02
XW =	.1359-01	ZW =	-.9942-00	MW =	-.1242-01
XQ =	-.6682-00	ZQ =	-.1603+01	MQ =	-.2620+01
XUD =	.0005	ZUD =	.0000	MUD =	.0000
XWD =	.0000	ZWD =	.0000	MWD =	.0000
XQD =	.0000	ZQD =	.0000	MQD =	.0000
XD =	.1028+01	ZD =	.7277+01	MD =	.3238+01
XT =	.3645+02	ZT =	-.1676+03	MT =	.1986+01

IN STABILITY AXES, U = .7100+02 AND W = 0.0
XIY = .2120+05 AND XIXZ = -.4450+04

Table A.16 RUN NO. 6

CANADAIR CL-84 42.KNOTS LEVEL FLIGHT SAS OFF

INPUT DATA Stability Derivatives

UNITS ARE 1 PER RADIAN
DIMENSIONAL DERIVATIVES TIMES INERTIA
(STABILITY AXES)

DXDU =	-.7758+02	DZDU =	-.8309+02	DMDU =	-.1051+03
DXDW =	.4726+01	DZDW =	-.9961+02	DMDW =	-.2634+03
DXDQ =	-.9228+02	DZDQ =	-.8665+02	DMDQ =	-.1257+05
DXDUD =	-.0000	DZDUD =	-.0000	DMDUD =	-.0000
DXDWD =	-.0000	DZDWD =	-.0000	DMDWD =	-.0000
DXDQD =	-.0000	DZDQD =	.0000	DMDQD =	.0000
DXDE =	.3575+03	DZDE =	.2531+04	DMDE =	.6865+05
DXDT =	.1258+05	DZDT =	-.3750+05	DMDT =	.4214+05

U =	.7071+02	LZ =	.6358+01	GAMA =	-.3097-03
MACH =	.6356-01	RHO =	.2380-02	S =	.2333+03
MAC =	.7000+01	IXZ =	-.4450+04	IY =	.2120+05
FT =	-.0000	XI =	-.0000	TDT =	-.0000
LX =	-.0000	LY =	-.0000	LZ =	-.0000
CL =	.3000	CD =	.0000	W =	.1120+05
IX =	.1837+05	IZ =	.3363+05	G =	.3220+02

DIMENSIONAL STABILITY DERIVATIVES, PER RADIAN,
STABILITY AXES

XU =	-.2230-00	ZU =	-.2389-00	MU =	-.4958-02
XW =	.1359-01	ZW =	-.2582-00	MW =	-.1242-01
XQ =	-.2653-00	ZQ =	-.2491-00	MQ =	-.5929-00
XUD =	.0000	ZUD =	.0000	MUD =	.0000
XWD =	.0000	ZWD =	.0000	MWD =	.0000
XQD =	.0000	ZQD =	.0000	MQD =	.0000
XD =	.1028+01	ZD =	.7277+01	MD =	.3238+01
XT =	.3645+02	ZT =	-.1076+03	MT =	.1988+01

IN STABILITY AXES, U = .7100+02 AND W = 0.0
ZIY = .2120+05 AND ZIXZ = -.4450+04

Table A.17 RUN NO. 6

CANADAIR CL-84 42.KNOTS LEVEL FLIGHT SAS ON

INPUT DATA Stability Derivatives

DIMENSIONAL DERIVATIVES TIMES INERTIA
UNITS ARE 1 PER RADIAN
(STABILITY AXES)

DYDV =	-.3142+02	DLDV =	-.2138+03	DNDV =	.3480+03
DYDP =	-.7167+02	DLDP =	-.4044+05	DNDP =	-.5500+04
DYDR =	.4145+03	DLDR =	-.2244+05	DNDR =	-.4473+05
DYDVD =	-.0000	DLDVD =	-.0000	DNDVD =	-.0000
DYDPD =	-.0000	DLDPD =	-.0000	DNDPD =	-.0000
DYDRD =	-.0000	DLDRD =	.0000	DNDRD =	.0000
DYDA =	.5666-00	DLDA =	.5508+05	DNDA =	.5600+04
DYDR =	-.3293+03	DLDR =	.4038+05	DNDR =	.5544+05
U =	.7071+02	UZ =	.6358+01	GAMA =	-.3097-03
MACH =	.6356-01	RHO =	.2380-02	S =	.2333+03
MAC =	.7000+01	IXZ =	-.4450+04	IY =	.2120+05
HT =	-.0000	XI =	-.0000	TDT =	-.0000
LX =	-.0000	LY =	-.0000	LZ =	-.0000
CL =	.0000	CD =	.0000	W =	.1120+05
IX =	.1837+05	IZ =	.3383+05	G =	.3220+02
SPAN =	.3330+02				

DIMENSIONAL STABILITY DERIVATIVES,PER RADIAN,
STABILITY AXES

YV =	-.9033-01	LV =	-.1164-01	NV =	.1029-01
YP =	-.2061-00	LP =	-.2201+01	NP =	-.1626-00
YR =	.1192+01	LR =	-.1222+01	NR =	-.1322+01
YVD =	.0000	LVD =	.0000	NVD =	.0000
YPD =	.0000	LPD =	.0000	NPD =	.0000
YRD =	.0000	LRD =	.0000	NRD =	.0000
YA =	.1629-02	LA =	.2998+01	NA =	.1655-00
YDR=	-.9467-00	LDR=	.2198+01	NDR=	.1639+01

DIMENSIONAL DERIVATIVES, PRIMED

YV =	-.9033-01	LV =	-.1460-01	NV =	.1261-01
YP =	-.2061-00	LP =	-.2233+01	NP =	.1355-00
YR =	.1192+01	LR =	-.9309-00	NR =	-.1239+01
YVD =	.0000	LVD =	.0000	NVD =	.0000
YPD =	.0000	LPD =	.0000	NPD =	.0000
YRD =	.0000	LRD =	.0000	NRD =	.0000
YA =	.1629-02	LA =	.3056+01	NA =	-.2442-00
YDR=	-.9467-00	LDR=	.1860+01	NDR=	.1440+01

IN STABILITY AXES, U= .7100+02
IXX= .1837+05 IZZ= .3383+05 IXZ=-.4450+04

Table A.18 RUN NO. 6

CANADAIR CL-84 42.KNOTS LEVEL FLIGHT SAS OFF

INPUT DATA Stability Derivatives

DIMENSIONAL DERIVATIVES TIMES INERTIA
UNITS ARE 1 PER RADIAN
(STABILITY AXES)

DYDV =	-.3142+02	DLDV =	-.2138+03	DNDV =	.3480+03
DYDP =	-.7132+02	DLDP =	-.7379+04	DNDP =	.5811+03
DYDR =	.4149+03	DLDR =	.3766+04	DNDR =	-.1189+05
DYDVD =	-.0000	DLDVD =	-.0000	DNDVD =	-.0000
DYDPD =	-.0000	DLDPD =	-.0000	DNDPD =	-.0000
DYDRD =	-.0000	DLDRD =	.0000	DNDRD =	.0000
DYDA =	.5666-00	DLDA =	.5508+05	DNDA =	.5600+04
DYDR =	-.3293+03	DLDR =	.4038+05	DNDR =	.5544+05

U =	.7071+02	UZ =	.6358+01	GAMA =	-.3097-03
MACH =	.6356-01	RHO =	.2380-02	S =	.2333+03
MAC =	.7000+01	IXZ =	-.4450+04	IY =	.2120+05
HT =	-.0000	XI =	-.0000	TDT =	-.0000
LX =	-.0000	LY =	-.0000	LZ =	-.0000
CL =	.0000	CD =	.0000	W =	.1120+05
IX =	.1837+05	IZ =	.3383+05	G =	.3220+02
SPAN =	.3330+02				

DIMENSIONAL STABILITY DERIVATIVES, PER RADIAN,
STABILITY AXES

YV =	-.9033-01	LV =	-.1164-01	NV =	.1029-01
YP =	-.2050-00	LP =	-.4017-00	NP =	.1718-01
YR =	.1193+01	LR =	.2050-00	NR =	-.3515-00
YVD =	.0000	LVD =	.0000	NVD =	.0000
YPD =	.0000	LPD =	.0000	NPD =	.0000
YRD =	.0000	LRD =	.0000	NRD =	.0000
YA =	.1629-02	LA =	.2998+01	NA =	.1655-00
YDR=	-.9467-00	LDR=	.2196+01	NDR=	.1639+01

DIMENSIONAL DERIVATIVES, PRIMED

YV =	-.9033-01	LV =	-.1460-01	NV =	.1261-01
YP =	-.2050-00	LP =	-.4192-00	NP =	.7470-01
YR =	.1193+01	LR =	.2997-00	NR =	-.4038-00
YVD =	.0000	LVD =	.0000	NVD =	.0000
YPD =	.0000	LPD =	.0000	NPD =	.0000
YRD =	.0000	LRD =	.0000	NRD =	.0000
YA =	.1629-02	LA =	.3056+01	NA =	-.2442-00
YDR=	-.9467-00	LDR=	.1860+01	NDR=	.1440+01

IN STABILITY AXES, U= .7100+02
,IXX= .1837+05 IZZ= .3383+05 IXZ=-.4450+04

Table A.19 RUN NO. 9

CANADAIR CL-84 42.KNOTS DESCENT 16.FT/SEC SAS ON

INPUT DATA Stability Derivatives

UNITS ARE 1 PER RADIAN
DIMENSIONAL DERIVATIVES TIMES INERTIA
(STABILITY AXES)

DXDU =	-.8662+02	DZDU =	-.8483+02	DMDU =	-.1857+03
DXDW =	.1138+02	DZDW =	-.7025+02	DMDW =	-.2730+03
DXDQ =	-.5375+03	DZDQ =	-.1393+04	DMDQ =	-.5192+05
DXDUD =	-.0000	DZDUD =	-.0000	DMDUD =	-.0000
DXDWD =	-.0000	DZDWD =	-.0000	DMDWD =	-.0000
DXDQD =	-.0000	DZDQD =	.0000	DMDQD =	.0000
DXDE =	.7269+03	DZDE =	.2272+04	DMDE =	.6391+05
DXDT =	.2633+04	DZDT =	-.3901+05	DMDT =	.4584+05

U =	.6754+02	UZ =	.2190+02	GAMA =	-.1302+02
MACH =	.6356-01	RHO =	.2380-02	S =	.2333+03
MAC =	.7000+01	IXZ =	-.7359+04	IY =	.2120+05
HT =	-.0000	XI =	-.0000	TDT =	-.0000
LX =	-.0000	LY =	-.0000	LZ =	-.0000
CL =	.0000	CD =	.0000	W =	.1120+05
IX =	.2106+05	IZ =	.3114+05	G =	.3220+02

DIMENSIONAL STABILITY DERIVATIVES, PER RADIAN,
STABILITY AXES

XU =	-.2490-00	ZU =	-.2439-00	MU =	-.8759-02
XW =	.3272-01	ZW =	-.2020-00	MW =	-.1288-01
XQ =	-.1545+01	ZQ =	-.4005+01	MQ =	-.2449+01
XUD =	.0000	ZUD =	.0000	MUD =	.0000
XWD =	.0000	ZWD =	.0000	MWD =	.0000
XQD =	.0000	ZQD =	.0000	MQD =	.0000
XD =	.2090+01	ZD =	.6532+01	MD =	.3015+01
XT =	.7570+01	ZT =	-.1122+03	MT =	.2162+01

IN STABILITY AXES, U = .7100+02 AND W = 0.0
ZIY = .2120+05 AND ZIXZ = -.7359+04

Table A.20 RUN NO. 9

CANADAIR CL-84 42.KNOTS DESCENT 16.FT/SEC SAS OFF

INPUT DATA Stability Derivatives

UNITS ARE 1 PER RADIAN
DIMENSIONAL DERIVATIVES TIMES INERTIA
(STABILITY AXES)

DXDU =	-.8662+02	DZDU =	-.3443+02	DMDU =	-.1857+03
DXDW =	.1138+02	DZDW =	-.7025+02	DMDW =	-.2730+03
DXDQ =	-.9872+02	DZDQ =	-.7253+02	DMDQ =	-.1257+05
DXDUD =	-.0000	DZDUD =	-.0000	DMDUD =	-.0000
DXDWD =	-.0000	DZDWD =	-.0000	DMDWD =	-.0000
DXDQD =	-.0000	DZDQD =	.0000	DMDQD =	.0000
DXDE =	.7269+03	DZDE =	.2272+04	DMDE =	.6391+05
DXDT =	.2633+04	DZDT =	-.3901+05	DMDT =	.4584+05

U =	.6754+02	UZ =	.2190+02	GAMA =	-.1302+02
MACH =	.6356-01	RHO =	.2380-02	S =	.2333+03
MAC =	.7000+01	IXZ =	-.7359+04	IY =	.2120+05
HT =	-.0000	XI =	-.0000	TDT =	-.0000
LX =	-.0000	LY =	-.0000	LZ =	-.0000
CL =	.0000	CD =	.0000	W =	.1120+05
IX =	.2106+05	IZ =	.3114+05	G =	.3220+02

DIMENSIONAL STABILITY DERIVATIVES, PER RADIAN,
STABILITY AXES

XU =	-.2490-00	ZU =	-.2439-00	MU =	-.8759-02
XW =	.3272-01	ZW =	-.2020-00	MW =	-.1288-01
XQ =	-.2551-00	ZQ =	-.2085-00	MQ =	-.5929-00
XUD =	.0000	ZUD =	.0000	MUD =	.0000
XWD =	.0000	ZWD =	.0000	MWD =	.0000
XQD =	.0000	ZQD =	.0000	MQD =	.0000
XD =	.2090+01	ZD =	.6532+01	MD =	.3015+01
XT =	.7570+01	ZT =	-.1122+03	MT =	.2162+01

IN STABILITY AXES, U = .7100+02 AND W = 0.0
ZIY = .2120+05 AND ZIXZ = -.7359+04

Table A.21 RUN NO. 9

CANADAIR CL-84 42.KNOTS DESCENT 1[illegible].FT/SEC SAS ON

INPUT DATA Stability Derivatives

DIMENSIONAL DERIVATIVES TIMES INERTIA
UNITS ARE 1 PER RADIAN
(STABILITY AXES)

DYDV	=	-.2933+02	DLDV	=	-.1289+03	DNDV	= .3933+03
DYDP	=	.2775+02	DLDP	=	-.4675+05	DNDP	= -.3901+04
DYDR	=	.4095+03	DLDR	=	-.2172+05	DNDR	= -.3254+05
DYDVD	=	-.0000	DLDVD	=	-.0000	DNDVD	= -.0000
DYDPD	=	-.0000	DLDPD	=	-.0000	DNDPD	= -.0000
DYDRD	=	-.0000	DLDRD	=	.0000	DNDRD	= .0000
DYDA	=	.3943-00	DLDA	=	.5365+05	DNDA	= -.7229+04
DYDR	=	-.3048+03	DLDR	=	.9211+05	DNDR	= .3711+05

U	=	.6754+02	UZ	=	.2190+02	GAMA	= -.1302+02
MACH	=	.6356-01	RHO	=	.2380-02	S	= .2333+03
MAC	=	.7000+01	IXZ	=	-.7359+04	IY	= .2120+05
HT	=	-.0000	XI	=	-.0000	TDT	= -.0000
LX	=	-.0000	LY	=	-.0000	LZ	= -.0000
CL	=	.0000	CD	=	.0000	W	= .1120+05
IX	=	.2106+05	IZ	=	.3114+05	G	= .3220+02
SPAN	=	.3330+02					

DIMENSIONAL STABILITY DERIVATIVES, PER RADIAN,
STABILITY AXES

YV	=	-.8432-01	LV	=	-.6121-02	NV	= .1263-01
YP	=	.7987-01	LP	=	-.2220+01	NP	= -.1253-00
YR	=	.1177+01	LR	=	-.1031+01	NR	= -.1045+01
YVD	=	.0000	LVD	=	.0000	NVD	= .0000
YPD	=	.0000	LPD	=	.0000	NPD	= .0000
YRD	=	.0000	LRD	=	.0000	NRD	= .0000
YA	=	.1134-02	LA	=	.2547+01	NA	= -.2321-00
YDR	=	-.8763-00	LDR	=	.2474+01	NDR	= .1192+01

DIMENSIONAL DERIVATIVES, PRIMED

YV	=	-.8432-01	LV	=	-.1148-01	NV	= .1672-01
YP	=	.7987-01	LP	=	-.2372+01	NP	= .4744-00
YR	=	.1177+01	LR	=	-.7262-00	NR	= -.9520-00
YVD	=	.0000	LVD	=	.0000	NVD	= .0000
YPD	=	.0000	LPD	=	.0000	NPD	= .0000
YRD	=	.0000	LRD	=	.0000	NRD	= .0000
YA	=	.1134-02	LA	=	.2865+01	NA	= -.9911-00
YDR	=	-.8763-00	LDR	=	.2243+01	NDR	= .7212-00

IN STABILITY AXES, U= .7100+02
.IXX= .2106+05 IZZ= .3114+05 IXZ=-.7359+04

Table A.22 RUN NO. 9

CANADAIR CL-84 42.KNOTS DESCENT 16.FT/SEC SAS OFF

INPUT DATA Stability Derivatives

DIMENSIONAL DERIVATIVES TIMES INERTIA
UNITS ARE 1 PER RADIAN
(STABILITY AXES)

DYDV =	-.2933+02	DLDV =	-.1289+03	DNDV =	.3933+03
DYDP =	.2808+02	DLDP =	-.7713+04	DNDP =	-.1084+04
DYDR =	.4097+03	DLDR =	.3044+04	DNDR =	-.1157+05
DYDVD =	-.0000	DLDVD =	-.0000	DNDVD =	-.0000
DYDPD =	-.0000	DLDPD =	-.0000	DNDPD =	-.0000
DYDRD =	-.0000	DLDRD =	.0000	DNDRD =	.0000
DYDA =	.3943-00	DLDA =	.5365+05	DNDA =	-.7229+04
DYDR =	-.3046+03	DLDR =	.5211+05	DNDR =	.3711+05

U =	.6754+02	UZ =	.2190+02	GAMA =	-.1302+02
MACH =	.6356-01	RHO =	.2380-02	S =	.2333+03
MAC =	.7000+01	IXZ =	-.7359+04	IY =	.2120+05
HT =	-.0000	XI =	-.0000	TDT =	-.0000
LX =	-.0000	LY =	-.0000	LZ =	-.0000
CL =	.0000	CD =	.0000	W =	.1120+05
IX =	.2106+05	IZ =	.3114+05	G =	.3220+02
SPAN =	.3330+02				

DIMENSIONAL STABILITY DERIVATIVES,PER RADIAN,
STABILITY AXES

YV =	-.8432-01	LV =	-.6121-02	NV =	.1263-01
YP =	.8073-01	LP =	-.3330-00	NP =	-.3461-01
YR =	.1178+01	LR =	.1445-00	NR =	-.3715-00
YVD =	.0000	LVD =	.0000	NVD =	.0000
YPD =	.0000	LPD =	.0000	NPD =	.0000
YRD =	.0000	LRD =	.0000	NRD =	.0000
YA =	.1134-02	LA =	.2547+01	NA =	-.2321-00
YDR=	-.8763-00	LDR=	.2474+01	NDR=	.1192+01

DIMENSIONAL DERIVATIVES, PRIMED

YV =	-.8432-01	LV =	-.1146-01	NV =	.1672-01
YP =	.8073-01	LP =	-.3497-00	NP =	.5214-01
YR =	.1178+01	LR =	.2991-00	NR =	-.4820-00
YVD =	.0000	LVD =	.0000	NVD =	.0000
YPD =	.0000	LPD =	.0000	NPD =	.0000
YRD =	.0000	LRD =	.0000	NRD =	.0000
YA =	.1134-02	LA =	.2865+01	NA =	-.9911-00
YDR=	-.8763-00	LDR=	.2243+01	NDR=	.7212-00

IN STABILITY AXES, U= .7100+02
IXX= .2106+05 IZZ= .3114+05 IXZ=-.7359+04

Table A.23 RUN NO. 13

CANADAIR CL-84 80.KNOTS LEVEL FLIGHT SAS ON

INPUT DATA Stability Derivatives

UNITS ARE 1 PER RADIAN
DIMENSIONAL DERIVATIVES TIMES INERTIA
(STABILITY AXES)

DXDU	=	-.3755+02	DZDU	=	-.1344+03	DMDU	=	.1135+03
DXDW	=	.1329+02	DZDW	=	-.2331+03	DMDW	=	-.5982+03
DXDQ	=	-.1549+03	DZDQ	=	-.2564+04	DMDQ	=	-.7160+05
DXDUD	=	-.0000	DZDUD	=	-.0000	DMDUD	=	-.0000
DXDWD	=	-.0000	DZDWD	=	-.0000	DMDWD	=	-.0000
DXDQD	=	-.0000	DZDQD	=	.0000	DMDQD	=	.0000
DXDE	=	.4707+03	DZDE	=	.3553+04	DMDE	=	.8993+05
DXDT	=	.3279+05	DZDT	=	-.2432+05	DMDT	=	.1091+05
U	=	.1345+03	UZ	=	-.1201+02	GAMA	=	-.2436-02
MACH	=	.1209+00	RHO	=	.2360-02	S	=	.2333+03
MAC	=	.7000+01	IXZ	=	.6573+03	IY	=	.2050+05
MT	=	-.0000	XI	=	-.0000	TDT	=	-.0000
LY	=	-.0000	LY	=	-.0000	LZ	=	-.0000
CL	=	.0000	CD	=	.0000	M	=	.1120+05
IX	=	.1019+05	IZ	=	.3451+05	G	=	.3220+02

DIMENSIONAL STABILITY DERIVATIVES, PER RADIAN,
STABILITY AXES

XU	=	-.1080+00	ZU	=	-.3864-00	MU	=	.5537-02
XW	=	.3821-01	ZW	=	-.6702+00	MW	=	-.2918-01
XQ	=	-.4453-00	ZQ	=	-.7429+01	MQ	=	-.3493+01
XUD	=	.0000	ZUD	=	.0000	MUD	=	.0000
XWD	=	.0000	ZWD	=	.0000	MWD	=	.0000
XQD	=	.0000	ZQD	=	.0000	MQD	=	.0000
XD	=	.1353+01	ZD	=	.1021+02	MD	=	.4387+01
XT	=	.9427+02	ZT	=	-.6992-02	MT	=	.5322-00

IN STABILITY AXES, U = .1360+03 AND U = 0.0
ZIY = .2050+05 AND ZIXZ = .6573+03

Table A.24 RUN NO. 13

CANADAIR CL-84 80.KNOTS LEVEL FLIGHT SAS OFF

INPUT DATA Stability Derivatives

UNITS ARE 1 PER RADIAN
DIMENSIONAL DERIVATIVES TIMES INERTIA
(STABILITY AXES)

DXDU =	-.3759+02	DZDU =	-.1344+03	DMDU =	.1135+03
DXDW =	.1329+02	DZDW =	-.2331+03	DMDW =	-.5982+03
DXDQ =	-.2038+03	DZDQ =	-.1305+04	DMDQ =	-.3578+05
DXDUC =	-.0000	DZDUC =	-.0000	DMDUC =	-.0000
DXDWD =	-.0000	DZDWD =	-.0000	DMDWD =	-.0000
DXDQD =	-.0100	DZDQD =	.0000	DMDQD =	.0000
DXDE =	.4707+03	DZDE =	.3553+04	DMDE =	.8993+05
DXDT =	.3279+05	DZDT =	-.2432+05	DMDT =	.1091+05

U =	.1345+03	W =	-.1201+02	GAMA =	-.2436-02
MACH =	.1209+00	RHO =	.2350-02	S =	.2333+03
MAC =	.7000+01	IXZ =	.6573+03	IY =	.2050+05
UT =	-.0000	XI =	-.0000	TDT =	-.0000
LX =	-.0000	LY =	-.0000	LZ =	-.0000
CL =	.0000	CD =	.0000	W =	.1120+05
IX =	.1019+05	IZ =	.3451+05	G =	.3220+02

DIMENSIONAL STABILITY DERIVATIVES, PER RADIAN,
STABILITY AXES

XU =	-.1080+00	ZU =	-.3884-00	MU =	.5537-02
XW =	.3821-01	ZW =	-.6702-00	MW =	-.2918-01
XQ =	-.5859-00	ZQ =	-.3738+01	MQ =	-.1745+01
XUD =	.0000	ZUD =	.0000	MUD =	.0000
XWD =	.0000	ZWD =	.0000	MWD =	.0000
XQD =	.0000	ZQD =	.0000	MQD =	.0000
XD =	.1353+04	ZD =	.1021+02	MD =	.4397+01
XT =	.9427+02	ZT =	-.6992+02	MT =	.5322-00

IN STABILITY AXES, U = .1350+03 AND W = 0.0
ZIY = .2050+05 AND ZIXZ = .6573+03

Table A. 25 RUN NO. 13

CANADAIR CL-84 60.KNOTS LEVEL FLIGHT SAS ON

INPUT DATA Stability Derivatives

DIMENSIONAL DERIVATIVES TIMES INERTIA
UNITS ARE 1 PER RADIAN
(STABILITY AXES)

CYDV =	-.5435+02	DLDV =	-.4912+03	DNDV =	.4514+03
CYDP =	-.2546+03	DLDP =	-.7541+05	DNDP =	.1677+05
CYDR =	.7642+03	DLDR =	.5127+05	DNDR =	-.8411+05
DYDVD =	-.0000	DLDVD =	-.0000	DNDVD =	-.0000
DYDPD =	-.0000	DLDPD =	-.0000	DNDPD =	-.0000
DYDRD =	-.0000	DLDRD =	.0000	DNDRD =	.0000
DYDA =	.2747-00	DLDA =	.9538+05	DNDA =	-.9232+04
DYDR =	-.1192+04	DLDR =	-.6728+05	DNDR =	.1294+06

U =	.1345+03	UZ =	-.1201+02	GAMA =	-.2436-02
MACH =	.1209+00	RHO =	.2380-02	S =	.2333+03
MAC =	.7000+01	IXZ =	.6573+03	IY =	.2050+05
HT =	-.0000	XI =	-.0000	TOT =	-.0000
LX =	-.0000	LY =	-.0000	LZ =	-.0000
CL =	.0000	CD =	.0000	W =	.1120+05
IX =	.1819+05	IZ =	.3451+05	G =	.3220+02
SPAN =	.3330+02				

DIMENSIONAL STABILITY DERIVATIVES,PER RADIAN,
STABILITY AXES

YV =	-.1563-00	LV =	-.2700-01	NV =	.1308-01
YP =	-.7320-00	LP =	-.4146+01	NP =	.4859-00
YR =	.2197+01	LR =	.2819+01	NR =	-.2437+01
YVD =	.0000	LVD =	.0000	NVD =	.0000
YPD =	.0000	LPD =	.0000	NPD =	.0000
YRD =	.0000	LRD =	.0000	NRD =	.0000
YA =	.7898-03	LA =	.5244+01	NA =	-.2675-00
YDR=	-.3427+01	LDR=	-.3699+01	NDR=	.3750+01

DIMENSIONAL DERIVATIVES, PRIMED

YV =	-.1563-00	LV =	-.2655-01	NV =	.1258-01
YP =	-.7320-00	LP =	-.4131+01	NP =	.4075-00
YR =	.2197+01	LR =	.2732+01	NR =	-.2387+01
YVD =	.0000	LVD =	.0000	NVD =	.0000
YPD =	.0000	LPD =	.0000	NPD =	.0000
YRD =	.0000	LRD =	.0000	NRD =	.0000
YA =	.7898-03	LA =	.5237+01	NA =	-.1679-00
YDR=	-.3427+01	LDR=	-.3566+01	NDR=	.3684+01

IN STABILITY AXES, U= .1350+03
,IXX= .1819+05 IZZ= .3451+05 IXZ= .6573+03

Table A. 26 RUN NO. 13

CANADAIR CL-84 80.KNOTS LEVEL FLIGHT SAS OFF

INPUT DATA Stability Derivatives

DIMENSIONAL DERIVATIVES TIMES INERTIA
UNITS ARE 1 PER RADIAN
(STABILITY AXES)

DYDV =	-.5435+02	DLDV =	-.4912+03	DNDV =	.4514+03
DYDP =	-.2565+03	DLDP =	-.1686+05	DNDP =	.5415+04
DYDR =	.7849+03	DLDR =	.1323+05	DNDR =	-.1476+05
DYDVD =	-.0000	DLDVD =	-.0000	DNDVD =	-.0000
DYDPD =	-.0000	DLDPD =	-.0000	DNDPD =	-.0000
DYDRD =	-.0000	DLDRD =	.0000	DNDRD =	.0000
DYDA =	.2747-00	DLDA =	.9536+05	DNDA =	-.9232+04
DYDR =	-.1192+04	DLDR =	-.6728+05	DNDR =	.1294+06

U =	.1345+03	UZ =	-.1208+02	GAMA =	-.2436-02
MACH =	.1209+00	RHO =	.2380-02	S =	.2333+03
MAC =	.7000+01	IXZ =	.6573+03	IY =	.2050+05
MT =	-.0000	XI =	-.0000	TDT =	-.0000
LX =	-.0000	LY =	-.0000	LZ =	-.0000
CL =	.0000	CD =	.0000	W =	.1120+05
IX =	.1819+05	IZ =	.3451+05	G =	.3220+02
SPAN =	.3330+02				

DIMENSIONAL STABILITY DERIVATIVES,PER RADIAN,
STABILITY AXES

YV =	-.1363-00	LV =	-.2700-01	NV =	.1308-01
YP =	-.7317-00	LP =	-.1037+01	NP =	.1569-00
YR =	.2199+01	LR =	.7273-00	NR =	-.4277-00
YVD =	.0000	LVD =	.0000	NVD =	.0000
YPD =	.0000	LPD =	.0000	NPD =	.0000
YRD =	.0000	LRD =	.0000	NRD =	.0000
YA =	.7896-03	LA =	.5244+01	NA =	-.2675-00
YDR=	-.3427+01	LDR=	-.3699+01	NDR=	.3750+01

DIMENSIONAL DERIVATIVES, PRIMED

YV =	-.1363-00	LV =	-.2655-01	NV =	.1258-01
YP =	-.7317-00	LP =	-.1032+01	NP =	.1374-00
YR =	.2199+01	LR =	.7124-00	NR =	-.4144-00
YVD =	.0000	LVD =	.0000	NVD =	.0000
YPD =	.0000	LPD =	.0000	NPD =	.0000
YRD =	.0000	LRD =	.0000	NRD =	.0000
YA =	.7896-03	LA =	.5237+01	NA =	-.1679-00
YDR=	-.3427+01	LDR=	-.3566+01	NDR=	.3684+01

IN STABILITY AXES, U= .1350+03
,IXX= .1819+05 IZZ= .3451+05 IXZ= .6573+03

Table A. 27 RUN NO. 15

CANADAIR CL-84 80.KNOTS DESCENT 30.FT.SEC SAS ON

INPUT DATA Stability Derivatives

UNITS ARE 1 PER RADIAN
DIMENSIONAL DERIVATIVES TIMES INERTIA
(STABILITY AXES)

DXDU =	-.5712+02	DZDU =	-.3409+03	DMDU =	-.6767+02
DXDW =	-.1683+02	DZDW =	-.2837+03	DMDW =	-.9758+03
DXDQ =	-.3361+02	DZDQ =	-.2653+04	DMDQ =	-.7226+05
DXDUD =	-.0000	DZDUD =	-.0000	DMDUD =	-.0000
DXDWD =	-.0000	DZDWD =	-.0000	DMDWD =	-.0000
DXDQD =	-.0000	DZDQD =	.0000	DMDQD =	.0000
DXDE =	.2699+03	DZDE =	.3462+04	DMDE =	.3944+05
DXDT =	.2672+05	DZDT =	-.3146+05	DMDT =	.2058+05

U =	.1364+03	UZ =	.7886+01	GAMA =	-.1284+02
MACH =	.1209+00	RHO =	.2380-02	S =	.2333+03
MAC =	.7920+01	IXZ =	-.1745+04	IY =	.2050+05
HT =	-.0300	XI =	-.1000	TDT =	-.0000
LX =	-.0000	LY =	-.0000	LZ =	-.0000
CL =	.0000	CD =	.0000	W =	.1120+05
IX =	.1835+05	IZ =	.3435+05	G =	.3220+02

DIMENSIONAL STABILITY DERIVATIVES, PER RADIAN,
STABILITY AXES

XU =	-.1942-00	ZU =	-.4051-00	MU =	-.3301-02
XW =	-.4639-01	ZW =	-.5281-00	MW =	-.4700-01
XQ =	-.9663-01	ZQ =	-.7627+01	MQ =	-.3525+01
XUD =	.0000	ZUD =	.0000	MUD =	.0000
XWD =	.0000	ZWD =	.0000	MWD =	.0000
XQD =	.0000	ZQD =	.0000	MQD =	.0000
XD =	.7472-00	ZD =	.1001+02	MD =	.4363+01
XT =	.7682+02	ZT =	-.9045+02	MT =	.1004+01

IN STABILITY AXES, U = .1350+03 AND W = 0.0
ZIY = .2050+05 AND ZIXZ = -.1745+04

Table A. 28 RUN NO. 15

CANADAIR CL-84 80.KNOTS DESCENT 30.FT/SEC SAS OFF

INPUT DATA Stability Derivatives

UNITS ARE 1 PER RADIAN
DIMENSIONAL DERIVATIVES TIMES INERTIA
(STABILITY AXES)

DXDU =	-.5712+02	DZDU =	-.1409+03	DMDU =	-.6767+02
DXDW =	-.1683+02	DZDW =	-.1837+03	DMDW =	-.9759+03
DXDQ =	.2960+02	DZDQ =	-.1391+04	DMDQ =	-.3670+05
DXDUD =	-.0000	DZDUD =	-.0000	DMDUD =	-.0000
DXDWD =	-.0000	DZDWD =	-.0000	DMDWD =	-.0000
DXDQD =	-.0000	DZDQD =	.0000	DMDQD =	.0000
DXDE =	.2599+03	DZDE =	.3492+04	DMDE =	.8944+05
DXDT =	.2672+03	DZDT =	-.3146+05	DMDT =	.2058+05

U =	.1348+03	UZ =	.7886+01	GAMA =	-.1284+02
MACH =	.1209+00	RHO =	.2390-02	S =	.2333+03
MAC =	.7000+01	IXZ =	-.1745+04	IY =	.2050+05
MT =	-.0000	XI =	-.0000	TDT =	-.0000
LX =	-.0000	LY =	-.0000	LZ =	-.0000
CL =	.0000	CD =	.0000	W =	.1120+05
IX =	.1535+05	IZ =	.3435+05	G =	.3220+02

DIMENSIONAL STABILITY DERIVATIVES, PER RADIAN,
STABILITY AXES

XU =	-.1542-00	ZU =	-.4091-00	MU =	-.3301-02
XW =	-.4039-01	ZW =	-.5281-00	MW =	-.4760-01
XQ =	.5222-01	ZQ =	-.3999+01	MQ =	-.1790+01
XUD =	.0000	ZUD =	.0000	MUD =	.0000
XWD =	.0000	ZWD =	.0000	MWD =	.0000
XQD =	.0000	ZQD =	.0000	MQD =	.0000
XE =	.7472-00	ZE =	.1001+02	ME =	.4363+01
XT =	.7682+02	ZT =	-.9045+02	MT =	.1004+01

IN STABILITY AXES, U = .1350+03 AND R = 0.0
ZIY = .2050+05 AND ZIXZ = -.1745+04

Table A. 29 RUN NO. 15

CANADAIR CL-84 80.KNOTS DESCENT 30.FT/SEC SAS ON

INPUT DATA

Stability Derivatives

DIMENSIONAL DERIVATIVES TIMES INERTIA
UNITS ARE 1 PER RADIAN
(STABILITY AXES)

)YDV =	-.5284+02	DLDV =	-.3173+03	DNDV =	.4692+03
)YDP =	-.1348+03	DLDP =	-.4213+05	DNDP =	.9540+03
)YDR =	.7992+03	DLDR =	.9509+04	DNDR =	-.6963+05
'DVD =	-.0000	DLDVD =	-.0000	DNDVD =	-.0000
'DPD =	-.0000	DLDPD =	-.0000	DNDPD =	-.0000
'DRD =	-.0000	DLDRD =	.0000	DNDRD =	.0000
)YDA =	-.1064+00	DLDA =	.8557+05	DNDA =	-.4258+04
)YDR =	-.1193+04	DLDR =	.3114+04	DNDR =	.1082+06

U =	.1350+03	UZ =	.7836+01	GAMA =	-.1284+02
MACH =	.1209+00	RHO =	.2380-02	S =	.2333+03
MAC =	.7000+01	IXZ =	-.1745+04	IY =	.2050+05
HT =	-.0000	XI =	-.0000	TDT =	-.0000
LX =	-.0000	LY =	-.0000	LZ =	-.0000
CL =	.0000	CD =	.0000	W =	.1120+05
IX =	.1835+05	IZ =	.3435+05	G =	.3220+02
SPAN =	.3330+02				

DIMENSIONAL STABILITY DERIVATIVES, PER RADIAN,
STABILITY AXES

YV =	-.1520-00	LV =	-.1729-01	NV =	.1366-01
YP =	-.3875-00	LP =	-.2296+01	NP =	.2777-01
YR =	.2298+01	LR =	.5182-00	NR =	-.2027+01
YVD =	.0000	LVD =	.0000	NVD =	.0000
YPD =	.0000	LPD =	.0000	NPD =	.0000
YRD =	.0000	LRD =	.0000	NRD =	.0000
YA =	-.3059-03	LA =	.3028+01	NA =	-.1240+00
YDR=	-.3444+01	LDR=	.1697-00	NDR=	.3150+01

DIMENSIONAL DERIVATIVES, PRIMED

YV =	-.1520-00	LV =	-.1868-01	NV =	.1466-01
YP =	-.3875-00	LP =	-.2310+01	NP =	.1458-00
YR =	.2298+01	LR =	.7144-00	NR =	-.2073+01
YVD =	.0000	LVD =	.0000	NVD =	.0000
YPD =	.0000	LPD =	.0000	NPD =	.0000
YRD =	.0000	LRD =	.0000	NRD =	.0000
YA =	-.3059-03	LA =	.3055+01	NA =	-.2805-00
YDR=	-.3444+01	LDR=	-.1305-00	NDR=	.3172+01

IN STABILITY AXES, U= .1350+03
IXX= .1835+05 IZZ= .3435+05 IXZ=-.1745+04

Table A. 30 RUN NO. 15

CANADAIR CL-84 80.KNOTS DESCENT 30.FT/SEC SAS OFF

INPUT DATA Stability Derivatives

DIMENSIONAL DERIVATIVES TIMES INERTIA
UNITS ARE 1 PER RADIAN
(STABILITY AXES)

DYDV =	-.5886+02	DLDV =	-.3173+03	DNDV =	.4692+03
DYDP =	-.1349+03	DLDP =	-.1115+05	DNDP =	.1771+04
DYDR =	.7985+03	DLDR =	.1175+05	DNDR =	-.1526+05
DYDVD =	-.0000	DLDVD =	-.0000	DNDVD =	-.0000
DYDPD =	-.0000	DLDPD =	-.0000	DNDPD =	-.0000
DYDRD =	-.0000	DLDRD =	.0000	DNDRD =	.0000
DYDA =	-.1064+00	DLDA =	.5557+05	DNDA =	-.4258+04
DYDR =	-.1196+04	DLDR =	.3114+04	DNDR =	.1082+06
U =	.1348+03	UZ =	.7956+01	GAMA =	-.1284+02
MACH =	.1209+00	AMC =	.2360-02	S =	.2333+03
MAC =	.7000+01	IXZ =	-.1745+04	IY =	.2050+05
HT =	-.0000	XT =	-.0000	TDT =	-.0000
LX =	-.0000	LY =	-.0000	LZ =	-.0000
CL =	.0000	CD =	.0000	T =	.1120+05
IX =	.1835+05	IZ =	.3435+05	G =	.3220+02
SPAN =	.3330+02				

DIMENSIONAL STABILITY DERIVATIVES,PER RADIAN,
STABILITY AXES

YV =	-.1520-00	LV =	-.1729-01	NV =	.1366-01
YP =	-.3678-00	LP =	-.6049-00	NP =	.5156-01
YR =	.2297+01	LR =	.6403-00	NR =	-.4443-00
YVD =	.0000	LVD =	.0000	NVD =	.0000
YPD =	.0000	LPD =	.0000	NPD =	.0000
YRD =	.0000	LRD =	.0000	NRD =	.0000
YA =	-.3059-03	LA =	.3028+01	NA =	-.1240+00
YDR=	-.3444+01	LDR=	.1697-00	NDR=	.3150+01

DIMENSIONAL DERIVATIVES, PRIMED

YV =	-.1520-00	LV =	-.1668-01	NV =	.1468-01
YP =	-.3678-00	LP =	-.6126-00	NP =	.8309-01
YR =	.2297+01	LR =	.6859-00	NR =	-.4814-00
YVD =	.0000	LVD =	.0000	NVD =	.0000
YPD =	.0000	LPD =	.0000	NPD =	.0000
YRD =	.0000	LRD =	.0000	NRD =	.0000
YA =	-.3059-03	LA =	.3055+01	NA =	-.2805-00
YDR=	-.3444+01	LDR=	-.1305-00	NDR=	.3172+01

IN STABILITY AXES, U= .1350+03
,IXX= .1835+05 IZZ= .3435+05 IXZ=-.1745+04

APPENDIX B

X-22A STABILITY DERIVATIVES

Introduction

The stability derivatives presented here are taken from Reference 31. For the reasons explained in the main text, only lateral derivatives are presented. The flight conditions are listed in Table 8 of the main text.

The printout contains some redundant information, such as Mach Number, which is arbitrarily set to zero, without affecting the accuracy of the derivatives. The yaw and roll derivatives are referred to the stick and pedals, and include the effects of control blending. These derivatives are denoted as NA, NR, YA, YR, LA, LR; and care should be taken to avoid confusion with the yaw rate derivatives, which are also denoted as NR, YR, LR. The yaw rate derivatives can be distinguished from the rudder pedal derivatives by noting that the latter are always printed adjacent to the YA, LA, NA derivatives. The inertias referred to stability axes are denoted ZIX,ZIZ,ZIXZ.

TABLE B-1 RUN NO. 1

BELL X-224 W=16770LB H=0FT UO= 10.0FPS GAMMA=-12.1DEG -AX= 0.0G

INPUT DATA

DIMENSIONAL STABILITY DERIVATIVES
UNITS ARE 1 PER RADIAN
(BODY AXES DIFFER BY .4972+01 DEGREES, POSITIVE FOR NOSE UP, FROM STABILITY AXES)

YV =	-.4700-00	LV =	-.1120+00	NV =	.1950-01
YP =	-.7700-00	LP =	-.2800-00	NP =	.0000
YR =	-.0000	LR =	-.1770-00	NR =	-.1480-00
YVD =	-.0000	LVD =	-.0000	NVD =	-.0000
YPD =	-.0000	LPD =	-.0000	NPD =	-.0000
YRD =	-.0000	LRD =	-.0000	NRD =	-.0000
YA =	.0000	LA =	.1970+01	NA =	.0000
YR =	.0000	LR =	.0000	NR =	.7000-00
U =	.1000+02	UZ =	.8700-00	GAMA =	-.1210+02
MACH =	.0000	RHO =	.0000	S =	.0000
MAC =	.0000	IXZ =	.2530+04	IY =	.5160+05
HT =	.0000	XI =	.0000	TDT =	.0000
LX =	.1600+02	LY =	.0000	LZ =	.0000
CL =	.0000	CD =	.0000	W =	.1677+05
IX =	.2175+05	IZ =	.4580+05	G =	.3220+02
SPAN =	.0000				

DIMENSIONAL STABILITY DERIVATIVES, PER RADIAN, STABILITY AXES

YV =	-.4700-00	LV =	-.1165+00	NV =	.2390-01
YP =	-.7671-00	LP =	-.2681-00	NP =	.2350-01
YR =	.6674-01	LR =	-.1261-00	NR =	-.1398-00
YVD =	.0000	LVD =	.0000	NVD =	.0000
YPD =	.0000	LPD =	.0000	NPD =	.0000
YRD =	.0000	LRD =	.0000	NRD =	.0000
YA =	.0000	LA =	.1986+01	NA =	-.8063-01
YR =	.0000	LR =	-.1295-00	NR =	.6935-00

DIMENSIONAL DERIVATIVES, PRIMED

YV =	-.4700-00	LV =	-.1170+00	NV =	.2496-01
YP =	-.7671-00	LP =	-.2686-00	NP =	.2592-01
YR =	.6674-01	LR =	-.1234+00	NR =	-.1388-00
YVD =	.0000	LVD =	.0000	NVD =	.0000
YPD =	.0000	LPD =	.0000	NPD =	.0000
YRD =	.0000	LRD =	.0000	NRD =	.0000
YA =	.0000	LA =	.1988+01	NA =	-.9858-01
YR =	.0000	LR =	-.1427-00	NR =	.6949-00

IN STABILITY AXES, U = .1004+02, ZIX = .2149+05
AND ZIZ = .4606+05

TABLE B-2 RUN NO, 1

X-22 + SAS W=16770LB H=0FT U0= 10.0FPS GAMMA=-12.1DEG -AX= 0.0G

INPUT DATA

DIMENSIONAL STABILITY DERIVATIVES
UNITS ARE 1 PER RADIAN
(BODY AXES DIFFER BY .4972+01 DEGREES, POSITIVE
FOR NOSE UP, FROM STABILITY AXES)

YV =	-.4700-00	LV =	-.1120+00	NV =	.1950-01
YP =	-.7700-00	LP =	-.3610+01	NP =	.0000
YR =	-.0000	LR =	-.1770-00	NR =	-.1728+01
YVD =	-.0000	LVD =	-.0000	NVD =	-.0000
YPD =	-.0000	LPD =	-.0000	NPD =	-.0000
YRD =	-.0000	LRD =	-.0000	NRD =	-.0000
YA =	.0000	LA =	.1970+01	NA =	.0000
YR =	.0000	LR =	.0000	NR =	.7000-00
U =	.1000+02	UZ =	.8700-00	GAMA =	-.1210+02
MACH =	.0000	RHO =	.0000	S =	.0000
MAC =	.0000	IXZ =	.2530+04	IY =	.3160+05
HT =	.0000	XI =	.0000	TDT =	.0000
LX =	.1600+02	LY =	.0000	LZ =	.0000
CL =	.0000	CD =	.0000	W =	.1677+05
IX =	.2175+05	IZ =	.4580+05	G =	.3220+02
SPAN =	.0000				

DIMENSIONAL STABILITY DERIVATIVES,PER RADIAN,
STABILITY AXES

YV =	-.4700-00	LV =	-.1165+00	NV =	.2390-01
YP =	-.7671-00	LP =	-.3638+01	NP =	.2950-00
YR =	.6674-01	LR =	.4556-00	NR =	-.1711+01
YVD =	.0000	LVD =	.0000	NVD =	.0000
YPD =	.0000	LPD =	.0000	NPD =	.0000
YRD =	.0000	LRD =	.0000	NRD =	.0000
YA =	.0000	LA =	.1986+01	NA =	-.8063-01
YR =	.0000	LR =	-.1293-00	NR =	.6935-00

DIMENSIONAL DERIVATIVES, PRIMED

YV =	-.4700-00	LV =	-.1170+00	NV =	.2496-01
YP =	-.7671-00	LP =	-.3644+01	NP =	.3279-00
YR =	.6674-01	LR =	.4886-00	NR =	-.1716+01
YVD =	.0000	LVD =	.0000	NVD =	.0000
YPD =	.0000	LPD =	.0000	NPD =	.0000
YRD =	.0000	LRD =	.0000	NRD =	.0000
YA =	.0000	LA =	.1988+01	NA =	-.9858-01
YR =	.0000	LR =	-.1427-00	NR =	.6949-00

IN STABILITY AXES, U = .1004+02, ZIX = .2149+05
AND ZIZ = .4606+05

TABLE B-3 RUN NO. 3

BELL X-22A W=16770LB H=0FT UO= 67.5FPS GAMMA= -7.1DEG -AX= 0.0G

INPUT DATA

DIMENSIONAL STABILITY DERIVATIVES
UNITS ARE 1 PER RADIAN
(BODY AXES DIFFER BY .4979+01 DEGREES, POSITIVE FOR NOSE UP, FROM STABILITY AXES)

YV =	-.3030-00	LV =	-.5800-01	NV =	.2200-02
YP =	-.1270+01	LP =	-.9300-00	NP =	-.2310-00
YR =	-.0000	LR =	.2340-00	NR =	-.4010-00
YVD =	-.0000	LVD =	-.0000	NVD =	-.0000
YPD =	-.0000	LPD =	-.0000	NPD =	-.0000
YRD =	-.0000	LRD =	-.0000	NRD =	-.0000
YA =	.0000	LA =	.2070+01	NA =	.7640-01
YR =	.0000	LR =	.3220-01	NR =	.7650-00
U =	.6750+02	UZ =	.5880+01	GAMA =	-.7100+01
MACH =	.0000	RHO =	.0000	S =	.0000
MAC =	.0000	IXZ =	.2530+04	IY =	.3160+05
HT =	.0000	XI =	.0000	TDT =	.0000
LX =	.1600+02	LY =	.0000	LZ =	.0000
CL =	.0000	CD =	.0000	W =	.1677+05
IX =	.2175+05	IZ =	.4560+05	G =	.3220+02
SPAN =	.0000				

DIMENSIONAL STABILITY DERIVATIVES,PER RADIAN, STABILITY AXES

YV =	-.3030-00	LV =	-.5988-01	NV =	.4557-02
YP =	-.1265+01	LP =	-.9164-00	NP =	-.1547-00
YR =	.1102+00	LR =	.3865-00	NR =	-.3808-00
YVD =	.0000	LVD =	.0000	NVD =	.0000
YPD =	.0000	LPD =	.0000	NPD =	.0000
YRD =	.0000	LRD =	.0000	NRD =	.0000
YA =	.0000	LA =	.2073+01	NA =	-.9146-02
YR =	.0000	LR =	-.1090+00	NR =	.7566-00

DIMENSIONAL DERIVATIVES, PRIMED

YV =	-.3030-00	LV =	-.5697-01	NV =	.5086-02
YP =	-.1265+01	LP =	-.9155-00	NP =	-.1465-00
YR =	.1102+00	LR =	.3941-00	NR =	-.3924-00
YVD =	.0000	LVD =	.0000	NVD =	.0000
YPD =	.0000	LPD =	.0000	NPD =	.0000
YRD =	.0000	LRD =	.0000	NRD =	.0000
YA =	.0000	LA =	.2073+01	NA =	-.2773-01
YR =	.0000	LR =	-.1235+00	NR =	.7578-00

IN STABILITY AXES, U = .6776+02, ZIX = .2149+05
AND ZIZ = .4606+05

TABLE B-4 RUN NO, 3

X-22 + SAS W=16770LB H=0FT U0= 67.5FPS GAMMA= -7.1DEG -AX= 0.0G

INPUT DATA

DIMENSIONAL STABILITY DERIVATIVES
UNITS ARE 1 PER RADIAN
(BODY AXES DIFFER BY .4979+01 DEGREES, POSITIVE FOR NOSE UP, FROM STABILITY AXES)

YV =	-.3030-00	LV =	-.5800-01	NV =	.2200-02
YP =	-.1270+01	LP =	-.4190+01	NP =	-.3510-00
YR =	-.0000	LR =	.1625-00	NR =	-.2101+01
YVD =	-.0000	LVD =	-.0000	NVD =	-.0000
YPD =	-.0000	LPD =	-.0000	NPD =	-.0000
YRD =	-.0000	LRD =	-.0000	NRD =	-.0000
YA =	.0000	LA =	.2070+01	NA =	.7640-01
YR =	.0000	LR =	.3220-01	NR =	.7650-00
U =	.6750+02	UZ =	.5880+01	GAMA =	-.7100+01
MACH =	.0000	RHO =	.0000	S =	.0000
MAC =	.0000	IXZ =	.2530+04	IY =	.3160+05
HT =	.0000	XI =	.0000	TDT =	.0000
LX =	.1600+02	LY =	.0000	LZ =	.0000
CL =	.0000	CD =	.0000	W =	.1677+05
IX =	.2175+05	IZ =	.4580+05	G =	.3220+02
SPAN =	.0000				

DIMENSIONAL STABILITY DERIVATIVES,PER RADIAN, STABILITY AXES

YV =	-.3030-00	LV =	-.5888-01	NV =	.4557-02
YP =	-.1265+01	LP =	-.4191+01	NP =	.5862-02
YR =	.1102+00	LR =	.9112-00	NR =	-.2065+01
YVD =	.0000	LVD =	.0000	NVD =	.0000
YPD =	.0000	LPD =	.0000	NPD =	.0000
YRD =	.0000	LRD =	.0000	NRD =	.0000
YA =	.0000	LA =	.2073+01	NA =	-.9146-02
YR =	.0000	LR =	-.1090+00	NR =	.7566-00

DIMENSIONAL DERIVATIVES, PRIMED

YV =	-.3030-00	LV =	-.5897-01	NV =	.5086-02
YP =	-.1265+01	LP =	-.4192+01	NP =	.4343-01
YR =	.1102+00	LR =	.9510-00	NR =	-.2074+01
YVD =	.0000	LVD =	.0000	NVD =	.0000
YPD =	.0000	LPD =	.0000	NPD =	.0000
YRD =	.0000	LRD =	.0000	NRD =	.0000
YA =	.0000	LA =	.2073+01	NA =	-.2773-01
YR =	.0000	LR =	-.1235+00	NR =	.7578-00

IN STABILITY AXES, U = .6776+02, ZIX = .2149+05
AND ZIZ = .4606+05

TABLE B-5 RUN NO. 5

BELL X-22A W=16770LB H=0FT UO=101.2FPS GAMMA=-10.00EG -AX= 0.0G

INPUT DATA

DIMENSIONAL STABILITY DERIVATIVES
UNITS ARE 1 PER RADIAN
(BODY AXES DIFFER BY .4970+01 DEGREES, POSITIVE FOR NOSE UP, FROM STABILITY AXES)

YV =	-.2310-00	LV =	-.4800-01	NV =	.4600-02
YP =	-.1160+01	LP =	-.1300+01	NP =	-.1520-00
YR =	-.0000	LR =	.3020-00	NR =	-.3790-00
YVD =	-.0000	LVD =	-.0000	NVD =	-.0000
YPD =	-.0000	LPD =	-.0000	NPD =	-.0000
YRD =	-.0000	LRD =	-.0000	NRD =	-.0000
YA =	.0000	LA =	.2200+01	NA =	.0000
YR =	.0000	LR =	.0000	NR =	.6550-00
U =	.1012+03	UZ =	.8000+01	GAMA =	-.1000+02
MACH =	.0000	RHO =	.0000	S =	.0000
MAC =	.0000	IXZ =	.2530+04	IY =	.3190+05
HT =	.0000	XI =	.0000	TDT =	.0000
LX =	.1600+02	LY =	.0000	LZ =	.0000
CL =	.0000	CD =	.0000	W =	.1677+05
IX =	.2175+05	IZ =	.4560+05	G =	.3220+02
SPAN =	.0000				

DIMENSIONAL STABILITY DERIVATIVES, PER RADIAN, STABILITY AXES

YV =	-.2310-00	LV =	-.4924-01	NV =	.6521-02
YP =	-.1156+01	LP =	-.1317+01	NP =	-.6315-01
YR =	.1005+00	LR =	.5645-00	NR =	-.3812-00
YVD =	.0000	LVD =	.0000	NVD =	.0000
YPD =	.0000	LPD =	.0000	NPD =	.0000
YRD =	.0000	LRD =	.0000	NRD =	.0000
YA =	.0000	LA =	.2218+01	NA =	-.9000-01
YR =	.0000	LR =	-.1209+00	NR =	.6489-00

DIMENSIONAL DERIVATIVES, PRIMED

YV =	-.2310-00	LV =	-.4937-01	NV =	.6969-02
YP =	-.1156+01	LP =	-.1316+01	NP =	-.5126-01
YR =	.1005+00	LR =	.5719-00	NR =	-.3864-00
YVD =	.0000	LVD =	.0000	NVD =	.0000
YPD =	.0000	LPD =	.0000	NPD =	.0000
YRD =	.0000	LRD =	.0000	NRD =	.0000
YA =	.0000	LA =	.2220+01	NA =	-.1101+00
YR =	.0000	LR =	-.1335-00	NR =	.6502-00

IN STABILITY AXES, U = .1016+03, ZIX = .2149+05
AND ZIZ = .4606+05

TABLE B-6 RUN NO, 5

X-22 + SAS W=16770LB H=0FT U0=101.2FPS GAMMA=-10.0DEG -AX= 0.0G

INPUT DATA

DIMENSIONAL STABILITY DERIVATIVES
UNITS ARE 1 PER RADIAN
(BODY AXES DIFFER BY .4970+01 DEGREES, POSITIVE FOR NOSE UP, FROM STABILITY AXES)

YV =	-.2310-00	LV =	-.4800-01	NV =	.4600-02
YP =	-.1160+01	LP =	-.3920+01	NP =	-.1520-00
YR =	-.0000	LR =	.3820-00	NR =	-.1859+01
YVD =	-.0000	LVD =	-.0000	NVD =	-.0000
YPD =	-.0000	LPD =	-.0000	NPD =	-.0000
YRD =	-.0000	LRD =	-.0000	NRD =	-.0000
YA =	.0000	LA =	.2200+01	NA =	.0000
YR =	.0000	LR =	.0000	NR =	.6550-00
U =	.1012+03	UZ =	.8800+01	GAMA =	-.1000+02
MACH =	.0000	RHO =	.0000	S =	.0000
MAC =	.0000	IXZ =	.2530+04	IY =	.3160+05
HT =	.0000	XI =	.0000	TDT =	.0000
LX =	.1600+02	LY =	.0000	LZ =	.0000
CL =	.0000	CD =	.0000	W =	.1677+05
IX =	.2175+05	IZ =	.4580+05	G =	.3220+02
SPAN =	.0000				

DIMENSIONAL STABILITY DERIVATIVES,PER RADIAN, STABILITY AXES

YV =	-.2310-00	LV =	-.4924-01	NV =	.6521-02
YP =	-.1156+01	LP =	-.3972+01	NP =	.1706-00
YR =	.1005+00	LR =	.1065+01	NR =	-.1851+01
YVD =	.0000	LVD =	.0000	NVD =	.0000
YPD =	.0000	LPD =	.0000	NPD =	.0000
YRD =	.0000	LRD =	.0000	NRD =	.0000
YA =	.0000	LA =	.2218+01	NA =	-.9000-01
YR =	.0000	LR =	-.1209+00	NR =	.6489-00

DIMENSIONAL DERIVATIVES, PRIMED

YV =	-.2310-00	LV =	-.4937-01	NV =	.6969-02
YP =	-.1156+01	LP =	-.3976+01	NP =	.2066-00
YR =	.1005+00	LR =	.1101+01	NR =	-.1861+01
YVD =	.0000	LVD =	.0000	NVD =	.0000
YPD =	.0000	LPD =	.0000	NPD =	.0000
YRD =	.0000	LRD =	.0000	NRD =	.0000
YA =	.0000	LA =	.2220+01	NA =	-.1101+00
YR =	.0000	LR =	-.1335-00	NR =	.6502-00

IN STABILITY AXES, U = .1016+03, ZIX = .2149+05
AND ZIZ = .4606+05

TABLE B-7 RUN NO. 7

BELL X-22A W=16770LB H=0FT U0=168.9FPS GAMMA=-13.5DEG -AX= 0.0G

INPUT DATA

DIMENSIONAL STABILITY DERIVATIVES
UNITS ARE 1 PER RADIAN
(BODY AXES DIFFER BY .4974+01 DEGREES, POSITIVE FOR NOSE UP, FROM STABILITY AXES)

YV =	-.2360-00	LV =	-.4700-01	NV =	.4000-02
YP =	-.1140+01	LP =	-.1840+01	NP =	-.7900-01
YR =	-.0000	LR =	.6640-00	NR =	-.4250-00
YVD =	-.0000	LVD =	-.0000	NVD =	-.0000
YPD =	-.0000	LPD =	-.0000	NPD =	-.0000
YRD =	-.0000	LRD =	-.0000	NRD =	-.0000
YA =	.0000	LA =	.2020+01	NA =	.2180-01
YR =	.0000	LR =	-.1290-00	NR =	.5350-00
U =	.1689+03	UZ =	.1470+02	GAMA =	-.1350+02
MACH =	.0000	RHO =	.0006	S =	.0000
MAC =	.0000	IXZ =	.2530+04	IY =	.5160+05
HT =	.0000	XI =	.0000	TDT =	.0000
LX =	.1600+02	LY =	.0000	LZ =	.0000
CL =	.0000	CD =	.0000	W =	.1677+05
IX =	.2175+05	IZ =	.4580+05	G =	.3220+02
SPAN =	.0000				

DIMENSIONAL STABILITY DERIVATIVES, PER RADIAN, STABILITY AXES

YV =	-.2360-00	LV =	-.4012-01	NV =	.5887-02
YP =	-.1136+01	LP =	-.1916+01	NP =	.3666-01
YR =	.9684-01	LR =	.1106+01	NR =	-.4544-00
YVD =	.0000	LVD =	.0000	NVD =	.0000
YPD =	.0000	LPD =	.0000	NPD =	.0000
YRD =	.0000	LRD =	.0000	NRD =	.0000
YA =	.0000	LA =	.2032+01	NA =	-.6112-01
YR =	.0000	LR =	-.2289-00	NR =	.5353-00

DIMENSIONAL DERIVATIVES, PRIMED

YV =	-.2360-00	LV =	-.4024-01	NV =	.6323-02
YP =	-.1136+01	LP =	-.1917+01	NP =	.5392-01
YR =	.9684-01	LR =	.1114+01	NR =	-.4646-00
YVD =	.0000	LVD =	.0000	NVD =	.0000
YPD =	.0000	LPD =	.0000	NPD =	.0000
YRD =	.0000	LRD =	.0000	NRD =	.0000
YA =	.0000	LA =	.2034+01	NA =	-.7944-01
YR =	.0000	LP =	-.2393-00	NR =	.5375-00

IN STABILITY AXES, U = .1695+03, ZIX = .2149+05
AND ZIZ = .4606+05

TABLE B-8 RUN NO, 7

X-22 + SAS W=16770LB H=0FT U0=168.9FPS GAMMA=-13.5DEG -AX= 0.0G

INPUT DATA

DIMENSIONAL STABILITY DERIVATIVES
UNITS ARE 1 PER RADIAN
(BODY AXES DIFFER BY .4974+01 DEGREES, POSITIVE
FOR NOSE UP, FROM STABILITY AXES)

YV =	-.2360-00	LV =	-.4700-01	NV =	.4000-02
YP =	-.1140+01	LP =	-.2112+01	NP =	-.8190-01
YR =	-.0000	LR =	.1153+01	NR =	-.1635+01
YVD =	-.0000	LVD =	-.0000	NVD =	-.0000
YPD =	-.0000	LPD =	-.0000	NPD =	-.0000
YRD =	-.0000	LRD =	-.0000	NRD =	-.0000
YA =	.0000	LA =	.2020+01	NA =	.2180-01
YR =	.0000	LR =	-.1290-00	NR =	.5350-00
U =	.1689+03	UZ =	.1470+02	GAMA =	-.1350+02
MACH =	.0000	RHO =	.0000	S =	.0000
MAC =	.0000	IXZ =	.2530+04	IY =	.3160+05
HT =	.0000	XI =	.0000	TDT =	.0000
LX =	.1600+02	LY =	.0000	LZ =	.0000
CL =	.0000	CD =	.0000	W =	.1677+05
IX =	.2175+05	IZ =	.4580+05	G =	.3220+02
SPAN =	.0000				

DIMENSIONAL STABILITY DERIVATIVES,PER RADIAN,
STABILITY AXES

YV =	-.2360-00	LV =	-.4812-01	NV =	.5887-02
YP =	-.1136+01	LP =	-.2233+01	NP =	.1499-00
YR =	.9884-01	LR =	.1642+01	NR =	-.1661+01
YVD =	.0000	LVD =	.0000	NVD =	.0000
YPD =	.0000	LPD =	.0000	NPD =	.0000
YRD =	.0000	LRD =	.0000	NRD =	.0000
YA =	.0000	LA =	.2032+01	NA =	-.6112-01
YR =	.0000	LR =	-.2289-00	NR =	.5353-00

DIMENSIONAL DERIVATIVES, PRIMED

YV =	-.2360-00	LV =	-.4824-01	NV =	.6323-02
YP =	-.1136+01	LP =	-.2236+01	NP =	.1700-00
YR =	.9884-01	LR =	.1675+01	NR =	-.1677+01
YVD =	.0000	LVD =	.0000	NVD =	.0000
YPD =	.0000	LPD =	.0000	NPD =	.0000
YRD =	.0000	LRD =	.0000	NRD =	.0000
YA =	.0000	LA =	.2034+01	NA =	-.7944-01
YR =	.0000	LR =	-.2393-00	NR =	.5375-00

IN STABILITY AXES, U = .1695+03, ZIX = .2149+05
AND ZIZ = .4606+05

TABLE B-9 RUN NO. 9

BELL X-22A W=16770LB H=0FT U0=219.5FPS GAMMA= 0.0DEG -AX= 0.0G

INPUT DATA

DIMENSIONAL STABILITY DERIVATIVES
UNITS ARE 1 PER RADIAN
(BODY AXES DIFFER BY .4973+01 DEGREES, POSITIVE
FOR NOSE UP, FROM STABILITY AXES)

YV =	-.3670-00	LV =	-.4900-01	NV =	.4700-02
YP =	-.1050+01	LP =	-.4040+01	NP =	-.3800-01
YR =	-.0000	LR =	.4600-00	NR =	-.4220-00
YVD =	-.0000	LVD =	-.0000	NVD =	-.0000
YPD =	-.0000	LPD =	-.0000	NPD =	-.0000
YRD =	-.0000	LRD =	-.0000	NRD =	-.0000
YA =	.0000	LA =	.2340+01	NA =	.1660-00
YR =	.0000	LR =	.1740-00	NR =	.4490-00
U =	.2195+03	UZ =	.1910+02	GAMA =	.0000
MACH =	.0000	RHO =	.0000	S =	.0000
MAC =	.0000	IXZ =	.2550+04	IY =	.3160+05
HT =	.0000	XI =	.0000	TDT =	.0000
LX =	.1600+02	LY =	.0000	LZ =	.0000
CL =	.0000	CD =	.0000	W =	.1677+05
IX =	.2175+05	IZ =	.4580+05	G =	.3220+02
SPAN =	.0000				

DIMENSIONAL STABILITY DERIVATIVES,PER RADIAN,
STABILITY AXES

YV =	-.3670-00	LV =	-.5027-01	NV =	.6662-02
YP =	-.1046+01	LP =	-.4097+01	NP =	.1651-00
YR =	.9102-01	LR =	.8921-00	NR =	-.4463-00
YVD =	.0000	LVD =	.0000	NVD =	.0000
YPD =	.0000	LPD =	.0000	NPD =	.0000
YRD =	.0000	LRD =	.0000	NRD =	.0000
YA =	.0000	LA =	.2328+01	NA =	.6866-01
YR =	.0000	LR =	.9247-01	NR =	.4377-00

DIMENSIONAL DERIVATIVES, PRIMED

YV =	-.3670-00	LV =	-.5040-01	NV =	.7118-02
YP =	-.1046+01	LP =	-.4101+01	NP =	.2021-00
YR =	.9102-01	LR =	.9009-00	NR =	-.4545-00
YVD =	.0000	LVD =	.0000	NVD =	.0000
YPD =	.0000	LPD =	.0000	NPD =	.0000
YRD =	.0000	LRD =	.0000	NRD =	.0000
YA =	.0000	LA =	.2327+01	NA =	.4770-01
YR =	.0000	LR =	.8904-01	NR =	.4370-00

IN STABILITY AXES, U = .2203+03, ZIX = .2149+05
AND ZIZ = .4606+05

TABLE B-10 RUN NO, 9

X-22 + SAS W=16770LB H=0FT U0=219,5FPS GAMMA= 0,0DEG -AX= 0,0G

INPUT DATA

DIMENSIONAL STABILITY DERIVATIVES
UNITS ARE 1 PER RADIAN
(BODY AXES DIFFER BY ,4973+01 DEGREES, POSITIVE
FOR NOSE UP, FROM STABILITY AXES)

YV =	-,3670-00	LV =	-,4900-01	NV =	,4700-02
YP =	-,1050+01	LP =	-,4040+01	NP =	-,3800-01
YR =	-,0000	LR =	,8500-01	NR =	-,1397+01
YVD =	-,0000	LVD =	-,0000	NVD =	-,0000
YPD =	-,0000	LPD =	-,0000	NPD =	-,0000
YRD =	-,0000	LRD =	-,0000	NRD =	-,0000
YA =	,0000	LA =	,2340+01	NA =	,1660-00
YR =	,0000	LR =	,1740-00	NR =	,4490-00
U =	,2195+03	UZ =	,1910+02	GAMA =	,0000
MACH =	,0000	RHO =	,0000	S =	,0000
MAC =	,0000	IXZ =	,2530+04	IY =	,3160+05
HT =	,0000	XI =	,0000	TDT =	,0000
LX =	,1600+02	LY =	,0000	LZ =	,0000
CL =	,0000	CD =	,0000	W =	,1677+05
IX =	,2175+05	IZ =	,4580+05	G =	,3220+02
SPAN =	,0000				

DIMENSIONAL STABILITY DERIVATIVES,PER RADIAN,
STABILITY AXES

YV =	-,3670-00	LV =	-,5027-01	NV =	,6662-02
YP =	-,1046+01	LP =	-,4080+01	NP =	,2475-00
YR =	,9102-01	LR =	,6949-00	NR =	-,1393+01
YVD =	,0000	LVD =	,0000	NVD =	,0000
YPD =	,0000	LPD =	,0000	NPD =	,0000
YRD =	,0000	LRD =	,0000	NRD =	,0000
YA =	,0000	LA =	,2328+01	NA =	,6866-01
YR =	,0000	LR =	,9247-01	NR =	,4377-00

DIMENSIONAL DERIVATIVES, PRIMED

YV =	-,3670-00	LV =	-,5040-01	NV =	,7118-02
YP =	-,1046+01	LP =	-,4086+01	NP =	,2844-00
YR =	,9102-01	LR =	,7219-00	NR =	-,1400+01
YVD =	,0000	LVD =	,0000	NVD =	,0000
YPD =	,0000	LPD =	,0000	NPD =	,0000
YRD =	,0000	LRD =	,0000	NRD =	,0000
YA =	,0000	LA =	,2327+01	NA =	,4770-01
YR =	,0000	LR =	,8404-01	NR =	,4370-00

IN STABILITY AXES, U = ,2203+03, ZIX = ,2149+05
AND ZIZ = ,4606+05

TABLE B-11 RUN NO. 12

BELL X-22A W=16770LB H=0FT UO= 0.0FPS GAMMA= 0.0DEG =AX=.211G

INPUT DATA

DIMENSIONAL STABILITY DERIVATIVES
UNITS ARE 1 PER RADIAN
(BODY AXES DIFFER BY .9000+02 DEGREES, POSITIVE
FOR NOSE UP, FROM STABILITY AXES)

YV	=	-.4700-00	LV	=	-.1120+00	NV	= .1950-01
YP	=	-.7700-00	LP	=	-.2800-00	NP	= .0000
YR	=	-.0000	LR	=	-.1770-00	NR	= -.1480-00
YVD	=	-.0000	LVD	=	-.0000	NVD	= -.0000
YPD	=	-.0000	LPD	=	-.0000	NPD	= -.0000
YRD	=	-.0000	LRD	=	-.0000	NRD	= -.0000
YA	=	.0000	LA	=	.1970+01	NA	= .0000
YR	=	.0000	LR	=	.0000	NR	= .7000-00
U	=	.0000	UZ	=	.0000	GAMA	= .0000
MACH	=	.0000	RHO	=	.0000	S	= .0000
MAC	=	.0000	IXZ	=	.2530+04	IY	= .3160+05
HT	=	.0000	XI	=	.0000	TDT	= .0000
LX	=	.1600+02	LY	=	.0000	LZ	= .0000
CL	=	.0000	CD	=	.0000	W	= .1677+05
IX	=	.2175+05	IZ	=	.4580+05	G	= .3220+02
SPAN	=	.0000					

DIMENSIONAL STABILITY DERIVATIVES,PER RADIAN,
STABILITY AXES

YV	=	-.4700-00	LV	=	-.1950-01	NV	= .1120+00
YP	=	.1067-07	LP	=	-.1480-00	NP	= -.1770-00
YR	=	.7700-00	LR	=	-.3892-08	NR	= -.2800-00
YVD	=	.0000	LVD	=	.0000	NVD	= .0000
YPD	=	.0000	LPD	=	.0000	NPD	= .0000
YRD	=	.0000	LRD	=	.0000	NRD	= .0000
YA	=	.0000	LA	=	-.1296-07	NA	= -.1970+01
YR	=	.0000	LR	=	-.7000-00	NR	= -.2042-07

DIMENSIONAL DERIVATIVES, PRIMED

YV	=	-.4700-00	LV	=	-.1240-01	NV	= .1112+00
YP	=	.1067-07	LP	=	-.1568-00	NP	= -.1967-00
YR	=	.7700-00	LR	=	-.1557-01	NR	= -.2836-00
YVD	=	.0000	LVD	=	.0000	NVD	= .0000
YPD	=	.0000	LPD	=	.0000	NPD	= .0000
YRD	=	.0000	LRD	=	.0000	NRD	= .0000
YA	=	.0000	LA	=	-.1095+00	NA	= -.1996+01
YR	=	.0000	LR	=	-.7045-00	NR	= -.8248-01

IN STABILITY AXES, U = .0000 , ZIX = .4580+05
AND ZIZ = .2175+05

TABLE B-12 RUN NO. 12

X-22 + SAS W=16770LB H=0FT U0= 0.0FPS GAMMA= 0.0DEG -AX=.211G

INPUT DATA

DIMENSIONAL STABILITY DERIVATIVES
UNITS ARE 1 PER RADIAN
(BODY AXES DIFFER BY .9000+02 DEGREES, POSITIVE
FOR NOSE UP, FROM STABILITY AXES)

YV =	-.4700-00	LV =	-.1120+00	NV =	.1950-01
YP =	-.7700-00	LP =	-.3610+01	NP =	.0000
YR =	-.0000	LR =	-.1770-00	NR =	-.1728+01
YVD =	-.0000	LVD =	-.0000	NVD =	-.0000
YPD =	-.0000	LPD =	-.0000	NPD =	-.0000
YRD =	-.0000	LRD =	-.0000	NRD =	-.0000
YA =	.0000	LA =	.1970+01	NA =	.0000
YR =	.0000	LR =	.0000	NR =	.7000-00
U =	.0000	UZ =	.0000	GAMA =	.0000
MACH =	.0000	RHO =	.0000	S =	.0000
MAC =	.0000	IXZ =	.2530+04	IY =	.3160+05
HT =	.0000	XI =	.0000	TDT =	.0000
LX =	.1600+02	LY =	.0000	LZ =	.0000
CL =	.0000	CD =	.0000	W =	.1677+05
IX =	.2175+05	IZ =	.4580+05	G =	.3220+02
SPAN =	.0000				

DIMENSIONAL STABILITY DERIVATIVES,PER RADIAN,
STABILITY AXES

YV =	-.4700-00	LV =	-.1950-01	NV =	.1120+00
YP =	.1067-07	LP =	-.1728+01	NP =	-.1770-00
YR =	.7700-00	LR =	-.4769-07	NR =	-.3610+01
YVD =	.0000	LVD =	.0000	NVD =	.0000
YPD =	.0000	LPD =	.0000	NPD =	.0000
YRD =	.0000	LRD =	.0000	NRD =	.0000
YA =	.0000	LA =	-.1296-07	NA =	-.1970+01
YR =	.0000	LR =	-.7000-00	NR =	-.2042-07

DIMENSIONAL DERIVATIVES, PRIMED

YV =	-.4700-00	LV =	-.1340-01	NV =	.1112+00
YP =	.1067-07	LP =	-.1749+01	NP =	-.3829-00
YR =	.7700-00	LR =	-.2007-00	NR =	-.3657+01
YVD =	.0000	LVD =	.0000	NVD =	.0000
YPD =	.0000	LPD =	.0000	NPD =	.0000
YRD =	.0000	LRD =	.0000	NRD =	.0000
YA =	.0000	LA =	-.1095+00	NA =	-.1996+01
YR =	.0000	LR =	-.7045-00	NR =	-.8248-01

IN STABILITY AXES, U = .0000 , ZIX = .4580+05
AND ZIZ = .2175+05

REFERENCES

1. Wolkovitch, J.; and Hoffman, J. A.: Stability and Control of Helicopters in Steep Approaches. MRI Report No. 2284-1 (USAAVLABS Technical Report 70-74A), Mechanics Research, Inc., Los Angeles, California, January 1971.

2. Chang, S. S. L.: Synthesis of Optimal Control Systems. McGraw-Hill Book Co., Inc., 1961.

3. Deckert, W. H.; and Hickey, D. H.: Summary and Analysis of Feasibility-Study Designs of V/STOL Transport Aircraft. J. Aircraft, vol. 7, no. 1, Jan.-Feb. 1970, pp. 66-71.

4. Hiscocks, R. D.: STOL Aircraft-A Perspective. The Aeronautical Journal, vol. 72, no. 685, January 1968, pp. 11-33.

5. Cornish, J. J.; and Tanner, R. F.: High Lift Techniques for STOL Aircraft. Society of Automotive Engineers, Paper 670245, 1967.

6. Alvarez-Calderon, A.: Design and Tests of Inverting Flaps and of Wing Span Flaps. Society of Automotive Engineers, Paper 680646.

7. Whittley, D. C.: Maximum Lift Coefficient for STOL Aircraft: A Critical Review, Proc. CAL/USAAVLABS Symposium on Aerodynamic Problems Associated with V/STOL Aircraft. AD 657563, 1966.

8. Hancock, G. J.: On the Rolling Up of a Trailing Vortex Sheet. Aeronautical Journal, vol. 74, no. 717, Sept. 1970, pp. 749-752.

9. Johnston, G. W.: Some Recent Aerodynamic Advances in STOL Aircraft. J. Aircraft, September - October 1965.

10. Strand, T.; and Levinsky, E. S.: Wind-Tunnel Tests of a Free-Wing Tilt-Propeller V/STOL Airplane Model. AFFDL-TR-69-80, 1969.

11. Campbell, J. P.: Vertical Takeoff and Landing Aircraft. MacMillan, New York, 1962.

12. Quigley, Hervey C.; Innis, Robert C.; and Holzhauser, Curt A.: A Flight Investigation of the Performance, Handling Qualities, and Operational Characteristics of a Deflected Slipstream STOL Transport Airplane Having Four Interconnected Propellers. NASA TN D-2231, March 1964.

13. Innis, R. C.; Holzhauser, C. A.; and Gallant, R. P.: Flight Tests Under IFR with an STOL Transport Aircraft. NASA TN D-4939, 1968.

14. Down, H. W.; Jones, G. E.; and Satterwhite, J. J.: XC-142A Limited Category II Stability and Control Tests. AFFTC TR-68-9, 1968.

15. Rhodes, W. B.: Initial Military Flight Tests of the X-22A VTOL Research Aircraft. AIAA Paper No. 69-319, March 1969.

16. Giulianetti, Demo J.,; Biggers, James C.; and Maki, Ralph L.: Longitudinal and Lateral-Directional Aerodynamic Characteristics of a Large-Scale, V/STOL Model with Four Tilting Ducted Fans Arranged in a Dual Tandem Configuration. NASA TN D-3490, 1966.

17. Kelly, H. L.; and Champine, R. A.: Flight Operating Problems and Aerodynamic and Performance Characteristics of a Fixed-Wing, Tilt-Duct.VTOL Research Aircraft, NASA TN D-1802, 1963.

18. Anon: The Hummingbird XV-4B. VTOL Research Program, AFFDL-TR-69-75 (AD-700436), 1969.

19. Gerdes, R. M.; and Hynes, C.S.; Factors Affecting Handling Qualities of a Lift-Fan Aircraft During Steep Terminal Area Approaches. American Helicopter Society 27th Annual National V/STOL Forum, Washington, D.C. May 1971. Preprint No. 544.

20. McCormick, B. W.: Aerodynamics of V/STOL Flight. Academic Press, New York, 1967.

21. Kuhn, R. E.: Semi-Empirical Procedure for Estimating Lift and Drag Characteristics of Propeller-Wing-Flap Configurations for Vertical and Short-Take-Off-and-Landing Airplanes. NASA Memo 1-16-59L, 1959.

22. Kuhn, R. E.; and Draper, J. W.: An Investigation of a Wing Propeller Configuration Employing Large-Chord Plain Flaps and Large-Diameter Propellers for Low-Speed Flight and Vertical Take-Off. NACA TN 3307, 1954.

23. Goodson, Kenneth W.: "Longitudinal Aerodynamic Characteristics of a Flapped Tilt-Wing Four-Propeller V/STOL Transport Model". NASA TN D-3217, February 1966.

24. Anon: U.S. and Canadian VTOL Aircraft. Aviation Week and Space Technology, vol. 90, no. 10, March 10, 1969, p. 157.

25. Black, Ernest L.; and Booth, George C.: "Correlation of Aerodynamic Stability and Control Derivatives Obtained from Flight Tests and Wind Tunnel Tests on the XC-142A Airplane". AFFDL-TR-68-167, November 1968.

26. Abbott, Ira H.; and Von Doenhoff, Albert E.: "Theory of Wing Sections". Dover Edition, 1958.

27. Kelley, H. L.; Reeder, J. P.; and Champine, R. A.: Summary of a Flight-Test Evaluation of the CL-84 Tilt-Wing V/STOL Aircraft. NASA TM X-1914, March 1970.

28. Longhurst, W. S.: A Report on Stability and Control Testing of a Tilt-Wing V/STOL Aircraft. S.A.E. Paper 660315, 1966.

29. Wolkovitch, J.; and Walton, R. P.: VTOL and Helicopter Approximate Transfer Functions and Closed-Loop Handling Qualities. STI TR 128-1 (ASTIA AD-470137), June 1965.

30. Brookhaus, R.: Mixed Pilot and Automatic Longitudinal Control During Landing Approach. Paper presented to AGARD Flight Mechanics Panel, 1966.

31. Gaul, J. W.; Kaiser, R. P.; Onega, G. T.; and DeCanio, F. T.: Application of Optimal Control Theory to VTOL Flight Control System Design. AFFDL-TR-67-102, 1967.

32. Wiener, N.: Extrapolation, Interpolation and Smoothing of Stationary Time Series. John Wiley and Sons, 1949.

33. Newton, C. G.; Gould, L. A.; and Kaiser, J. F.: Analytical Design of Linear Feedback Controls. John Wiley and Sons, 1957.

34. Kalman, R. E.; and Englar, T.: Fundamental Study of Adaptive Control Systems. United States Air Force Rept. ASD-TR-61-27, vol. I and II, March 1962.

35. Magdaleno, R.; and Wolkovitch, J.: Performance Criteria for Linear Constant-Coefficient Systems with Random Inputs. United States Air Force Rept. ASD-TDR-62-470 (ASTIA AD-297805), January 1963.

36. Tobak, M.: On the Minimization of Airplane Responses to Random Gusts. NACA TN 3290, 1957.

37. Whitbeck, R. F.: A Frequency Domain Approach to Linear Optimal Control. J. Aircraft, July-August 1968.

38. Willis, B. H.; and Brockett, R. W.: The Frequency Domain Solution of Regulator Problems. Proc. J.A.C.C., 1965.

39. Etkin, B.: A Simple Method for the Analogue Computation of the Mean-Square Response of Airplanes to Atmospheric Turbulence. University of Toronto UTIA Tech. Note 32, January 1960.

40. Ashkenas, I. L.; and McRuer, D. T.: Approximate Airframe Transfer Functions and Application to Single Sensor Control Systems. WADD TR 58-82, 1958.

"The aeronautical and space activities of the United States shall be conducted so as to contribute . . . to the expansion of human knowledge of phenomena in the atmosphere and space. The Administration shall provide for the widest practicable and appropriate dissemination of information concerning its activities and the results thereof."

—NATIONAL AERONAUTICS AND SPACE ACT OF 1958

NASA SCIENTIFIC AND TECHNICAL PUBLICATIONS

TECHNICAL REPORTS: Scientific and technical information considered important, complete, and a lasting contribution to existing knowledge.

TECHNICAL NOTES: Information less broad in scope but nevertheless of importance as a contribution to existing knowledge.

TECHNICAL MEMORANDUMS: Information receiving limited distribution because of preliminary data, security classification, or other reasons.

CONTRACTOR REPORTS: Scientific and technical information generated under a NASA contract or grant and considered an important contribution to existing knowledge.

TECHNICAL TRANSLATIONS: Information published in a foreign language considered to merit NASA distribution in English.

SPECIAL PUBLICATIONS: Information derived from or of value to NASA activities. Publications include conference proceedings, monographs, data compilations, handbooks, sourcebooks, and special bibliographies.

TECHNOLOGY UTILIZATION PUBLICATIONS: Information on technology used by NASA that may be of particular interest in commercial and other non-aerospace applications. Publications include Tech Briefs, Technology Utilization Reports and Technology Surveys.

Details on the availability of these publications may be obtained from:

SCIENTIFIC AND TECHNICAL INFORMATION OFFICE

NATIONAL AERONAUTICS AND SPACE ADMINISTRATION

Washington, D.C. 20546